PLASMA DYNAMICS

XIII. PLASMA DYNAMICS

Academic and Research Staff

Prof. William P. Allis
Prof. Abraham Bers
Prof. George Bekefi
Prof. Sanborn C. Brown
Prof. Sow-Hsin Chen
Prof. Bruno Coppi
Prof. Thomas H. Dupree
Prof. E. Victor George
Prof. Elias P. Gyftopoulos
Prof. Hermann A. Haus
Prof. Lawrence M. Lidsky
Prof. James E. McCune
Prof. Peter A. Politzer
Prof. Dieter J. Sigmar
Prof. Louis D. Smullin
Prof. Robert J. Taylor
Dr. Edward G. Apgar
Dr. Giuseppe F. Bosia
Dr. Gradus J. Boxman
Dr. Alberto Brusadin
Dr. Bert C. J. M. DeKock
Dr. J. Michael Drake
Dr. Enrico Grilli
Dr. Giampietro Lampis
Dr. Bernard J. Meddens
Dr. D. Bruce Montgomery*
Dr. Arnoldus A. M. Oomens
Dr. Ronald R. Parker
Dr. Francesco Pegoraro
Dr. Leonardo Pieroni
Dr. Arthur H. M. Ross
Dr. Sergio Segre
Dr. R. Van Heijningen
Dr. Gregory N. Rewoldt
John J. McCarthy
William J. Mulligan
Allan R. Reiman

Graduate Students

Charles T. Breuer
Leslie Bromberg
Natale M. Ceglio
Frank W. Chambers
Hark C. Chan
Franklin R. Chang
Tsi-Pin Choong
Wing-Shek Chow
Paul W. Chrisman, Jr.
John A. Combs
Donald L. Cook
David A. Ehst
Nathaniel J. Fisch
Jay L. Fisher
Alan R. Forbes
Ricardo M. O. Galvao
Keith C. Garel
Ady Hershcovitch
Steven P. Hirshman
James C. Hsia
Dennis J. Huber
Saeed Z. Jabbawy
David L. Kaplan
Charles F. F. Karney
Peter T. Kenyon
David S. Komm
Craig Kullberg
John L. Kulp, Jr.
Ping Lee
Francois Martin
Mark L. McKinstry
John L. Miller
Paul E. Morgan
Thaddeus Orzechowski
David O. Overskei
Aniket Pant
Louis R. Pasquarelli
Gerald D. Pine
Robert H. Price
Charles A. Primmerman
Donald Prosnitz
Paul A. Roth
David S. Stone
Miloslav S. Tekula
David J. Tetrault
Kim Theilhaber
Alan L. Throop
Ben M. Tucker
Ernesto C. Vanterpool
Marcio L. Vianna
Yi-Ming Wang
Duncan C. Watson
Charles W. Werner
David M. Wildman
Stephen M. Wolfe

*Dr. D. Bruce Montgomery is at the Francis Bitter National Magnet Laboratory.

XIII. PLASMA DYNAMICS

A. Confinement Systems

RESEARCH OBJECTIVES AND SUMMARY OF RESEARCH

1. Physics of High-Temperature Plasmas

U.S. Atomic Energy Commission (Contract AT(11-1)-3070)

Bruno Coppi

An understanding of the physics of high-temperature plasmas is of primary importance in the solution of the problem of controlled thermonuclear fusion. One of the goals in this field of research is the magnetic confinement and heating of plasmas with densities of the order of 10^{14} particles/cm^3 and thermal energies between 5 keV and 10 keV. The macroscopic transport properties (e.g., particle diffusion, thermal conductivity, and electrical resistivity) of plasmas in these regimes are weakly affected by two-body collisions between particles. These plasmas are significantly influenced by the types of collective modes such as density fluctuations caused by microinstabilities that can be excited in them.

We have carried out a theoretical and experimental program in this general area during 1974 and presented relevant contributions at national and international conferences. Several papers have been published in professional journals. Our primary focus has been the experimental effort developed around the Alcator machine. Our purpose has been to realize plasmas capable of sustaining very high current densities without becoming macroscopically unstable, in order to achieve the highest possible rate of resistive heating of the plasma itself.

We may point out the following achievements:

a. Average plasma densities in deuterium of $\sim 2 \times 10^{14}$/cm^3, which represents a record for toroidal plasma experiments with relatively long energy replacement times (~20 msec).

b. Record values of average current densities ($700 \div 800$ A/cm^2) corresponding to total plasma currents of ~200 kA.

c. Duration of plasma equilibria up to 300 msec without the assistance of a feedback system; this also is a record.

d. Production of stable plasmas with evidence from particle density measurements, thermonuclear neutron production, and electrical resistivity of a high degree of purity (that is, $Z \approx 1$).

A new experimental facility (Rector) that was proposed in 1973 has been brought into operation and is being used to investigate the confinement properties of toroidal plasma columns with noncircular cross sections. The main objective of the experiment has been achieved, since a plasma cross section with 2:1 elongation has been obtained and proved to be stable. To our knowledge, this is the first time that a relatively long-lived toroidal configuration with noncircular cross section and without a surrounding metallic shell has been realized.

The Thomson scattering system developed by the Euratom-CNEN laboratory of Frascati and the sophisticated electrical diagnostic system developed by collaborators of the Euratom-F.O.M. Laboratory at Jutphaas have been operated successfully and have already provided a firm basis for the understanding of the new plasma regimes that have been attained.

XIII. PLASMA DYNAMICS

B. Laser-Plasma Interactions

RESEARCH OBJECTIVES AND SUMMARY OF RESEARCH

National Science Foundation (Grant GK-37979X1)

E. Victor George

An experimental program is under way to study the interaction of high peak power lasers with target plasmas. The general aspect of this research is directed toward understanding the precise details of the interaction, including the amount of energy deposited (by the interaction) in the plasma by the laser. We are also examining the use of plasma spectroscopy as a diagnostic probe of plasma turbulence. The interaction program is divided into two basic, though interrelated, areas of research: CO_2 and dye laser interactions with low-density (n_e in the range 10^{14}-10^{17} cm^{-3}) helium target plasmas; and studies on the plasma produced by irradiating a solid target with an ~10 J, ~1 ns CO_2 laser. Details of our experimental program were given in Quarterly Progress Report No. 112 (pp. 54-55).

In studying the interaction of intense laser pulses with "low" density (n_e in the range 10^{14}-10^{17} cm^{-3}) target plasmas it is necessary to choose suitable diagnostic tools. During the past several years we have developed the experimental techniques for obtaining both spatially and temporally resolved emission line shapes from plasmas, and hence we have concentrated our diagnostic effort in this direction. Our present interest is focused on detecting the strength of the laser-plasma interaction using optical satellites. The strength of the satellite lines depends on the average plasma field fluctuations. The positions of these lines yield the local electron density. We feel that the shape of the satellite line, when properly unfolded from its "natural" shape, should yield the turbulent spectrum of the plasma fluctuations.

A prerequisite for using this technique is to ascertain the "natural" line shape of the satellite line or lines, and to determine the effect on the emission spectra of a high-power CO_2 laser beam. This work has been highly successful and is nearing completion.

Before undertaking plasma experiments we decided that it was imperative to observe the satellite or satellites caused by the oscillating laser field, that is, $\omega_\ell = \omega_{CO_2}$ in a helium target plasma. From such work we have developed a theoretical model that determines the "natural" satellite line profile. These predictions compare well with experiment. Details of the theoretical model and a brief description of the experimental apparatus have been published.[1] A comprehensive article on this work is being prepared for publication.

Experimental apparatus for the optical mixing stimulated plasmon production and laser-solid target experiments are nearing completion, and progress on this work will be reported at a later date.

References

1. D. Prosnitz and E. V. George, "Emission Profiles of Laser-Induced Optical Satellite Lines in a Helium Plasma," Phys. Rev. Letters 32, 1282 (1974).

(XIII. PLASMA DYNAMICS)

1. THREE-DIMENSIONAL DISPERSION RELATIONS FOR THIRD-ORDER LASER-PLASMA INTERACTIONS. II

National Science Foundation (Grant GK-37979X1)

Duncan C. Watson, Abraham Bers

Introduction

We shall use the theory of coherent wave coupling in three dimensions, which was presented in Quarterly Progress Report No. 113 (pp. 117-126), to extend our unified description of laser-driven instabilities[1] to the filamentation[2] and modulation[3] instabilities.

Isolation of Specific Instabilities from the Determinantal Equation

For very small $|E_L|$ not all of

$$(K_+)_M, (K_+)_S, (K)_M, (K)_S, (K_-)_M, (K_-)_S \tag{1}$$

can simultaneously be of order unity. Let $(K_+)_M$, $(K_-)_M$ be small and the rest of (1) of order unity. Use the result that

$$\left(C_+^-\right)_{MM} = \left({}_+C^+\right)_{MM} = \left(C_-^+\right)_{MM} = \left({}_-C^-\right)_{MM} = 0. \tag{2}$$

Then to order $|E_L|$ we have[3]

$$0 = \begin{vmatrix} (K_+)_M + |E_L|^2 \left({}_+C_+^{+-}\right)_{MM} & E_L\left({}_+C^+\right)_{MS} & E_L^2\left({}_+C_-^{++}\right)_{MM} \\ E_L^*\left(C_+^-\right)_{SM} & (K)_S & E_L\left(C_-^+\right)_{SM} \\ E_L^{*2}\left({}_-C_+^{--}\right)_{MM} & E_L^*\left({}_-C^-\right)_{MS} & (K_-)_M + |E_L|^2 \left({}_-C_-^{+-}\right)_{MM} \end{vmatrix} \tag{3}$$

This describes the self-filamentation and self-modulation of the laser light. The 2×2 upper-left and lower-right subdeterminants describe the modified Brillouin instability. The additional roots thus introduced are not important, since the modified Brillouin growth rate goes to zero in the region of $(\vec{k}, \omega)$ space where the filamentation and modulation roots are found, that is, the neighborhood of the origin $(\vec{0}, 0)$. Contrast this with the case of the coalescence[1] of the modified-decay and oscillating-two-stream instabilities, where both have appreciable growth rates in the same region of $\vec{k}$-space.

Three-Dimensional Dispersion Relation

From (3), taking only the electron contributions to the nonlinear currents,[1] and assuming the phase-velocity disparities

$$|\omega_{--}/k_{--}|, |\omega_{++}/k_{++}| > |\omega_{-}/k_{-}|, |\omega_{+}/k_{+}| \gg v_{Te} \gg |\omega/k|, \tag{4}$$

we get

$$0 = \begin{vmatrix} 1 - \dfrac{\omega_p^2 + k_+^2 c^2}{\omega_+^2} + |X^2| & \dfrac{X}{k\lambda_D} & XY \\ \dfrac{X^*}{k\lambda_D} & \dfrac{1}{k^2\lambda_D^2}\left[1 - \dfrac{k^2 c_s^2}{\omega^2}\right] & \dfrac{Y}{k\lambda_D} \\ X^*Y^* & \dfrac{Y^*}{k\lambda_D} & 1 - \dfrac{\omega_p^2 + k_-^2 c^2}{\omega_-^2} + |Y^2| \end{vmatrix} \tag{5}$$

where

$$X = \frac{v_{Le}}{v_{Te}} \frac{\omega_{pe}}{\omega_+} (\vec{e}_{M+} \cdot \vec{e}_L) \tag{6}$$

$$Y = \frac{v_{Le}}{v_{Te}} \frac{\omega_{pe}}{\omega_-} (\vec{e}_{M-} \cdot \vec{e}_L). \tag{7}$$

We expand (5) and obtain the dispersion relation

$$1 - \frac{k^2 c_s^2}{\omega^2} = \frac{V_{Laser}^2}{4v_{Te}^2} \frac{k^2 c_s^2}{\omega^2} \left\{ \frac{\omega_{pe}^2 (\vec{e}_{M+} \cdot \vec{e}_L)^2}{\omega_+^2 - \omega_p^2 - k_+^2 c^2} + \frac{\omega_{pe}^2 (\vec{e}_{M-} \cdot \vec{e}_L)^2}{\omega_-^2 - \omega_p^2 - k_-^2 c^2} \right\}. \tag{8}$$

We now use (8) to describe the filamentation and modulation instabilities by specifying the region of $(\vec{k}, \omega)$-space as follows. Consider the neighborhood of the origin $(\vec{0}, 0)$ where the hypersurfaces

$$(K_+)_M = 0, \qquad (K_-)_M = 0 \tag{9}$$

are tangent, so that correspondingly

$$(\vec{k}_\pm, \omega_\pm) = (\pm\vec{k}_L, \pm\omega_L). \tag{10}$$

We expand the electromagnetic dispersion functions about the tangent point to first order in frequency and to second order in wavevector. Then with damping ignored (8) becomes the dispersion relation for

Three-dimensional Filamentation and Modulation Instability

$$1-\frac{k^2c_s^2}{\omega^2}=\frac{V_{Laser}^2}{8v_{Te}^2}\frac{k^2c_s^2}{\omega^2}\frac{\omega_p}{\omega_L}\left\{\frac{\omega_p(\vec{e}_{M+}\cdot\vec{e}_L)^2}{\omega-\vec{k}\cdot\vec{v}_g^L-\left(k^2c^2/2\omega_L\right)}-\frac{\omega_p(\vec{e}_{M-}\cdot\vec{e}_L)^2}{\omega-\vec{k}\cdot\vec{v}_g^L+\left(k^2c^2/2\omega_L\right)}\right\}. \tag{11}$$

Physical Mechanisms Leading to Instability

The physical mechanisms underlying the filamentation and modulation instabilities can be described in macroscopic terms. Suppose that the laser pump wave acquires a slight modulation, or equivalently that two small electromagnetic sidebands are superimposed on the steady uniform laser pump. Furthermore, suppose that the phase velocity of this modulation is less than the ion sound speed c_s. Then the radiation pressure pattern arising from the modulation of the laser intensity will lead to density striations in the plasma which constitute variations in the dielectric constant of the plasma. Since this constant decreases with density, these variations in dielectric constant focus the laser light into the less dense plasma regions. This increases the radiation pressure in those regions, thereby further expelling the plasma and increasing the depth of the density striations.

This process can be visualized most easily in the case wherein the modulation is directly across the laser beam and its phase velocity is zero. This is the "filamentation instability." The plasma acquires density striations in the form of parallel slabs lying in the direction of laser propagation. The performance of the resulting parallel-slab dielectric waveguide as a means of confining the laser radiation to the regions between the slabs can be calculated. This performance factor for the slab waveguide, together with radiation-pressure calculations of the rate at which the plasma-slab structure increases in strength, yields the growth rate for the filamentation instability, as we shall now show.

It can be seen from (11) that the growth rate of the filamentation instability depends very little on the orientation of the density striations with respect to the polarization of the laser, provided these striations have a wavelength much greater than that of the laser. For illustrative purposes, therefore, take the striation wavevector perpendicular to the laser polarization. A cross section of the irradiated plasma in the plane of the laser propagation and the striation wavevector is shown in Fig. XIII-1.

Treat the plasma density striations as a given static structure, that is, a sinusoidal

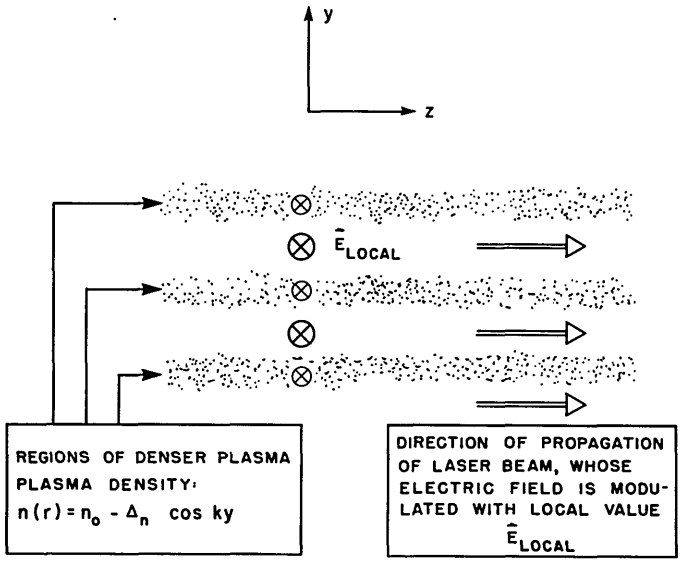

Fig. XIII-1. Cross section of plasma undergoing filamentation instability.

index-profile dielectric-slab waveguide. The performance of this waveguide may be found by standard methods. The result to first order in the index variations is

$$E_{Local} = \left\{ 1 + \frac{\omega_L^2}{k^2 c^2} \frac{\Delta\epsilon}{\epsilon_o} \cos ky \right\} E_1. \tag{12}$$

Now the refractive index is a decreasing function of plasma density

$$\frac{\epsilon}{\epsilon_o} = 1 - \frac{\omega_p^2}{\omega_L^2} = 1 - \frac{1}{\omega_L^2} \frac{n_e q^2}{m_e \epsilon_o}. \tag{13}$$

We use (12) and (13) to relate the variation in the "radiation pressure" (more strictly termed the effective pressure of coherent oscillations) to the variation in plasma density:

$$n_o \Delta \langle v_{Local}^2 \rangle = \frac{2}{k^2 c^2} \left(-\Delta n \omega_{po}^2 \right) \langle v_{Laser}^2 \rangle \tag{14}$$

$$\Delta p_{\substack{\text{coherent} \\ \text{oscillations}}} = n_o \Delta \langle v_{Local}^2 \rangle / 2. \tag{15}$$

Also

$$\Delta p_{Thermal} = v_{Te}^2 \Delta n. \tag{16}$$

Thus the "ponderomotive force" overcomes the electron thermal pressure gradient if

$$\frac{\omega_{po}^2}{k^2c^2}\,\frac{V_{Laser}^2}{2} > v_{Te}^2, \tag{17}$$

$$\frac{V_{Laser}^2}{4c^2} = \frac{|V_{Le}^2|}{2c^2} > \frac{k^2v_{Te}^2}{2\omega_{pe}^2} = \frac{k^2c_s^2}{2\omega_{pi}^2}. \tag{18}$$

For a fixed striation spatial frequency k, (18) fixes the threshold laser intensity. For a fixed laser intensity, (18) delimits the neighborhood of the origin in which the wavevector $\vec{k}$ of the instability can exist. When the inequality (18) is satisfied, the striations can grow in time with growth rate γ and all quantities associated with them have temporal variation $e^{\gamma t}$. The electrons are forced into the regions of higher plasma density and drag the ions with them. To the extent that the neutralization is not complete, there will exist a small electrostatic field with wavevector and frequency

$$(\vec{k}, \omega) = (k\vec{e}_y, i\gamma). \tag{19}$$

For the ions, the linearized quasi-static fluid equations are

$$\frac{\partial \vec{v}_i}{\partial t} = \frac{q_i}{m_i} E_{static}\vec{e}_y \tag{20}$$

$$\frac{\partial n_i}{\partial t} = -n_{oi}\nabla \cdot \vec{v}_i. \tag{21}$$

These quasi-static quantities have temporal variation $e^{\gamma t}$, and therefore

$$\frac{\Delta n_i}{n_{oi}} = \frac{kq_i}{\gamma^2 m_i} E_{static}^{peak}. \tag{22}$$

For the electrons, the linearized quasi-static fluid equations are

$$\frac{\partial \vec{v}_e}{\partial t} = -\frac{\Delta p}{n_o} - \frac{\nabla\langle v_{coherent}^2\rangle}{2} + \frac{q_e}{m_e} E_{static}\vec{e}_y \tag{23}$$

$$\frac{\partial n_e}{\partial t} = -n_{oe}\nabla \cdot \vec{v}_e. \tag{24}$$

These quasi-static quantities have temporal variation $e^{\gamma t}$, and therefore

$$\frac{\Delta n_e}{n_{oe}} = \frac{kq_e}{\left(\gamma^2 + k^2 v_{Te}^2 - \frac{V_{Laser}^2}{2c^2}\omega_{pe}^2\right) m_e} E_{static}^{peak}. \tag{25}$$

Substituting in Poisson's equation and assuming quasi neutrality, we obtain the formula for the growth rate of the filamentation instability:

$$\gamma^2 = \frac{V_{Laser}^2}{2c^2}\omega_{pi}^2 - k^2 c_s^2. \tag{26}$$

The more exact result from the generalized coupling-of-modes approach embodied in (11) is that the growth rate of the filamentation instability satisfies the biquadratic

$$\gamma^2 = \frac{V_{Laser}^2}{2c^2}\omega_{pi}^2\left[\frac{k^4c^4}{k^4c^4 + 4\gamma^2\omega_L^2}\right] - k^2c_s^2. \tag{27}$$

The quantity in brackets is the correction factor to the waveguide performance caused by the finite temporal growth rate of its refractive-index striations. For striations with wavevector $\vec{k}$ not perpendicular to the laser polarization $\vec{e}_L$, (11) and hence (27) contains an additional geometric correction factor satisfying the inequalities

$$\frac{k_L^2}{k_L^2 + k^2} \leq (e_{M+} \cdot e_L)^2 = (e_{M-} \cdot e_L)^2 \leq 1. \tag{28}$$

Thus in physical terms we may explain the dispersion relation (11) for the case of filamentation instability, that is, the case

$$\vec{k} \cdot \vec{k}_L = 0. \tag{29}$$

For the modulation instability, the striation wavevector $\vec{k}$ is still almost perpendicular to the laser wavevector $\vec{k}_L$. This allows the laser modulation pattern to move along the laser beam with the laser light group velocity, while the phase velocity of the plasma striations is still less than, or comparable to, the ion sound speed. Again, for illustrative purposes, take $\vec{k}$ perpendicular to the laser polarization $\vec{e}_L$. A cross section through the plasma that is undergoing the modulation instability is shown in Fig. XIII-2.

The basic physical mechanisms for the filamentation and modulation instabilities are the same. Spatial variations in laser light intensity set up a ponderomotive force, more precisely a gradient in the effective pressure of coherent oscillations. The ponderomotive force drives plasma into regions of less intense laser light. These denser regions have a lower refractive index than other regions, so that the laser light is further

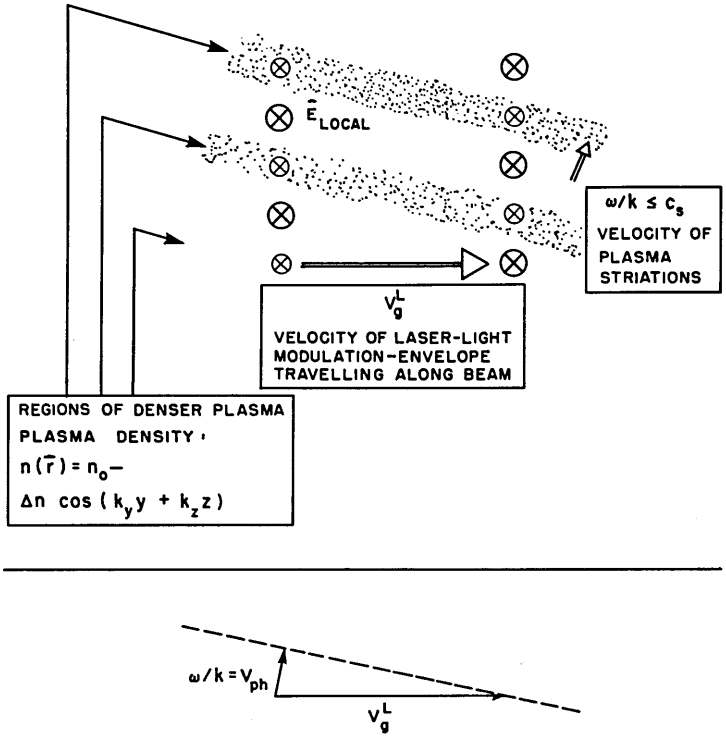

Fig. XIII-2. Cross section of plasma undergoing modulation instability.

repelled from them and the positive feedback loop is completed. We shall not try to rederive the modulation growth rate from this macroscopic picture, since this involves calculating the performance of the inclined traveling dielectric-slab waveguide sketched in Fig. XIII-2 and would not provide additional physical insight. Rather, for growth-rate calculations we refer to the general dispersion relation (11) and take the case

$$0 \neq \vec{k} \cdot \vec{k}_L \ll k k_L. \tag{30}$$

By neglecting the geometric factors $(\vec{e}_{M\pm} \cdot \vec{e}_L)^2$, the dispersion relation becomes a quartic in ω for fixed $\vec{k}$ of the following form [compare (27)]:

$$-\omega^2 = \frac{V_{Laser}^2}{2c^2}\,\omega_{pi}^2 \left[\frac{k^4c^4}{k^4c^4 - 4\left(\omega - \vec{k}\cdot\vec{v}_g^L\right)^2 \omega_L^2}\right] - k^2c_s^2, \tag{31}$$

which must be solved numerically.

References

1. D. C. Watson and A. Bers, Quarterly Progress Report No. 113, Research Laboratory of Electronics, M.I.T., April 15, 1974, pp. 59-74.

2. J. W. Shearer and J. L. Eddleman, Phys. Fluids 16, 1753 (1973).

3. J. Drake, P. K. Kaw, Y. C. Lee, G. Schmidt, C. S. Liu, and M. N. Rosenbluth, Phys. Fluids 17, 778 (1974).

2. THREE-DIMENSIONAL PULSE RESPONSE FOR WAVE-WAVE INTERACTIONS IN THE PRESENCE OF INHOMOGENEITY

National Science Foundation (Grant GK-37979X1)

Frank W. Chambers, Abraham Bers

In this report we examine the three-dimensional pulse response of wave-wave interactions in an infinitely extended but inhomogeneous plasma. We apply this to the laser-pellet plasma interactions described for a homogeneous plasma in a previous report.[1] We begin by deriving the one-dimensional mode-coupling equations from a general integral description of a mode by WKB techniques. We determine the dominant inhomogeneity effect, that is, the dephasing introduced in the coupling coefficient. We generalize the partial differential equations including dephasing effects only to three dimensions. Then we solve the three-dimensional equations first by making appropriate velocity transformations similar to those for the homogeneous case.[2] The one-dimensional solution of Rosenbluth et al.[3,4] is reviewed and generalized to solve the transformed three-dimensional equation. The technique for constructing the entire three-dimensional space-time response in the presence of inhomogeneity from the calculated responses for specific triplets of coupled waves is presented. Finally, the three-dimensional inhomogeneous responses for the previously discussed laser-plasma instabilities are calculated.

A single mode in a plasma with inhomogeneity and an external source current may be represented by

$$\iint \overline{\overline{D}}\left(\vec{r}-\vec{r}',\ t-t',\ \frac{\vec{r}+\vec{r}'}{2}\right) \vec{E}_1(\vec{r}',t')\, d^3r'dt' = \frac{-\vec{J}_{1\,NL}(\vec{r},t)}{-i\omega_1 \epsilon_o}. \tag{1}$$

The nonlocal or dispersive nature of the medium is included in the integration over the primed coordinates; the inhomogeneity is included in $\overline{\overline{D}}$ which depends on the average position $(\vec{r}+\vec{r}')/2$, as well as the separation $\vec{r}-\vec{r}'$. The nonlinear interactions are included in the external current $\vec{J}_{1\,NL}$ that is due to the presence of other modes in the plasma. For three-wave coupling of modes the current driving, say, mode 1 because of modes 2 and 3 is

$$\vec{J}^{(2)}_{1\,NL} = \overline{\overline{\sigma}}^{(2)}_{1\,NL} \vec{E}_2 \vec{E}_3, \tag{2}$$

where the necessary tensor-vector contraction on the right-hand side is understood and

the superscript 2 indicates that the conductivity and nonlinear current are second order in electric fields. The factor $(-\omega_1 \epsilon_o)$ is included in Eq. 1 so $\overline{\overline{D}}$ will have the conventional normalization.

Equation 1 is an integral equation for the $\vec{E}$ field of mode 1; we wish to reduce it to a differential equation for the space-time evolution of the mode. To simplify the problem and highlight the inhomogeneous effects, we shall replace $\overline{\overline{D}}$ with a scalar D and take $\vec{E}_1$ parallel to $\vec{J}^{(2)}_{1\,NL}$, we shall allow the variables to depend only on x, and take the inhomogeneity to be in the x direction. We begin by assuming that the electric fields can be represented by WKB modes

$$E_i(x,t) = E_{i0} u_i(x,t) \exp\left[i \int_0^x k(x)\, dx - i\omega t \right]. \tag{3}$$

A transformation is made to local coordinates, and D and E_1 are expanded in Taylor's series. The equations are then separated by order, under the assumption of a weak space-time dependence; D and $u_1(x,t)$ are zeroth order, $\partial D/\partial x$ and $\partial u_1/\partial x$, $\partial u_1/\partial t$ are first order. The integrations in Eq. 1 become Fourier-Laplace transforms and the resultant equations dividing out E_{10} are

$$\text{Zeroth Order:} \quad D(k(x), \omega, x)\, u_1(x,t) = 0. \tag{4}$$

$$\text{First Order:} \quad \frac{-i}{2} \frac{\partial^2}{\partial k^2} D(k(x), \omega, x) \frac{\partial k(x)}{\partial x} u_1(x,t) + i \frac{\partial}{\partial \omega} D(k(x), \omega, x) \frac{\partial u_1(x,t)}{\partial t}$$

$$- i \frac{\partial}{\partial k} D(k(x), \omega, x) \frac{\partial u_1(x,t)}{\partial x} - \frac{i}{2} \frac{\partial}{\partial k} \frac{\partial D(k(x), \omega, x)}{\partial x} u_1(x,t) = \frac{-J^{(2)}_{1\,NL}(x,t)}{-i\omega_1 \epsilon_o E_{10}}. \tag{5}$$

Equation 4 is the local dispersion relation and gives k(x) as a function of ω and x. Equation 5 describes the pulse evolution resulting from both WKB and nonlinear effects; these effects can be separated by allowing

$$u_1(x,t) \rightarrow \underbrace{u_1(x,t)}_{\substack{\text{nonlinear} \\ \text{effects}}} \times \underbrace{U_1(x)}_{\substack{\text{WKB} \\ \text{effects}}}. \tag{6}$$

We substitute Eq. 6 in Eq. 5. Then the resulting equation can be separated to yield the equation for $U_1(x)$

$$\frac{1}{2} \frac{\partial^2}{\partial k^2} D(k(x), \omega, x) \frac{\partial k(x)}{\partial x} U_1(x) - \frac{\partial}{\partial k} D(k(x), \omega, x) \frac{\partial U_1(x)}{\partial x} - \frac{1}{2} \frac{\partial}{\partial k} \frac{\partial D(k(x), \omega, x)}{\partial x} U_1(x) = 0. \tag{7}$$

This differential equation describes the spatial dependence of the mode amplitude $U_1(x)$ caused by WKB effects. Presumably it can be solved and the mode electric fields in the plasma can then be described by

$$\mathscr{E}_i(x) = E_{i0} U_i(x). \tag{8}$$

These spatially dependent modes form a new basis in which to describe the nonlinear interaction. Defining a local group velocity and an energy density as

$$v_{gi}(x) = \left.\frac{\frac{-\partial D(k(x), \omega, x)}{\partial k}}{\frac{\partial D(k(x), \omega, x)}{\partial \omega}}\right|_{\omega_i, k_i} \tag{9}$$

$$\langle W_{i0}(x) \rangle = \frac{\omega_i \epsilon_0}{4} \mathscr{E}_i^*(x) \frac{\partial D(k(x), \omega, x)}{\partial \omega} \mathscr{E}_i(x), \tag{10}$$

we find that the equation describing the nonlinear interaction is

$$\frac{\partial u_1(x,t)}{\partial t} + v_{g1}(x) \frac{\partial u_1(x,t)}{\partial x} = \left\{\frac{-\sigma_{1\,NL}^{(2)} \mathscr{E}_2(x) \mathscr{E}_3(x) \mathscr{E}_1^*(x)}{4\langle W_{i0}(x) \rangle}\right\} u_2(x,t)\, u_3(x,t)$$

$$\times \exp\left[-i \int_0^x \{k_1(x) - k_2(x) - k_3(x)\}\, dx + i(\omega_1 - \omega_2 - \omega_3)\, t\right]. \tag{11}$$

Equation 11 looks similar to the usual homogeneous coupling-of-modes equation that has been derived more rigorously elsewhere.[5] The group velocity now depends on position, the portion of the coupling coefficient in braces also depends on position, and there is an x-dependent phase factor. Henceforth in our further calculations we shall assume exact frequency matching

$$\omega_1 - \omega_2 - \omega_3 = 0, \tag{12}$$

and exact wave-number matching at x = 0 and linearize our mismatch about that point. Thus

$$k_1(x) - k_2(x) - k_3(x) \approx K'x \tag{13}$$

$$K' \equiv \frac{\partial}{\partial x} [k_1(x) - k_2(x) - k_3(x)]\Big|_{x=0}. \tag{14}$$

The problem that we wish to consider now is three-wave coupling where each mode amplitude is described by an equation of the form of (11). We include a weak phenomenological damping $\gamma_i(x)$ that may be position-dependent. The equations describing the interaction with these approximations are

$$\left(\frac{\partial}{\partial t} + v_{g1}(x)\frac{\partial}{\partial x} + \gamma_1(x)\right) u_1 = K_1 u_2 u_3 \, e^{-iK'x^2/2} \tag{15}$$

$$\left(\frac{\partial}{\partial t} + v_{g2}(x)\frac{\partial}{\partial x} + \gamma_2(x)\right) u_2 = K_2 u_1 u_3^* \, e^{+iK'x^2/2} \tag{16}$$

$$\left(\frac{\partial}{\partial t} + v_{g3}(x)\frac{\partial}{\partial x} + \gamma_3(x)\right) u_3 = K_3 u_1 u_2^* \, e^{+iK'x^2/2}, \tag{17}$$

where the K_i are determined by permutations of Eq. 11. We make the strong pump approximation so $u_1 \rightarrow u_{10}$, independent of space and time. Now Eqs. 16 and 17 are coupled linear equations describing the system whose pulse response we seek.

In solving (16) and (17) we do not want to include all x dependencies of the parameters but rather to determine the dominant effect and calculate only that. We must compare the mismatch in the exponent with the varying coefficients in the differential equation. If the plasma parameters vary over the scale length L, we would expect the varying coefficients $v_{gi}(x)$, $K_i(x)$, and $\gamma_i(x)$ to modify the solution significantly, but only over this scale length. The mismatch, however, enters the problem differently. We know that if the mismatch in frequency, $\delta\omega$, becomes comparable to the growth rate γ_o ($\gamma_o^2 = |K_2K_3||u_{10}|^2$, then with our present normalizations) the growth is suppressed.[5] Since our mismatch in k increases linearly with position $\delta k = K'x$, we can solve for the distance from the origin, ℓ_{crit}, at which the mismatch in k corresponds to a mismatch in ω that will suppress the coupling. The mismatches are related through the mode group velocity so that

$$\delta\omega = v_g K' \ell_{crit} = \gamma_o. \tag{18}$$

We can approximate $K' = k/L$ and consequently

$$k\ell_{crit} \sim \frac{\gamma_o}{v_g} L \ll kL. \tag{19}$$

The last inequality follows because γ_o/v_g can be considered as a spatial growth rate and, since we are considering weak coupling, $\gamma_o/v_g \ll k$ and hence $\ell_{crit} \ll L$. This tells us that as the pulse response spreads mismatch effects will become important when the pulse edge has propagated a distance ℓ_{crit} and other effects will not be important until the pulse spreads a distance L. Hence we are concerned only with dephasing effects and we shall assume that on the scale of ℓ_{crit}, v_{gi}, γ_i and K_i are constant. Of course, in several instances, the estimation $K' = k/L$ is not adequate and the inhomogeneity effects attributable to $\gamma_i(x)$, $v_{gi}(x)$, and $K_i(x)$ may become significant.

By including only the mismatch as the largest inhomogeneity effect, we can convert Eqs. 15-17 from the mode E-field amplitudes $u_i(r,t)$ to the more conventional normalized action density $a_i(r,t)$. There is a weak spatial dependence in the conversion factor

which, in keeping with our previous approximations, we shall neglect. We identify $K_2 a_{10} = K_3 a_{10} = \gamma_o$, since we are assuming conservative interactions.[5] Furthermore, we generalize the equations to three dimensions by taking dot products with the group velocities. Note that this does not change the mismatch factor because the inhomogeneity is assumed only in the x direction. Since we have assumed a large amplitude pump and can insert a point excitation in mode 2, we can rewrite Eqs. 16 and 17 as

$$\left(\frac{\partial}{\partial t} + \vec{v}_{g2} \cdot \frac{\partial}{\partial \vec{r}} + \gamma_2\right) a_2 = \gamma_o a_3^* e^{+iK'x^2/2} + a_{20}\delta^3(\vec{r})\,\delta(t) \tag{20}$$

$$\left(\frac{\partial}{\partial t} + \vec{v}_{g3} \cdot \frac{\partial}{\partial \vec{r}} + \gamma_3\right) a_3 = \gamma_o a_2^* e^{+iK'x^2/2}. \tag{21}$$

The space-time evolution of the pulse described by these equations with $K' = 0$ has been discussed in a previous report.[2] Our approach will be to reduce Eqs. 22 and 23 to a one-dimensional coupled pair of equations by rewriting them for a moving, rotated observer. We will recover the one-dimensional equations which have already been solved elsewhere.[4]

Restricting our two group velocities to lie in the x-y plane, let us consider an observer traveling at $\vec{V}_y$, where $\vec{V}_y$ is determined as in Fig. XIII-3, such that the observer sees the two modes propagating in exactly opposite directions. We choose the $\hat{y}$ direction so that this observer motion does not introduce any time dependence in the mismatch factor. We make the transformation

$$\vec{r}' = \vec{r} + \vec{V}_y t \tag{22}$$

$$t' = t. \tag{23}$$

Further, we define $\vec{V}_2, \vec{V}_3$ which are antiparallel as

$$\vec{V}_2 = \vec{v}_{g2} - \vec{V}_y \tag{24}$$

$$\vec{V}_3 = \vec{v}_{g3} - \vec{V}_y. \tag{25}$$

Finally, we make a rotation of coordinates from x, y to $r_\parallel, r_\perp$, where $r_\parallel$ is parallel to $\vec{V}_2, \vec{V}_3$. With these two changes of reference frame Eqs. 20 and 21 in two dimensions become

$$\left(\frac{\partial}{\partial t'} + \vec{V}_2 \cdot \frac{\partial}{\partial \vec{r}_\parallel} + \gamma_2\right) a_2 = \gamma_o a_3^* \exp\{iK'/2\,(r_\parallel^2 \cos^2\theta + 2r_\parallel r_\perp \cos\theta \sin\theta + r_\perp^2 \sin^2\theta)\}$$

$$+ a_{20}\delta(r_\parallel)\,\delta(r_\perp)\,\delta(t) \tag{26}$$

$$\left(\frac{\partial}{\partial t'} + \vec{V}_3 \cdot \frac{\partial}{\partial r_{\|}} + \gamma_3\right) a_3 = \gamma_o a_2^* \exp\{iK'/2\ (r_{\|}^2 \cos^2\theta + 2r_{\|}r_{\perp}\cos\theta\sin\theta + r_{\perp}^2 \sin^2\theta)\}. \tag{27}$$

These equations are fairly complex, especially since they contain terms that mix $r_{\|}$ and $r_{\perp}$. They do have one vastly simplifying feature; there are only derivatives with respect to $r_{\|}$. We propose a solution of the form $a_i = a_i(r_{\|})\ \delta(r_{\perp})$. If we put this in Eqs. 26 and 27 and integrate over $r_{\perp}$, we obtain

$$\left(\frac{\partial}{\partial t'} + \vec{V}_2 \cdot \frac{\partial}{\partial \vec{r}_{\|}} + \gamma_2\right) a_2 = \gamma_o a_3^* \exp\{iK'/2\ r_{\|}^2 \cos^2\theta\} + a_{20}\delta(r_{\|})\ \delta(t) \tag{28}$$

$$\left(\frac{\partial}{\partial t'} + \vec{V}_3 \cdot \frac{\partial}{\partial \vec{r}_{\|}} + \gamma_3\right) a_3 = \gamma_o a_2^* \exp\{iK'/2\ r_{\|}^2 \cos^2\theta\}. \tag{29}$$

These equations are essentially one-dimensional, since $\vec{V}_2, \vec{V}_3$ are parallel to $\vec{r}_{\|}$. They correspond to the equations whose pulse response has been calculated by Rosenbluth, White, and Liu[4] if $\vec{V}_2 \cdot \vec{V}_3 < 0$ and we let $K' \rightarrow K' \cos^2\theta$. Although there are numerous algebraic and typographical errors in the paper of Rosenbluth et al., the conclusions presented are correct for an infinite inhomogeneous plasma and may be summarized as follows. At first the pulse grows and spreads as if the inhomogeneity were not present. It grows at approximately the homogeneous growth rate until a gain of $e^{\pi\lambda}$ has taken place, where $\lambda = \gamma_o^2/\left(K'\cos^2\theta\, V_2 V_3\right)$. At this point the pulse gain saturates, although the pulse still spreads out spatially at the group velocities of the two modes. As $K' \rightarrow 0$ the pulse never saturates, and the absolute instability is recovered. These conclusions apply only when the damping is negligible, but this is the most interesting case. After the very lengthy task of correcting the algebraic errors of Rosenbluth et al. we have applied the approach to the $\vec{V}_2 \cdot \vec{V}_3 > 0$ case, and we have found, as have others,[3] that the same result applies; that is, unaffected growth until a gain of $e^{\pi\lambda}$ has occurred and then saturation. Note that when the pulse is in the process of saturating the pulse structure becomes very complex[4] and our qualitative description is not sufficient. We can associate the $\cos^2\theta$, which we used to modify the K', as modifying the V_2 and V_3. It may be seen from Fig. XIII-3 that this changes λ. Thus

$$\lambda = \frac{\gamma_o^2}{K'V_2V_3\cos^2\theta} = \frac{\gamma_o^2}{K'|v_{g2x}v_{g3x}|}. \tag{30}$$

This is illustrated schematically in Fig. XIII-4 which shows an unstable pulse in two dimensions. We illustrate the pulse growing, propagating, and saturating. Note that this result is different from the "two" or "three" dimensional solutions of Liu,

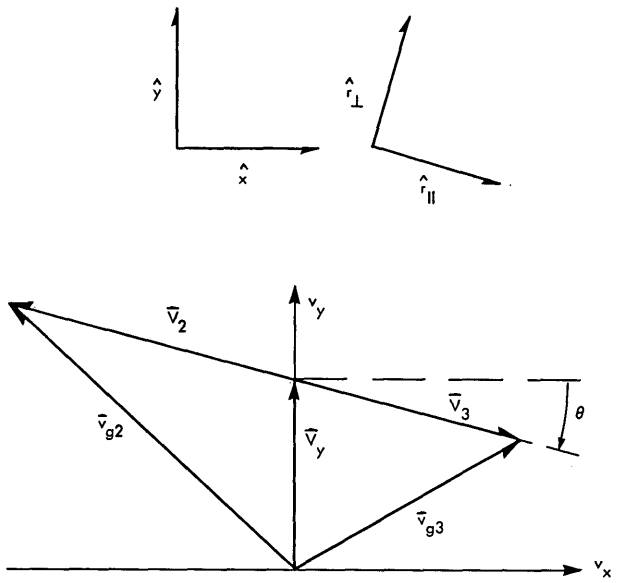

Fig. XIII-3. Coordinate systems used in transforming the inhomogeneous mode-coupling equations. The transformation to a moving observer is indicated in the $(v_x\text{-}v_y)$-plane. The angle θ is defined. The rotation in real space from $\hat{x}, \hat{y}$ to an $\hat{r}_{||}, \hat{r}_\perp$ basis is indicated in the upper diagram.

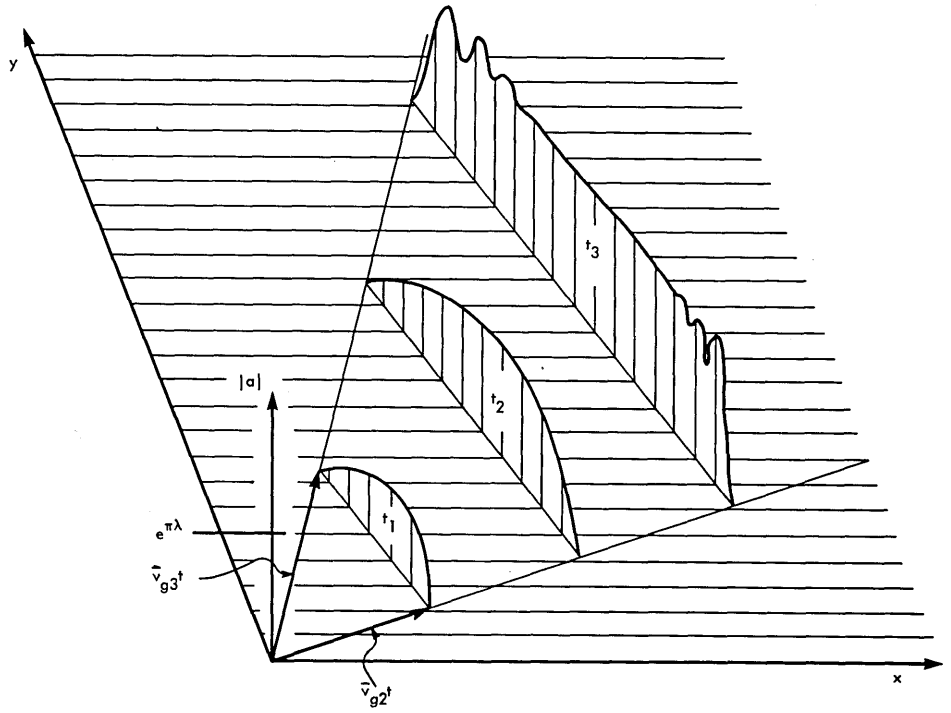

Fig. XIII-4. Space-time pulse evolution. Pulse amplitude vs position is shown at three successive times. At $t = t_3$ saturation has occurred after a gain of $e^{\pi\lambda}$.

Rosenbluth, and White,[6] where a sheet initial excitation is used and the y dependence of the pulse response is lost.

One aspect of the resulting pulse response requires a closer look. This is the surprising result that if either wave is propagating purely in the y direction, $\lambda \to \infty$ and we are led back to the homogeneous plasma result. We can see this immediately from Eqs. 20 and 21. Suppose mode 3 propagates only in the y direction, then if we make the substitution $a_3 = \bar{a}_3 \exp(+iK'x^2/2)$, we can commute the exponent through the differential operator that has only $\partial/\partial y$ and cancel $\exp(+iK'x^2/2)$ from either side of (21). When we substitute for a_3^* in (20) the inhomogeneous exponents again cancel and we are left with the usual homogeneous coupled-mode equations.

This result has a simple physical explanation. Suppose $v_{g2x} \gg v_{g3x}$. Then mode 3 will be produced all along x with its phase shifted by approximately $\exp(+iK'x^2/2)$ to produce maximum growth of the system. When, however, the mode 3 produced at various x's propagate into the same region (which will never happen if $v_{g3x} = 0$) they can interfere destructively because of their shifted phases. This interference is illustrated schematically in Fig. XIII-5, which is a diagram for a computer algorithm to integrate the inhomogeneous mode-coupling equations. The scheme is to propagate the waves one step at a time and then couple them through the coupling terms in Eqs. 20 and 21. The

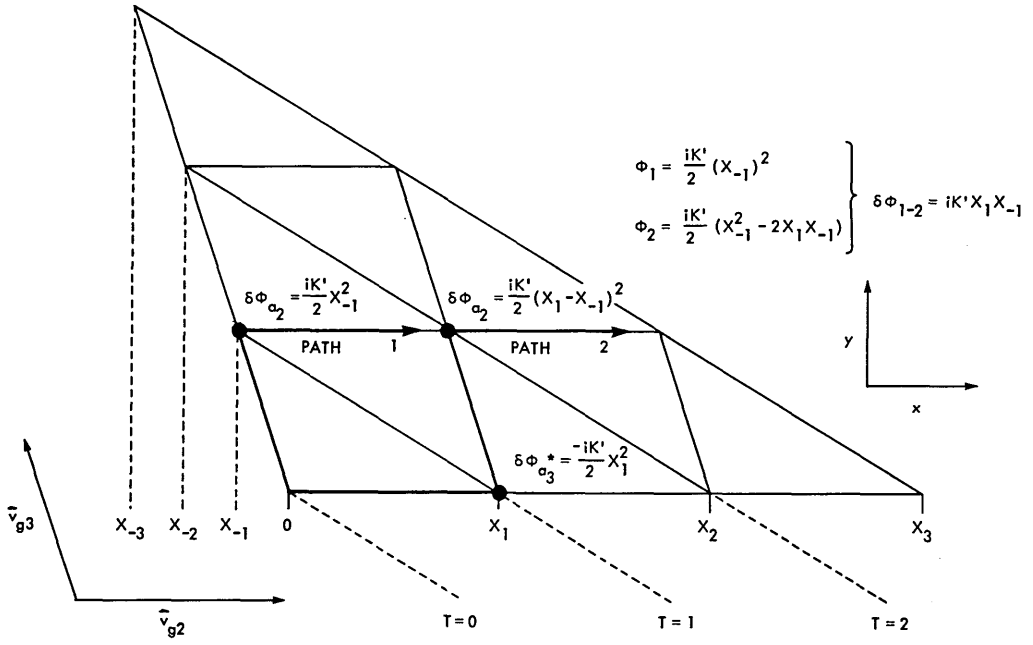

Fig. XIII-5. Accumulated phase for mode 2 at T = 2 on two different paths. Each coupling is indicated by a large dot and the phase change introduced in the produced wave (a_2 or a_3^*) is indicated by the dot.

dark lines labeled 1 and 2 are separate paths both of which produce mode 2 at T = 2. Path 1 involves only one coupling at $x = X_{-1}$. The phase shift introduced by this coupling is $\exp\left(iK'X_{-1}^2/2\right)$ and the black dot indicates the coupling. On path 2 we start with mode 2, convert to mode 3 at T = 1, and go back to mode 2 at T = 2. The total phase introduced by the couplings is indicated in Fig. XIII-5. We note that the difference in accumulated phase is $\delta\phi = K'X_1X_{-1}$, and since $X_1 \sim V_{g2x}T$ and $X_{-1} \sim v_{g3x}T$ the mismatch enters as the product of the x components of the group velocities. It is obvious from Fig. XIII-5 that if, say, $\vec{v}_{g3}$ were in the y direction phase shifts would be introduced but that these shifts would be path-independent and hence would not lead to destructive interference.

This destructive interference causes the instability to saturate in gain. Anything that can work to destroy it can reduce the effect of the inhomogeneity, for example, finite interaction length[7,8] or the addition of small random fluctuations to the mismatch.[9] While discussing the 90° scattering problem it should be noted that at 90° $k_x \to 0$ and we can no longer use the WKB approximation. This problem has been addressed by Liu, Rosenbluth, and White.[10,11]

Another interesting effect may occur at 90° propagation for one of the modes. Specifically, the K' may diverge such that the product $K'v_{g2x}v_{g3x}$ remains finite. This occurs if the dispersion relation is of the form

$$f(k) = \omega^2 - \omega_{pe}^2(x). \tag{31}$$

Both the electromagnetic wave and the electron plasma oscillation dispersion are of this form. If we assume that the density varies linearly in space over a scale length L, that is, $n = n_o(1 + x/L)$, then $\partial\omega_{pe}/\partial x = \omega_{pe}/2L$ and it follows that

$$\frac{\partial k}{\partial x} = \frac{-\omega_{pe}^2}{2\omega L v_{gx}}. \tag{32}$$

We recall the formula for K' from (14), and if we assume that all three mode dispersion relations are of the form of (31), we can write

$$K'v_{g2x}v_{g3x} = \frac{\omega_{pe}^2}{2L}\left\{\frac{-v_{g2x}v_{g3x}}{\omega_1 v_{g1x}} + \frac{v_{g3x}}{\omega_2} + \frac{v_{g2x}}{\omega_3}\right\}. \tag{33}$$

Now there is no zero in K' or divergence in λ at 90°; this will be seen later in the computed results. We must use great caution in believing the results at 90° because of the breakdown of the WKB theory.

Now we shall illustrate how to construct the response in three dimensions,

considering all possible coupled waves. This process is similar to work reported previously.[2] We are given $\vec{k}_1$ as $\vec{k}_{Laser}$ fixed along the x axis (plane polarized with $\vec{E}_{Laser}$ along the z axis). Given an angle for $\vec{k}_2$, we can calculate $\vec{k}_2$ and $\vec{k}_3$ so that ω and $\vec{k}$ matching conditions are satisfied. This determines the one-wave triplet described by Eqs. 20 and 21 for which the pulse response is known. We then step the angle of $\vec{k}_2$ and repeat the procedure. The spatial response is now made up of all responses for the different wave triplets growing and saturating in accordance with the previously presented solution. Since this is rather difficult to represent graphically, we present the saturation amplitude as a function of the angle of $\vec{k}_2$. If the group velocity of mode 2 is much larger than that of mode 3, as in Raman, Brillouin, and plasmon-phonon interactions, the angle of $\vec{k}_2$ is essentially the direction in which the spatial pulse response lies.

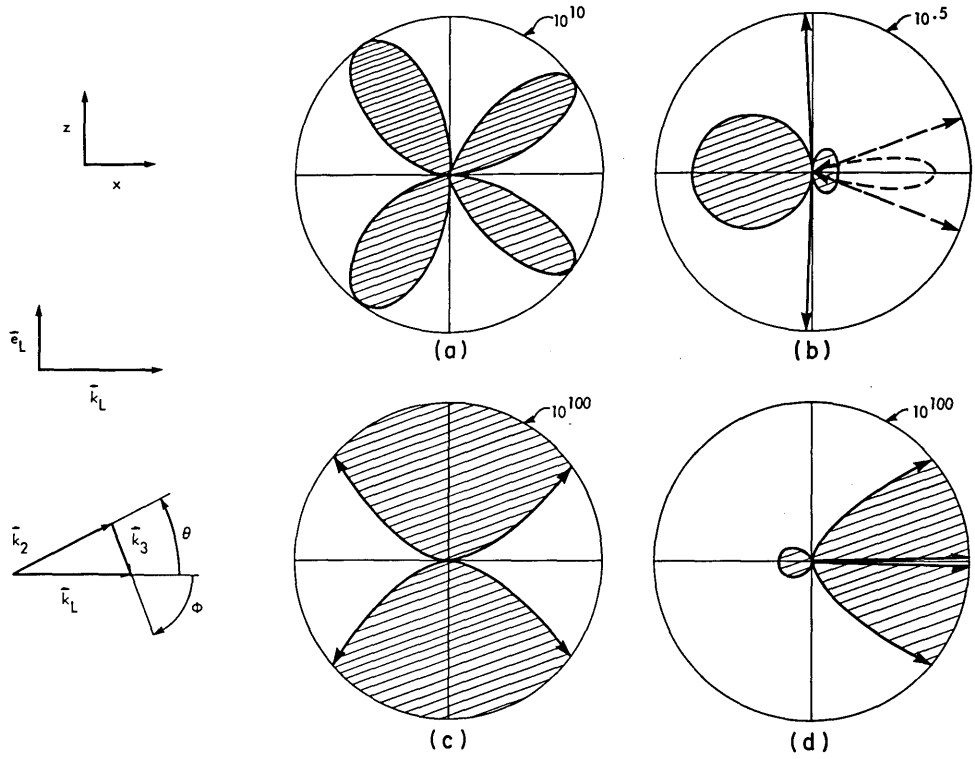

Fig. XIII-6. Inhomogeneous gain $\log_{10}(e^{\pi\lambda})$ vs θ, the $\vec{k}_2$ angle, for laser-plasma interactions. Plasma parameters are T_e = 1 keV, T_i = 50 eV, P = 10^{15} W/cm^2, L = 100 μm. Interactions are (a) two-plasmon at ω_{pe}/ω_ℓ = .475; (b) Raman at ω_{pe}/ω_ℓ = .45; (c) plasmon-phonon at ω_{pe}/ω_ℓ = .9; (d) Brillouin at ω_{pe}/ω_ℓ = .9. For the Raman case gain vs ϕ, the $\vec{k}_3$ angle is plotted as a dashed line. The gain $e^{\pi\lambda}$ in each case is indicated in the upper right of each circle. The geometry is shown in the diagrams on the left. Gains are calculated for the x-z plane with the laser propagating in the x direction, plane-polarized in the z direction.

The results of this inhomogeneous calculation for the various instabilities are presented in Fig. XIII-6 for typical plasma parameters. The response is plotted in the x-z plane with the laser propagating in the x direction and plane-polarized in the z direction. The final saturated gain vs the angle θ of the wavevector $\vec{k}_2$ is plotted in polar coordinates.

In Fig. XIII-6a we present the two-plasmon gain as $\log_{10}(e^{\pi\lambda(\theta)})$ vs angle. The maximum gain is 10^{10}. The largest gain occurs when $\vec{k}_2$ is approximately at 45° and 135°. Referring to Eq. 33, we find that the dominant mismatch (since $v_{g1x} \gg v_{g2x}, v_{g3x}$) is due to the plasmons. Since $\omega_2 \approx \omega_3 \approx \omega_{pe}$ and $v_{g2x} \propto k_{2x}$ and $v_{g3x} \propto k_{3x}$, and $k_{2x} + k_{3x} = k_{1x}$, the factor $K'v_{g2x}v_{g3x}$ actually turns out to be a constant nearly independent of angle. Hence, as can be seen from Eq. 30, λ essentially traces out the variation of the coupling coefficient $\gamma_o^2(\theta)$; hence, the four-lobed pattern is similar to the spatial response that we described in a previous report.[1] It is important to note that the maximum gain is 10^{10}. Undoubtedly some other effect such as pump depletion or particle trapping will become important before this large gain has taken place. Hence for the two-plasmon instability with these parameters the mismatch effect of the inhomogeneity is negligible.

In Fig. XIII-6b we present the results for Raman scattering. We plot the gain vs the angle ϕ of $\vec{k}_3$ as a dashed line. The null at 90° arises because the calculation is in the x-z plane and in this plane the Raman coupling coefficient vanishes at 90°. Referring to Eq. 33, we find that the dominant mismatch, since $v_{g3} \ll v_{g1}, v_{g2}$, is the mismatch of the plasmon. This mismatch effectively suppresses the scattering and the maximum gain is $10^{.5}$. At an angle just past 90°, however, the plasmon mismatch (greatly reduced because v_{g2x} is small) exactly cancels the mismatch caused by the two electromagnetic waves and $\lambda \to \infty$. This special angle has been much discussed.[6, 11] We also plot gain vs angle for $\vec{k}_3$ and we can see that the ~90° scattering of the electromagnetic wave corresponds to a nearly forward-going plasmon. To produce Raman scatter at other than the special angle would require an incident laser power flux greater than the 10^{15} W/cm^2 which we assume.

In Fig. XIII-6c and 6d we present the results for the plasmon-phonon and Brillouin interactions. In performing these calculations we have ignored mismatch effects introduced on the ion acoustic wave by temperature and expansion velocity gradients, even though these effects may be important.[6] Hence our calculation of the effect of the mismatch will turn out to indicate that it is less important than actually it may be. The expression for $K'v_{g2x}v_{g3x}$ (Eq. 33) is modified by omitting the v_{g2x}/ω_3 term. The results for the plasmon-phonon interaction show tremendous gains wherever the coupling coefficient does not vanish. In this case there is also a special angle similar to the Raman case where $\lambda \to \infty$. At such large gains, however, the only conclusion that we can draw is that the mismatch has no effect because the very slow acoustic velocity

prevents the destructive interference from occurring except after a very long time. The Brillouin results show that the mismatch has very little effect in the near forward direction (at 0° the coupling coefficient vanishes). The reason for this is the mismatches of the two electromagnetic waves nearly cancel, as shown by Eq. 33. Even in the backward direction there is a gain of 10^{21}. At lower power levels the mismatch could limit the Brillouin scatter.

In summary, we have derived equations describing the mode amplitudes for nonlinear wave-wave interactions in an inhomogeneous infinite extent plasma. Using these equations and assuming that the dephasing effects are the dominant ones, we have solved for the three-dimensional pulse response. We have calculated the saturation amplitude vs angle for several instabilities of current interest in laser-induced fusion studies.

References

1. F. W. Chambers and A. Bers, "Two- and Three-Dimensional Stability Analysis for Second-Order Laser-Plasma Interactions," Quarterly Progress Report No. 113, Research Laboratory of Electronics, M.I.T., April 15, 1974, pp. 48-58.
2. A. Bers and F. W. Chambers, "Three-Dimensional Pulse Evolution of Coupled Wave-Wave Interactions," Quarterly Progress Report No. 113, Research Laboratory of Electronics, M.I.T., April 15, 1974, pp. 112-116.
3. M. N. Rosenbluth, "Parametric Instabilities in Inhomogeneous Media," Phys. Rev. Letters 29, 565 (1972).
4. M. N. Rosenbluth, R. B. White, and C. S. Liu, "Temporal Evolution of a Three-Wave Parametric Instability," Phys. Rev. Letters 31, 1190 (1973).
5. A. Bers, Notes on Lectures: Linear Waves and Instabilities in Plasma Physics, given at Ecole d'Eté de Physique Théorique, Les Houches, France, July 1972 (Gordon and Breach Publishers, London, in press); also M.I.T. Plasma Research Report 7210, July 1972 (unpublished).
6. C. S. Liu, M. N. Rosenbluth, and R. B. White, "Raman and Brillouin Scatterings of Electromagnetic Waves in Inhomogeneous Plasmas," Institute for Advanced Studies Report C00 3237-33, Princeton, New Jersey, 1973.
7. P. Kaw, R. B. White, D. Pesme, M. N. Rosenbluth, G. Laval, R. Varma, and R. Huff, "Linear Parametric Instabilities in Inhomogeneous Plasmas," Trieste Report IC/73/142 (Revised), March 1974.
8. R. B. White, P. Kaw, D. Pesme, M. N. Rosenbluth, G. Laval, R. Huff, and R. Varma, "Absolute Parametric Instabilities in Inhomogeneous Plasmas," Trieste Report IC/73/143, September 1973.
9. D. R. Nicholson and A. N. Kaufmann, "Parametric Instabilities in Turbulent, Inhomogeneous Plasmas," Phys. Rev. Letters 33, 1207 (1974).
10. C. S. Liu, M. N. Rosenbluth, and R. B. White, "Parametric Scattering Instabilities in Inhomogeneous Plasmas," Phys. Rev. Letters 31, 697 (1973).
11. C. S. Liu, M. N. Rosenbluth, and R. B. White, "Raman and Brillouin Sidescatter from Spherical Inhomogeneous Plasmas": Summary of a paper submitted to the Fifth Conference on Plasma Physics and Controlled Nuclear Fusion Research, Tokyo, Japan, November 1974.

XIII. PLASMA DYNAMICS

C. Symbolic Computation for Plasma Dynamics Problems

RESEARCH OBJECTIVES AND SUMMARY OF RESEARCH

National Science Foundation (Grant GK-37979X1)

Abraham Bers, Frank W. Chambers, Nathaniel J. Fisch, John L. Kulp, Jr.

We have completed the implementation of symbolic computation for studying nonlinear wave-wave interactions as described by the hydrodynamic, two-fluid model of a plasma in a magnetic field. We chose the hydrodynamic plasma model rather than the Vlasov plasma model because it is simpler to use in solving nonlinear equations by perturbation techniques. All required mathematical machinery was readily available on the MACSYMA system, and we have now implemented the solution of these equations to second order on MACSYMA so that any three-wave interaction in a magnetic field can be studied in detail. The implementation includes means for extracting approximate formulations, as well as exact numerical results, of the growth rate of parametric wave interactions driven by a pump wave. A report describing our research during the past two years on these aspects of symbolic computation in plasma physics is being prepared and will be published as a Research Laboratory of Electronics Technical Report. We have been able to derive approximate analytic formulations of the excitation of ion waves (ion acoustic, electrostatic ion cyclotron, and magnetoacoustic) by pump waves near the lower hybrid frequency. These interactions are of importance, since RF energy near the lower hybrid frequency can be linearly coupled into a plasma wave and the parametric excitation of large amplitude ion waves by such a plasma wave could lead to heating the ions.[1]

Theoretical work on higher order nonlinear interactions driven by a pump has been completed.[2] This work gives a unified description of such interactions to third order in the electric field, and will allow for systematic extension of symbolic computation to such interactions. We have shown that, based on this theory, at high pump powers some of the well-known interactions that have been studied independently to second order in the electric field coalesce and thereby acquire very different growth characteristics.[3]

Theoretical work on describing the time-space evaluation of nonlinear wave interactions also continues. We have shown how the evolution of pump-driven, coupled-mode instabilities can be studied in three dimensions, including the effects of plasma inhomogeneities. These studies have led us to propose a simple explanation for the observed 45° backscattering of light at three-halves of the laser frequency in laser-target experiments.[4, 5]

In the past year we have discovered a generalization of the resonance broadening concept that is applicable to all nonlinear interactions of weak turbulence theory.[6] This generalization allows us to describe correctly all wave-particle and wave-wave turbulent interactions, and we hope it will form the basis on which symbolic computation can be used for studying such interactions.

Our plans for next year are to extend symbolic computation to studying nonlinear wave interactions to third order in a magnetized plasma for both fluid and Vlasov models. We plan to complete the three-dimensional stability analysis of coupled-mode interactions, including the effects of finite geometry and pump depletion. We hope also to extend our understanding of resonance broadening to turbulent interactions in a magnetic field, and initiate symbolic computation for such phenomena of current interest.

References

1. C. F. F. Karney, S. M. Thesis, Department of Electrical Engineering, M. I. T., January 1974.

2. D. C. Watson, Ph.D. Thesis (to be submitted to the Department of Electrical Engineering, M. I. T., February 1975).

3. D. C. Watson and A. Bers, Abstract in Proc. Fourth Annual Anomalous Absorption Conference, Lawrence Livermore Laboratory, University of California, Livermore, California, April 8-10, 1974; Paper D4.

4. F. W. Chambers and A. Bers, Abstract in Proc. Fourth Annual Anomalous Absorption Conference, Lawrence Livermore Laboratory, University of California, Livermore, California, April 8-10, 1974; Paper A4.

5. F. W. Chambers and A. Bers, Bull. Am. Phys. Soc. 19, 881 (1974).

6. N. J. Fisch and A. Bers, Bull. Am. Phys. Soc. 19, 908 (1974).

XIII. PLASMA DYNAMICS

D. Intense Relativistic Beam-Plasma Interactions

RESEARCH OBJECTIVES AND SUMMARY OF RESEARCH

National Science Foundation (Grant GK-37979X1)

George Bekefi, Abraham Bers, Thaddeus Orzechowski, Marcio L. Vianna

Suppression of electrical breakdown in a vacuum gap between two electrodes subjected to intense electric fields is a problem of quite recent interest. The need to insulate the space between conductors so that voltages of millions of volts across 0.1-10 cm gaps can be maintained without breakdown for at least short periods of time (<1 μs) arises, for example, in the design of high-voltage transmission lines, energy storage systems, ion diodes, and microwave generators. By having a sufficiently strong magnetic field parallel to the emitting surface, it is hoped that most of the electrons can be turned back to the source and thus prevented from crossing the gap. The magnetic field may be provided by an external source or it may be self-generated by the current flow in the diode or transmission line, but it may also be a hybrid combination of both. This is the underlying idea of "magnetic insulation." The concept is by no means novel; it was exploited years ago in connection with the smooth-bore magnetron. What is new is the parameter range of currents and voltages which is far beyond anything that was attempted in the early days. The high voltages introduce relativistic effects, but more important, the tremendous current densities make it mandatory to account properly for self-electric and self-magnetic fields within the gap. Dense, hot plasmas are formed at the cathode (and anode) during the initial stages of electron beam formation and their presence has important consequences on the characteristics of the vacuum gap.

During the past year we began to study magnetic insulation, using as our energy source the Cogen III high-voltage facility. Through the generosity of the Sandia Laboratories we now have use of a second facility, Nereus, on which most of our future research will be based.

During the coming year we plan studies in the following areas.

a. The motion of cathode and anode plasma produced during the high-voltage pulse. This will be studied both in the absence of a magnetic field and in the presence of a large field oriented transversely to the plasma motion.

b. A magnetically insulated diode is a copious source of microwave radiation. We intend to study this radiation with a view to understanding the instability that caused it. Such a system could then be optimized for possible use as an efficient high-power microwave generator.

c. The blow-off-anode plasma may be used as a source of ions and the electron diode may be converted to an ion diode by suitable choice of geometry and by suitable preparation of the anode. Such a system has potential for use as an intense source of high-energy ions.

XIII. PLASMA DYNAMICS

E. Fusion Technology Studies

RESEARCH OBJECTIVES AND SUMMARY OF RESEARCH

U. S. Atomic Energy Commission (Contract AT(11-1)-3070)

Lawrence M. Lidsky, Peter A. Politzer, David J. Rose

We are expanding our work on the technological problems associated with the design and construction of a controlled thermonuclear reactor. Our goals are to evaluate the engineering requirements for a fusion reactor, to assess the possible applications of this power source, and to produce the engineering data required for the design of the reactor. We have in progress at present a study of the possibilities inherent in fission-fusion symbiosis. This concept envisions the use of fusion-generated neutrons for the production of fissionable fuels, as well as in the transmutation of radioactive waste products. Also in progress is an experimental study simulating the cyclic stresses that are expected in the first wall of a theta-pinch reactor. This program will determine the fatigue stress limits and fracture mechanisms for niobium and other first-wall candidate materials. We are participating in the development of an intense 14-MeV neutron source which is needed for testing possible reactor materials and a high-flux 14-MeV environment. We have built and are beginning preliminary measurements on a device that will allow us to observe the dynamics of fuel pellet interactions with high-energy density plasmas.

1. Fission-Fusion Symbiosis

U. S. Atomic Energy Commission (Contract AT(11-1)-3070)

Lawrence M. Lidsky

It appears likely that fusion reactors will be copious sources of excess neutrons. These may be used to produce power directly (usually through heavy-element fission), to generate fissile fuel for use in conventional fission reactors, or for nuclear transmutation. We have been assessing the relative merits of these various schemes with respect to various engineering and economic constraints. We shall concentrate our efforts on the optimization of fuel-breeding in conjunction with the Th-U^{233} cycle. A related goal is the development of a detailed engineering model of a helium-cooled symbiotic blanket based on HTGR technology.

2. High-Intensity Neutron Source

U. S. Atomic Energy Commission (Contract AT(11-1)-3070)

Lawrence M. Lidsky

Several years ago, we developed a conceptual design for an intense source of 14-MeV neutrons for use in fusion reactor materials testing. It appears likely that such a gas target source will be built. We are performing experimental measurements of the detailed behavior of the beam-heated jet in a quarter-scale intermittently pulsed model of the proposed device. Our goal is to compare theoretical predictions and extensive numerical computations (from several laboratories) with experimental results. The interaction is so complex and the engineering design so sensitive to behavior in the transonic interaction zone that experimental work is essential to guide the design of the full-scale source.

3. Pellet Fueling of Fusion Reactors

U. S. Atomic Energy Commission (Contract AT(11-1)-3070)

Peter A. Politzer, David J. Rose, Jay L. Fisher

We are engaged in a continuous analytic and experimental study of the possibility of refueling a steady-state fusion reactor by injection of small solid pellets, and of the physical processes that are involved. We are examining the transport of particles and energy across the low-temperature, high-density balloon region which separates the solid pellet from the thermonuclear plasma in order to derive criteria for the existence of this shielding balloon and to determine the optimum size and velocity for the pellet. In this study we want to optimize the distribution of ablated material in the reactor plasma. We are also constructing an experiment that will allow us to observe the first stages of the formation of the balloon in a hot dense plasma.

XIII. PLASMA DYNAMICS

F. Experimental Studies – Waves, Turbulence, and Radiation

RESEARCH OBJECTIVES AND SUMMARY OF RESEARCH

1. Plasma Diagnostics

U. S. Atomic Energy Commission (Contract AT(11-1)-3070)

George Bekefi, Robert J. Taylor

Our present objectives are focused on the diagnostics of a small toroidal device called Versator. During the coming year we are planning to carry out three experiments.

a. Electromagnetic Mode Studies on Versator

Experiments with Versator have shown that MHD fluctuations (10-20 kHz) are present and can easily be observed with magnetic probes placed on the outside of the windings. By placing pick-up coils at various $[\phi, \theta]$ coordinates, it has been determined that the most prominent mode is an $n = 1/2$ and $m = 3$ mode. Correlation exists between the magnetic signals and the electrostatic fluctuations as measured by a Langmuir-type electrostatic probe inside a plasma column. The correlation shows a peak at $r \approx a/2$. This measurement will be used to identify the location of rational surfaces.

We propose to expand the investigation by inserting small magnetic probes into the plasma to make correlation measurements of the externally seen fluctuations. We shall study local magnetic and electric perturbations, and measure the level of typical electric fields by a double-probe technique.

b. Wall Effects on Tokamak Equilibrium

We shall investigate how wall stabilization depends on various Tokamak parameters, such as size of the plasma, wall proximity, error fields, toroidal field, density, electron temperature, and ion mass.

c. Spectroscopic Studies

Ultraviolet and visible light emission studies in Versator show that during a negative voltage spike the O(V) and O(VI) line emissions decrease markedly and the O(IV) and O(II) line emissions increase. The temperature decrease takes place in less than 20 μs, and we believe that this cooling is not due to heat loss to the walls or to the influx of neutrals.

Using visible and ultraviolet spectroscopy, we shall investigate how the spatial evolution of the reduction of the temperature takes place in Versator and what impurities and impurity levels are responsible for the onset and the limiting of negative voltage spikes seen in Tokamaks.

2. Coherent Scattering Experiment: Scattering of 10.6 μm Radiation

U. S. Atomic Energy Commission (Contract AT(11-1)-3070)

Lawrence M. Lidsky

An experiment is in progress to resolve and measure the "ion" portion of the spectrum of radiation scattered from a plasma. In a quiescent plasma this measurement permits determination of the temperature of the ions, and in a turbulent system it yields the spectral characteristics of the low-frequency waves. An extremely stable 10.6 μm CO_2 laser oscillator and amplifier system has been constructed for this experiment. An optical system based on a liquid nitrogen-cooled electrically scanned Fabry-Perot interferometer and a liquid helium-cooled bandpass filter has been built and tested.

3. Linear Quadrupole Experiment: Plasma Equilibrium and Stability in Inhomogeneous Magnetic Fields

U. S. Atomic Energy Commission (Contract AT(11-1)-3070)

Peter A. Politzer, David O. Overskei, Michael D. Stiefel

We plan to use the SLIM steady-state linear quadrupole device to pursue three areas of investigation. The results of preliminary studies of plasma stability behavior in the vicinity of the neutral line under the influence of applied dc electric fields have been promising. The observations of changes in the equilibrium configuration agree well with theoretical models. We shall continue the equilibrium study and undertake a quantitative identification of the instabilities that occur in the neighborhood of the neutral line. Furthermore, we shall attempt to relate the instability spectrum to the observed increases in plasma temperature. In addition to this study, we are engaged in an experiment to demonstrate the existence of a trapped electron echo phenomenon in this device and to show that this effect can provide a useful diagnostic for determination of the distribution function of trapped electrons and of the scattering processes that affect them. Finally, we plan an investigation of trapped electron-driven instabilities, both because of the interest in experimental verification of trapped-particle instability theory for large devices and the effect that trapped-particle phenomena may have on the plasma behavior near the neutral line.

4. Strong Nonlinear Wave-Particle Effects

National Science Foundation (Grant GK-37979X1)

Peter A. Politzer, Ady Hershcovitch

We are investigating, both theoretically and experimentally, the nonlinear effects resulting from the presence of large amplitude electric field fluctuations in a counter-streaming electron beam system. The field fluctuations arise either from the growth to saturation of a spontaneous cyclotron instability or from externally applied fields, or from the superposition of these two. We have determined that as the spontaneous instability evolves in time, it shows a frequency shift that can be explained in terms of scattering and heating of the electrons by the wave. In this system we are able to determine the electron distribution function as a function of time. This permits direct observation of the velocity-space diffusion of the particles. We plan to use this technique to

determine the velocity-space diffusion coefficient for a superposition of the saturated instability field and several different spectra of applied turbulent fields. These results will then be compared with the predictions of strong turbulence theory to serve as an experimental test of various aspects of the theory.

5. Parametric Instabilities in Beam-Plasma Interaction

National Science Foundation (Grant GK-37979X1)

Ronald R. Parker, Alan E. Throop

Our study of parametrically induced instabilities generated by the linearly unstable interaction of beam-plasma systems continues. Details of our progress are reported in the article on the following page.

6. Nonlinear Saturation Experiment

National Science Foundation (Grant GK-37979X1)

Lawrence M. Lidsky

We are attempting to determine experimentally the effect of broadband ion cyclotron frequency turbulence on the propagation of various driven ion acoustic waves. The experimental conditions allow for the domination of various nonlinear coupling effects over collisional mapping. We plan to apply the results of these measurements to the prediction of the nonlinear limit of related plasma instabilities.

7. Trapped-Particle Experiment

National Science Foundation (Grant GK-37979X1)

Lawrence M. Lidsky

The theory of the cylindrical-geometry analog of the toroidal trapped-particle modes has been developed and the results have been used to predict the behavior of a particular set of trapped-particle modes. These modes have been experimentally detected for the first time and their linear properties have been measured. We are now measuring their nonlinear properties and comparing the results with the predictions of various nonlinear saturation models. Our goal is the prediction of the effect of various trapped-particle instabilities on particle and thermal transport in toroidal systems.

1. PARAMETRIC DECAY INSTABILITY AS A POSSIBLE SATURATION MECHANISM IN A WEAK BEAM-PLASMA SYSTEM

National Science Foundation (Grant GK-37979X1)

Ronald R. Parker, Alan L. Throop

Introduction

While the linear phase of weak beam-plasma (BP) interactions seems to be well understood,[1] a great deal of effort is being expended to try to understand the nonlinear evolution of the interaction.[2] In particular, the observed saturation of the linearly unstable BP waves has been explained in terms of beam trapping,[3] strong turbulence,[4] or other nonlinear processes.[5] Pump depletion caused by the parametric decay instability has generally been rejected as a saturation mechanism because the interaction involves a linearly unstable BP wave as a pump, and the resulting nonlinear interaction is often thought to be explosively unstable, since the uncoupled system involves a negative-energy wave.[4]

Recent experiments[6] have suggested, however, that a resonant transfer of energy from the unstable BP wave to other plasma modes could be responsible for the observed saturation. We shall present a coupled-mode theory for the parametric decay instability in a weak BP system which suggests that under certain experimental conditions the interaction can be nonlinearly stabilized by the decay process.

After a brief discussion and summary of the general approach used in this report, we derive a generalized conservation theorem for the magnetized beam-plasma system and specialize it to the confined-flow case. We then derive a coupled-mode equation from this theorem and evaluate the coupling coefficient for the interaction that we are considering. Some of the properties of this system and the nonlinear evolution predicted by the set of coupled-mode equations are also discussed.

Outline of the Theory and Summary of Results

The interaction that we are considering is shown in Fig. XIII-7. We have evaluated the following dispersion relation for a linearly coupled weak electron beam and a magnetized background plasma column:[7]

$$D(\omega, k) = k^2 - \sum_s \frac{\omega_{ps}^2}{\omega_{Ds}^2} \frac{\left(k_z^2 + \frac{k_x^2}{f_s}\right)}{1 - \frac{v_{ts}^2}{\omega_{Ds}^2}\left(k_z^2 + \frac{k_x^2}{f_s}\right)}, \tag{1}$$

where ω_{ps} is the plasma frequency, $\omega_{Ds} = \omega - kv_{os}$ is the Doppler-shifted frequency because of a zero-order drift v_{os}, v_{ts} is the specie thermal velocity, $k_\perp$ is the geometrically determined radial wave number, and $f = 1 - \frac{\omega_{cs}^2}{\omega_{Ds}^2}$, with ω_{cs} the cyclotron frequency. The sum is over the plasma species. The electron plasma wave (Trivelpiece-Gould "T" mode) remains essentially unperturbed by the presence of the beam except in the resonant region just below ω_{pe} where the beam and plasma waves are in synchronism. The fast and slow space-charge beam waves interact strongly, however, in the presence of the reactive background plasma and couple below ω_{pe} to form conjugate modes with the same real frequency and wavelengths, but with equal and opposite growth rates. We denote the decaying BP mode as B and the growing BP mode as B'. Above ω_{pe} the two beam waves again become distinct modes. The plasma column also supports a low-frequency, lightly damped ion-acoustic (A) branch as shown in Fig. XIII-7. The linearly unstable BP wave grows convectively until it reaches a sufficient amplitude to decay resonantly into a backward-traveling T (Trivelpiece-Gould) mode and a forward-traveling A mode with frequencies and wavelengths consistent with the predicted values.

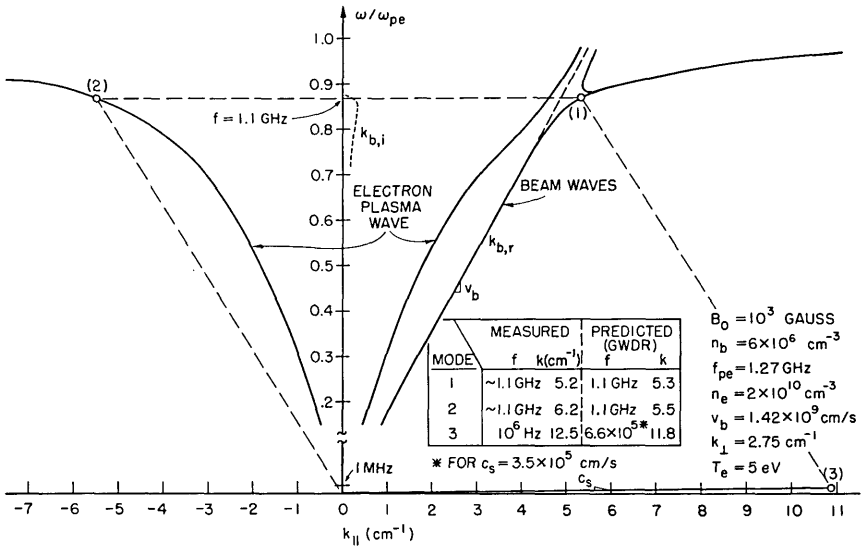

Fig. XIII-7. Guided-wave dispersion relation for the coupled beam and plasma waves. (Acoustic branch not to scale.) The parameters used in the calculation, as well as the predicted and experimentally measured mode frequencies and wave numbers, are listed.

Before discussing the theory in detail, it may be worthwhile to motivate the formalism by summarizing some of the most relevant results. We assume that the energy that is transferred between modes as a result of the nonlinear interaction gives rise to

slowly varying wave amplitudes $a(\bar{r}, t)$, whose behavior is described by coupled-mode equations of the form

$$\frac{d}{dt} a_M = K a_N a_P, \tag{2}$$

where the capitalized subscripts M, N, P denote the three coupled modes, and K is the coupling coefficient. Equations similar to (2) are written for each mode, and the resulting set of nonlinear equations is solved to obtain the nonlinear evolution of the system. The coupled-mode equation is obtained, as usual, from a conservation equation of the form

$$\frac{\partial}{\partial t} W_M + \nabla \cdot \bar{S}_M + P_{dM} = P_{ext, M} \tag{3}$$

which is derived by using the generalized approach of Bers and Penfield.[8] Here, W_M and S_M are the small-signal energy and power flow, P_{dM} represents the power dissipation, and $P_{ext, M}$ represents a source term for a mode M. For the BP system, the source term arises from the nonlinear coupling and gives rise to the spatial and temporal changes in mode energy. Initially, we shall neglect the resistive dissipative effects represented by p_d. Since, however, the linear BP interaction is a reactive type of instability[9] and involves <u>two</u> waves at the <u>same</u> real frequency and wavelength, we are forced to account explicitly for the finite growth and decay rates of the BP waves. Therefore we view the parametric interaction as a four-wave coupling involving the modes A, T, B, and B'. The formalism leads to a coupling coefficient that is complex, instead of to the usual form which is either pure real or pure imaginary.[10] It is found that K contains resonant terms as a result of the presence of the BP modes, but that the overall contribution of these terms to the interaction is small. The formalism concludes that the small-signal energy of either BP mode taken independently, W_B or $W_{B'}$, is identically zero. Instead, to derive the coupled-mode equations, we utilize a quantity defined from the adjoint system denoted $\tilde{W}_B$, which is a complex quantity composed of parts of both growing and decaying BP modes. We find that $\tilde{W}_B$ can still be written as $\epsilon_o E_B^2 \omega \frac{\partial \mathcal{D}}{\partial \omega}$ if this quantity is now evaluated at the complex frequency $\tilde{\omega}_B = \omega_{Br} + j\gamma$. Furthermore, the nonlinear stability of the system depends on the parity of the real part of $\tilde{W}_B$, and results in the physically satisfying condition that the system is nonlinearly stable for $\mathrm{Re}\,(\tilde{W}_B) > 0$ and explosively unstable for $\mathrm{Re}\,(\tilde{W}_B) < 0$.

Generalized Energy Conservation Equation

To derive an energy theorem like Eq. 3, we shall use a fluid model for the system, since all waves are lightly damped and kinetic effects may be neglected. We simply combine the force and continuity equation for each of the three plasma species, together with Poisson's equation, to get a form of the conservation equation that is commensurate

with the form of a coupled-mode equation. For each of the plasma variables (density n and velocity v), the first-order quantities associated with the plasma electrons are denoted by subscript e, those associated with the plasma ions by subscript i, and those associated with the beam electrons by subscript β. Zero-order quantities are denoted by subscript zero for plasma variables and by b for beam variables. For example, we assume a form $n = n_o + n_e$ for the plasma electron density and $\bar{v} = \bar{v}_b + \bar{v}_\beta$ for the beam electron velocity. The seven equations in the resulting set are written twice — once as an uncoupled set of linearized equations, and again as a coupled set of nonlinear equations whose solutions have a slow time variation as a result of the nonlinear driving terms. We write the two sets of equations as follows:

$$\frac{\partial n_e}{\partial t} + \bar{\nabla} \cdot (n_o \bar{v}_e) = N_{e1}, {}^{0}_{2} \tag{4}$$

$$m_e n_o \frac{\partial \bar{v}_e}{\partial t} + q_e n_o \bar{\nabla}\phi - q_e n_o \bar{v}_e \times \bar{B}_o + m_e v_{te}^2 \bar{\nabla} n_e = \bar{F}_{e1}, {}^{0}_{2} \tag{5}$$

$$\frac{\partial n_i}{\partial t} + \bar{\nabla} \cdot (n_o \bar{v}_i) = N_{i1}, {}^{0}_{2} \tag{6}$$

$$m_i n_o \frac{\partial \bar{v}_i}{\partial t} + q_i n_o \bar{\nabla}\phi + q_i \bar{v}_i \times \bar{B}_o + m_i v_{ti}^2 \bar{\nabla} n_i = \bar{F}_{i1}, {}^{0}_{2} \tag{7}$$

$$\frac{\partial n_\beta}{\partial t} + \bar{\nabla} \cdot (n_\beta \bar{v}_b + n_b \bar{v}_\beta) = N_{b1}, {}^{0}_{2} \tag{8}$$

$$m_e n_b \frac{\partial \bar{v}_\beta}{\partial t} + m_e n_b (\bar{v}_b \cdot \bar{\nabla})\, \bar{v}_\beta + q_e n_b \bar{\nabla}\phi - q_e n_b \bar{v}_\beta \times \bar{B}_o + m_e v_{tb}^2 \bar{\nabla} n_\beta = \bar{F}_{b1}, {}^{0}_{2} \tag{9}$$

$$\epsilon_o \bar{\nabla} \cdot \bar{\nabla}\phi = -q_e (n_e + n_\beta) - q_i n_i, \tag{10}$$

where

$$\begin{aligned} N_{a1} &= -\bar{\nabla} \cdot (n_{a1} \bar{v}_{a1}) \\ F_{a1} &= -\frac{\eta}{2} \frac{m_a}{n_{ao}} v_{ta}^2 \bar{\nabla}\left(n_{a1}^2\right) - m_a n_{ao} (\bar{v}_{a1} \cdot \bar{\nabla})\, \bar{v}_{a1} \end{aligned} \tag{11}$$

with $v_{ta}^2 = \frac{\gamma k_B T_a}{m_a}$, $\eta = \gamma - 2$, $\gamma \approx 1$, and $a = e, i, \beta$ for each species. Here v_{ta} is the thermal velocity, and γ is the ratio of specific heats. For completeness we have left v_{tb} and v_{ti} nonzero, but later for simplicity we shall set them equal to zero. We have written the nonlinear terms as source terms on the right-hand side of the equations, and have denoted the nonlinear and linear sets of equations by subscripts 1 and 2. The right-hand side is zero for the linear equations.

We use a normal-mode form for the solutions, which may be written as follows. For the linear (subscript 2) solutions the modes exist independently and so have the form

$$\begin{Bmatrix} n_{e2}(\bar{r}, t) \\ \bar{v}_{e2}(\bar{r}, t) \\ n_{i2}(r, t) \\ \bar{v}_{i2}(r, t) \\ n_{\beta 2}(r, t) \\ \bar{v}_{\beta 2}(r, t) \\ \phi_2(r, t) \end{Bmatrix} = \begin{Bmatrix} \tilde{N}_{eM}(\omega_M, k_M) \\ \tilde{V}_{eM}(\omega_M, k_M) \\ \tilde{N}_{iM}(\omega_M, k_M) \\ \tilde{V}_{iM}(\omega_M, k_M) \\ \tilde{N}_{\beta M}(\omega_M, k_M) \\ \tilde{V}_{\beta M}(\omega_M, k_M) \\ \tilde{\Phi}_M(\omega_M, k_M) \end{Bmatrix} e^{j\Lambda_M} e^{\pm\gamma_M t} \tag{12}$$

where $\Lambda_M \equiv \omega_M t + \bar{k}_M \cdot \bar{r}$, and $\gamma_M > 0$ is the linear growth or decay rate for the mode M. Note that $\gamma_M \neq 0$ for modes B and B' even in the absence of dissipation. For the nonlinear (subscript 1) equations, the solutions are coupled by the nonlinear interactions, which give rise to a slowly varying amplitude $a_M(\bar{r}, t)$ that is identical for each variable. Thus the set of driven solutions may be written

$$\begin{Bmatrix} n_{e1}(\bar{r}, t) \\ \bar{v}_{e1}(\bar{r}, t) \\ n_{i1}(\bar{r}, t) \\ \bar{v}_{i1}(\bar{r}, t) \\ n_{\beta 1}(\bar{r}, t) \\ \bar{v}_{\beta 1}(\bar{r}, t) \\ \phi_1(\bar{r}, t) \end{Bmatrix} = \sum_M \begin{Bmatrix} \tilde{N}_{eM}(\omega_M, k_M) \\ \tilde{V}_{eM}(\omega_M, k_M) \\ \tilde{N}_{iM}(\omega_M, k_M) \\ \tilde{V}_{iM}(\omega_M, k_M) \\ \tilde{N}_{\beta M}(\omega_M, k_M) \\ \tilde{V}_{\beta M}(\omega_M, k_M) \\ \tilde{\Phi}_M(\omega_M, k_M) \end{Bmatrix} a_M(\bar{r}, t)\, e^{j\Lambda_M} e^{\pm\gamma_M t} + \text{complex conjugate} \tag{13}$$

where the sum is over the interacting modes. We assume that the interaction is resonant. That is,

$$\begin{aligned} \omega_{B, B'} &= \omega_A + \omega_T \\ \bar{k}_{B, B'} &= \bar{k}_A + \bar{k}_T \end{aligned} \tag{14}$$

and only these resonant combinations of the modes in Eq. 13 are of consequence.

To derive a conservation equation from the thirteen equations (4)-(10), we follow the generalized approach of Bers and Penfield.[8] The equations are multiplied by the appropriate quantities, and either added or combined until all terms reduce to a time-derivative or divergence of some quantity, as in Eq. 3. The nonlinear terms contribute to P_{ext}.

By setting the nonlinear terms to zero, the appropriate quantities can be identified as the small-signal energy and power flow. We outline the derivation here, again using subscripts 1 and 2 to denote the linear and nonlinear equations and solutions. We take

$$[\bar{v}_{e1}\cdot\overline{(5)}_2+\bar{v}_{i1}\cdot\overline{(7)}_2+\bar{v}_{\beta 1}\cdot\overline{(9)}_2]+[\bar{v}_{e2}\cdot\overline{(5)}_1+\bar{v}_{i2}\cdot\overline{(7)}_1+\bar{v}_{\beta 2}\cdot\overline{(9)}_1]$$

to get

$$\begin{aligned}
&\frac{d}{dt}\left(\sum_a m_a n_{ao}\bar{v}_{a1}\cdot\bar{v}_{a2}+\sum_a m_a\frac{v_{ta}^2}{n_{ao}}n_{a1}n_{a2}\right)\\
&\quad+\nabla\cdot\left(\sum_a m_a v_{ta}^2(n_{a2}\bar{v}_{a1}+n_{a1}\bar{v}_{a2})\right)\\
&\quad+\nabla\cdot(m_e n_b\bar{v}_b(\bar{v}_{\beta 1}\cdot\bar{v}_{\beta 2}))\\
&\quad\underbrace{+\sum_a q_a n_{ao}(\bar{v}_{a2}\cdot\bar{\nabla}\phi_1+\bar{v}_{a1}\cdot\bar{\nabla}\phi_2)}\\
&=\sum_a\bar{v}_{a2}\cdot\bar{F}_{a1}+\sum_a\frac{m_a v_{ta}^2}{n_{ao}}n_{2a}N_{a1},
\end{aligned}\tag{15}$$

where the sum is over the three plasma species.

From Eqs. 4, 6, and 8 we have

$$\begin{aligned}
&\nabla\cdot\bar{J}_{t1}=\sum_a q_a N_{a1}\\
&\nabla\cdot\bar{J}_{t2}=0,
\end{aligned}\tag{16}$$

where the total current $\bar{J}_{t1}=\bar{J}_{p1}-\epsilon_o\frac{\partial}{\partial t}\bar{\nabla}\phi$, and the particle current $\bar{J}_{p1}=\sum_s q_a n_{ao}\bar{v}_{a1}+q_e\bar{v}_b n_{\beta 1}$. Thus, using $\bar{v}_b\cdot(\bar{v}_b\cdot\nabla)\,\bar{v}_\beta=\nabla\cdot[\bar{v}_b(\bar{v}_b\cdot\bar{v}_\beta)]$ and the beam force equation, we can rewrite the fourth term indicated by an underbrace in Eq. 15 as

$$\begin{aligned}
&\nabla\cdot\left[\bar{J}_{t1}\phi_2+\bar{J}_{t2}\phi_1+\frac{T_2\bar{J}_{b1}}{q_e}+\frac{T_1\bar{J}_{b2}}{q_e}+\frac{m_e v_{tb}^2}{n_b}\bar{v}_b n_{\beta 1}n_{\beta 2}\right]\\
&+\frac{\partial}{\partial t}\left[\epsilon_o\bar{\nabla}\phi_1\cdot\bar{\nabla}\phi_2+n_{\beta 1}T_2+n_{\beta 2}T_1\right]-\phi_2\sum_a q_a N_{a1}\\
&-T_2N_{b1}-\frac{n_{\beta 2}}{n_b}\bar{v}_b\cdot\bar{F}_{b1}-\bar{v}_b\cdot q_e(n_{\beta 1}\bar{v}_{\beta 2}+n_{\beta 2}\bar{v}_{\beta 1})\times B_o\\
&-m_e n_b(\bar{v}_{\beta 1}\cdot\bar{\nabla}T_2+\bar{v}_{\beta 2}\cdot\bar{\nabla}T_1),
\end{aligned}\tag{17}$$

where $T_1 \equiv m_e \bar{v}_{\beta 1} \cdot \bar{v}_b$, and $\bar{J}_{b1} = q_e(n_{\beta 1}\bar{v}_b + n_b \bar{v}_{\beta 1})$. By noting that $\bar{v}_b$ is parallel to $\bar{B}_o$ and by making the indicated substitution, Eq. 15 becomes

$$\frac{d}{dt}\left[\sum_a m_a n_{ao} \bar{v}_{a1} \cdot \bar{v}_{a2} + \sum_a \frac{m_a v_{ta}^2}{n_{ao}} n_{a1} n_{a2} + \epsilon_o \bar{\nabla}\phi_1 \cdot \bar{\nabla}\phi_2 + n_{\beta 1} T_2 + n_{\beta 2} T_1\right]$$

$$+ \nabla \cdot \left[\sum m_a v_{ta}^2 (n_{a2}\bar{v}_{a1} + n_{a1}\bar{v}_{a2}) + \bar{J}_{t1}\phi_2 + \bar{J}_{t2}\phi_1 + \frac{T_2 \bar{J}_{b1}}{q_e} + \frac{T_1 \bar{J}_{b2}}{q_e} + \frac{m_e v_{tb}^2}{n_b} n_{\beta 1} n_{\beta 2} \bar{v}_b\right]$$

$$+ m_e n_b \bar{v}_b \cdot [\bar{v}_{\beta 1} \times \nabla \times \bar{v}_{\beta 2} + \bar{v}_{\beta 2} \times \nabla \times \bar{v}_{\beta 1}]$$

$$= \sum_a \bar{v}_{2a} \cdot \bar{F}_{a1} + \sum_a m_a v_{ta}^2 \frac{n_{a2}}{n_{ao}} N_{a1} + \phi_2 \sum_a q_a N_{a1} + \bar{v}_b \cdot \frac{n_{\beta 2} \bar{F}_{b1}}{n_b} + T_2 N_{b1}. \qquad (18)$$

This has the desired form of a conservation theorem except for the third term on the left-hand side. This term can be neglected if we take the limit of an infinitely strong magnetic field B_o, so that a purely longitudinal motion of the particles results. Such an assumption also simplifies the dispersion relation to an analytically tractable form and allows us to rewrite $\bar{F}_{a1}$ in a more symmetric form:

$$\bar{F}_{a1} = -\frac{m_a n_{ao}}{2}\left[\eta \frac{v_{ta}^2}{n_{ao}} \bar{\nabla}(n_{a1} n_{a1}) + \nabla(\bar{v}_{a1} \cdot \bar{v}_{a1})\right]. \qquad (19)$$

The linear dispersion relation shown in Fig. XIII-7 is also negligibly modified if it is evaluated for $\omega_{ce}/\omega_{pe} \to \infty$ instead of $\omega_{ce}/\omega_{pe} \approx 3$. The infinite field limit appears, therefore, to be a valid approximation.

Coupled-Mode Equations

The form of the terms on both sides of Eq. 18 is already suggestive of a coupled-mode equation. Each term on the left-hand side of Eq. 18 involves the product of a linear solution times a nonlinear solution, while each term on the right-hand side involves the product of two nonlinear solutions times a linear solution. When the normal-mode form of the solutions is substituted in Eq. 18, each term on the left-hand side will contribute a single slowly varying amplitude, while the right-hand side will contribute a product of slowly varying amplitudes. The modes associated with each of the solutions

are chosen to satisfy the resonance conditions (Eq. 14).

To simplify the problem, we consider only coupling in time. If we write any one of the system variables x = n, v, or ϕ schematically as $x = a_M X_M e^{j\Lambda_M}$, we obtain a coupled-mode equation for $a_M(t)$ by letting

$$x_1 = a_M X_M e^{j\Lambda_M}$$
$$x_2 = X_M^* e^{-j\Lambda_M} \tag{20}$$

for any well-defined mode M, with only an oscillating dependence (e.g., modes A and T). With this form assumed for each of the plasma variables and in the absence of any nonlinear terms, Eq. 18 reduces to

$$\frac{d}{dt}(W_M) = 0, \tag{21}$$

where W_M is the small-signal wave energy given by a sum of terms of the form $X_M X_M^* = |X_M|^2$, as expected. With the nonlinear terms present, however, the resonance conditions (B, B' = A + T) restrict the product of modes which appear on the right-hand side to those that combine to give a slowly varying amplitude commensurate with the rate of change of $a_M(t)$, as we shall see.

The situation is slightly different for the case of the BP modes, which have both exponential and oscillating dependence. For example, if we attempt to evaluate the small-signal energy of the decaying mode B independently by letting

$$x_1 = a_B X_B e^{j\Lambda_B} e^{-\gamma t}$$
$$x_2 = X_{B'}^* e^{-j\Lambda_B} e^{-\gamma t}, \tag{22}$$

we obtain

$$\frac{d}{dt}\left[W_B e^{-2\gamma t}\right] = 0. \tag{23}$$

For the bracketed term to be independent of time the small-signal energy must be identically zero. We are unable, therefore, to write a conservation equation for $a_B(t)$. But we recognize that if we choose the normal-mode solutions so that a part of both BP modes at (ω_B, k_B) are combined; that is,

$$x_1 = a_B X_B e^{j\Lambda_B} e^{-\gamma t}$$

$$x_2 = X^*_{B'} e^{-j\Lambda_B} e^{\gamma t}, \tag{24}$$

then the expression corresponding to (21) becomes $\frac{d}{dt}(\tilde{W}_B) = 0$, where $\tilde{W}_B$ is now a complex quantity given by a sum of terms of the form $X_B X^*_{B'}$. This allows us to obtain an equation for the (slow) time evolution of $a_B(t)$ or $a_{B'}(t)$.

Before deriving the coupled-mode equation and coupling coefficient for the four modes, we must evaluate the normal-mode amplitudes. For any mode M, each amplitude can be obtained from the linearized Eqs. 4 through 10 in terms of a single quantity, say, the RF electron velocity V_{eM}. Assuming $v_{tb} = v_{ti} = 0$ and $B_o \to \infty$, we have

$$V_{iM} = -\mathscr{M} T_M V_{eM} \qquad N_{eM} = n_o \frac{V_{eM}}{v_M}$$

$$V_{\beta M} = \frac{\omega_M}{\omega_{DM}} T_M V_{eM} \qquad N_{\beta M} = \frac{n_b \omega_M k_M}{\omega_{DM}^2} T_M V_{eM} \tag{25}$$

$$\Phi_M = \frac{m_e}{q_e} v_M T_M V_{eM} \qquad N_{iM} = -\frac{n_o}{v_M} \mathscr{M} T_M V_{eM}$$

where

$$T_M = 1 - \frac{v_{te}^2}{v_M^2}, \quad \mathscr{M} = \frac{m_e}{m_i}, \quad \mathscr{N} = \frac{n_b}{n_o}, \quad v_M \equiv \frac{\omega_M}{k_{zM}}, \quad \omega_{DM} = \omega_M - k_{zM} v_b.$$

Here we may arbitrarily choose V_{eM} to be real and take the remaining amplitudes to be complex. It can also be shown that $V_{eB} = V_{eB'}$.

To derive the coupled-mode equation for the amplitudes of the decaying BP mode, $a_B(t)$, we substitute the solutions given by Eqs. 24 for the BP mode and Eqs. 20 for the A and T modes in Eq. 18, and use Eqs. 25 to simplify the resulting form of the coupling coefficient. For example, considering only the contribution of the first nonlinear term to Eq. 18, we have

$$\frac{d}{dt}(\tilde{W}_B a_B) = v_{e2(B'^*)} F_{e1(A+T)} \tag{26}$$

where the capitalized mode subscripts remind us of the restrictions imposed by the resonance conditions. But

$$F_{el(A+T)} = -m_e n_o \left\{ \frac{\eta v_{te}^2}{n_o^2} (-jk_B) N_{eA} N_{eT} a_A a_T e^{j(\Lambda_A+\Lambda_T)} + (-jk_B) V_{eA} V_{et} a_A a_T e^{j(\Lambda_A+\Lambda_T)} \right\}$$

$$= (jk_B) m_e n_o V_{eA} V_{eT} a_A a_T e^{j\Lambda_B} \left[1 + \frac{\eta v_{te}^2}{v_A v_T} \right] \tag{27}$$

and

$$v_{e2(B'^*)} = V_{eB'}^* e^{-j\Lambda_B} e^{\gamma t}.$$

The contribution of the first nonlinearity is given by

$$\tilde{W}_B \frac{d}{dt} a_B = (jk_B) m_e n_o V_{eA} V_{eT} V_{eB'}^* e^{\gamma t} a_A a_T \left(1 + \frac{\eta v_{te}^2}{v_A v_T} \right). \tag{28}$$

The other nonlinear contributions are evaluated in a similar manner to give

$$\frac{d}{dt} a_B = j m_e n_o V_{eA} V_{eT} V_{eB} e^{\gamma t} \left(\frac{\tilde{\omega}_B \tilde{K}_B}{\tilde{W}_B} \right) a_A a_T, \tag{29}$$

where

$$\tilde{K}_B = \left\{ \left[\frac{1}{v_A} + \frac{1}{v_T} + \frac{1}{\tilde{v}_B} + \frac{\eta v_{te}^2}{v_A v_T \tilde{v}_B} \right] - \left[\mathcal{M} T_A T_T \tilde{T}_B \left(\frac{1}{v_A} + \frac{1}{v_T} + \frac{1}{\tilde{v}_B} \right) \right] \right.$$

$$\left. + \frac{\mathcal{N} T_A T_T \tilde{T}_B}{\left(1 - \frac{v_b}{v_A}\right)\left(1 - \frac{v_b}{v_T}\right)\left(1 - \frac{v_b}{\tilde{v}_B}\right)} \left[\frac{1}{(v_A - v_b)} + \frac{1}{(v_T - v_b)} + \frac{1}{(\tilde{v}_B - v_b)} \right] \right\}. \tag{30}$$

Here we have used the fact that $\omega_{B'}^* = \omega_{B'}$, $k_{B'}^* = k_{B'}$, and $X_{B'}^* = X_{B'}$, where the last equality will be shown later.

In the expression for $\tilde{K}_B$ the first term in brackets in (30) comes from the nonlinearities arising from the plasma electrons, the second term arises from plasma ion nonlinearities, and the last term from the beam nonlinearities. Since $v_B = \frac{\omega_B}{k_B} \approx v_b$, the beam nonlinearities may cause a considerable enhancement in the magnitude of the coupling coefficient.

The coupled-mode equation for the growing BP mode (B') is obtained in a similar manner by letting

$$x_1 = a_{B'} X_{B'} e^{j\Lambda} e^{\gamma t}$$
$$x_2 = X_B^* e^{-j\Lambda} e^{-\gamma t}. \tag{31}$$

We then get

$$\frac{d}{dt} a_{B'} = jm_e n_o V_{eA} V_{eT} V_{eB'} e^{-\gamma t} \left(\frac{\tilde{\omega}_{B'} \tilde{K}_{B'}}{\tilde{W}_B} \right) a_A a_T, \tag{32}$$

where $\tilde{K}_{B'}$ has the same form as K_B with $\tilde{v}_B \rightarrow \tilde{v}_{B'}$ and $\tilde{K}_{B'} = \tilde{K}_{B'}^*$.

The coupled-mode equation for the acoustic mode is obtained by letting each system variable assume the usual form:

$$x_1 = a_A X_A e^{j\Lambda_A}$$
$$x_2 = X_A^* e^{-j\Lambda_A}.$$

Since we recall that $\omega_A = \omega_{B,B'} - \omega_T$ and $\bar{k}_A = \bar{k}_{B,B'} - \bar{k}_T$, the thermal contribution of the first nonlinearity is given by

$$W_A \frac{d}{dt} a_A = -v_{e2(A^*)} \left[-\frac{m_e n_o}{2} \frac{\eta v_{te}^2}{n_o} \nabla (n_{e1(B,B')} n_{e1(T^*)}) \right],$$

where the bracketed term becomes

$$-m_e n_o (-jk_A) \left[\frac{\eta v_{te}^2}{n_o^2} \left(a_B N_{eB} e^{-\gamma t} + a_{B'} N_{eB'} e^{\gamma t} \right) a_T^* N_{eT}^* \right] e^{j\Lambda_A} \tag{33}$$

and $v_{e2} = V_{eA}^* e^{-j\Lambda_A}$.

The thermal contribution therefore becomes

$$W_A \frac{da_A}{dt} = jm_e n_o V_{eA}^* V_{et}^* \frac{\eta v_{te}^2 \omega_A}{v_A v_T} \left[\frac{a_B V_{eB}}{v_B} e^{-\gamma t} + \frac{a_{B'} V_{eB'}}{v_{B'}} e^{\gamma t} \right] a_T^*. \tag{34}$$

Recalling that $\frac{V_{eB}}{v_B} = \frac{V_{eB'}^*}{v_{B'}^*}$ and comparing Eq. 34 with Eqs. 28, 29 and 32 we find

$$\frac{d}{dt} a_A = jm_e n_o V_{eA} V_{et} \frac{\omega_A}{W_A} \left[a_B V_{eB} \tilde{K}_B e^{-\gamma t} + a_B^* V_{eB}^* \tilde{K}_B^* e^{\gamma t} \right] a_T^*, \tag{35}$$

where we have used the fact that V_{eM} is taken to be real. Because the resonance conditions for the T mode and the A mode are symmetric, the equation for $a_T(t)$ is identical to Eq. 35 if the A and T subscripts are exchanged.

We can therefore summarize the four coupled-mode equations as follows:

$$\frac{d}{dt}A_B = jm_e n_o V_{eA} V_{eT} V_{eB}\, e^{\gamma t}\, \mathscr{C} A_A A_T$$

$$\frac{d}{dt}A_{B'} = jm_e n_o V_{eA} V_{eT} V_{eB}\, e^{-\gamma t}\, \mathscr{C}^* A_A A_T$$

$$\frac{d}{dt}A_A = jm_e n_o V_{eA} V_{eT} V_{eB} \left\{A_B \mathscr{C}\, e^{-\gamma t} + A_{B'} \mathscr{C}^*\, e^{\gamma t}\right\} A_T^*$$

$$\frac{d}{dt}A_T = jm_e n_o V_{eA} V_{eT} V_{eB} \left\{A_B \mathscr{C}\, e^{-\gamma t} + A_{B'} \mathscr{C}^*\, e^{\gamma t}\right\} A_A^* \tag{36}$$

where

$$A_M \equiv a_m \left(\frac{W_M}{\omega_M}\right)^{1/2}, \qquad \mathscr{C} \equiv \tilde{K}_B \left(\frac{\omega_A \omega_T \tilde{\omega}_B}{W_A W_T \tilde{W}_B}\right)^{1/2}.$$

In these equations, we have normalized the wave amplitudes to obtain a symmetrical form for the equations. We may obtain an alternative form for (36) by the transformation $\mathscr{A}_B = A_B\, e^{-\gamma t}$ and $\mathscr{A}_{B'} = A_{B'}\, e^{\gamma t}$. We then obtain

$$\left(\frac{d}{dt} + \gamma\right)\mathscr{A}_B = j(m_e n_o V_{eA} V_{et} V_{eB})\, \mathscr{C} A_A A_T$$

$$\left(\frac{d}{dt} - \gamma\right)\mathscr{A}_{B'} = j(m_e n_o V_{eA} V_{et} V_{eB})\, \mathscr{C}^* A_A A_T$$

$$\frac{d}{dt}A_A = j(m_e n_o V_{eA} V_{et} V_{eB})\left(\mathscr{C}\mathscr{A}_B + \mathscr{C}^*\mathscr{A}_{B'}\right) A_T^*$$

$$\frac{d}{dt}A_T = j(m_e n_o V_{eA} V_{et} V_{eB})\left(\mathscr{C}\mathscr{A}_B + \mathscr{C}^*\mathscr{A}_{B'}\right) A_A^*. \tag{37}$$

These equations differ from the usual form of the coupled-mode equation for the decay instability[11] in several ways. First, the interaction involves four equations instead of the three equations that result when only the growing BP wave is considered. The formalism still involves only second-order products. The coupling coefficient $\mathscr{C}$ is now complex, instead of being pure real or pure imaginary as for the usual three-wave case.[10] It is also interesting to note that the BP wave which appears as a source in the equations for A_A and A_T is a composite of both the growing and decaying modes. These equations were derived for the case of a dissipationless medium. We can include the effect of dissipation by treating it as an additional perturbation of the system in the

same manner as we have treated the reactive instability.

Properties of the Nonlinear System

a. Evaluation of $\tilde{W}_B$ and $\tilde{S}_B$

We have previously discussed the incentive for defining the complex quantity $\tilde{W}_B$ in connection with the BP waves. To evaluate $\tilde{W}_B$, we substitute the assumed form for the solutions:

$$x_1 = X_B e^{j\Lambda_B} e^{-\gamma t}$$
$$x_2 = X_{B'}^* e^{-j\Lambda_B} e^{\gamma t} = X_B e^{-i\Lambda_B} e^{\gamma t} \tag{38}$$

in Eq. 18 in the absence of nonlinear coupling. We shall now show that the conjugate mode amplitudes are equal; that is, $X_{B'}^* = X_B$. X_B is found from the set of equations described by

$$\bar{\bar{A}}(\tilde{\omega}, \tilde{k}) \cdot \bar{X}_B = 0, \tag{39}$$

where $\bar{\bar{A}}(\tilde{\omega}, \tilde{k})$ is in general a real matrix of the complex quantities $\tilde{\omega}$ and $\tilde{k}$. For example, for the simple cold beam-cold plasma case, Eq. 39 represents

$$\begin{bmatrix} \omega & -kn_o & 0 & 0 & 0 \\ 0 & m_e n_o \omega & 0 & 0 & -q_e n_o k \\ 0 & 0 & \omega_D & -kn_b & 0 \\ 0 & 0 & 0 & m_e n_o \omega_D & -q_e n_b k \\ q_e & 0 & q_e & 0 & -k^2 \epsilon_o \end{bmatrix} \begin{bmatrix} N_e(\omega, k) \\ V_e(\omega, k) \\ N_\beta(\omega, k) \\ V_\beta(\omega, k) \\ \Phi(\omega, k) \end{bmatrix} = 0. \tag{40}$$

For electrostatic waves the matrix $\bar{\bar{A}}(\tilde{\omega}, \tilde{k})$ will always have elements that are real functions of the complex variables $\tilde{\omega}$ and $\tilde{k}$ as long as the electric potential $\phi(r, t)$ is used as a system variable. Therefore

$$[A(\tilde{\omega}, \tilde{k})]^* = A(\tilde{\omega}^*, \tilde{k}^*). \tag{41}$$

Since X_B and $X_{B'}$ are conjugate modes, $X_{B'}$ is found from the same set of equations, with $\omega \rightarrow \omega^*$ and $k \rightarrow k^*$.

$$\bar{\bar{A}}(\omega^*, k^*) \cdot \bar{X}_{B'} = 0. \tag{42}$$

Taking the complex conjugate of this equation, we obtain

$$\overline{\overline{A}}(\omega, k) \cdot \overline{X}^*_{B'} = 0. \tag{43}$$

Comparing (39) and (43), we have $X^*_{B'} = X_B$. This relation holds for each of the seven normal-mode amplitudes.

To evaluate W_B, we substitute Eqs. 38 in the time-derivative term of Eq. 18 and use Eqs. 25 which relate the normal-mode amplitudes to obtain

$$\tilde{W}_B = m_e n_o V_{eB} V^*_{eB'} T_B T^*_{B'} \; 2 \left\{ \frac{k_B^2}{k_{zB}^2} \frac{\omega_B^2}{\omega_{pe}^2} + \frac{v_{te}^2}{v_B^2 T_B^2} + \mathcal{N} \frac{v_b k_B}{\omega_B} \frac{\omega_B^3}{\omega_D^3} \right\}. \tag{44}$$

In the infinite field limit the dispersion relation given by Eq. 1 becomes

$$\mathcal{D}(\omega, k) = \frac{k^2}{k_z^2} - \frac{\omega_{pe}^2}{\omega^2} \left(\frac{1}{T} + \mathcal{M} + \mathcal{N} \frac{\omega^2}{\omega_D^2} \right), \tag{45}$$

so that the braced term in Eq. 44 becomes $\frac{\omega^3}{2\omega_{pe}^2} \frac{\partial \mathcal{D}}{\partial \omega}$. Using the relation $T_M V_{eM} = -j \frac{E_M}{\omega_M} \frac{q_e}{m_e}$, we can express $\tilde{W}_B$ as

$$\tilde{W}_B = \epsilon_o \tilde{E}_B \tilde{E}^*_{B'} \, \omega \left. \frac{\partial \mathcal{D}}{\partial \omega} \right|_{\tilde{\omega}_B} = -\epsilon_o \tilde{E}_B^2 \omega \left. \frac{\partial \mathcal{D}}{\partial \omega} \right|_{\tilde{\omega}_B}. \tag{46}$$

The minus sign in the second expression appears because V_{eB} was chosen to be real. Thus $\tilde{W}_B$ is given by the usual expression for the mode energy, but the quantity must now be evaluated at the complex frequency ω_B. We can show similarly that

$$\tilde{S}_{2B} = \epsilon_o \tilde{E}_B \tilde{E}^*_{B'} \omega \left. \frac{\partial \mathcal{D}}{\partial k_z} \right|_{\tilde{\omega}_B}. \tag{47}$$

b. Coupling Coefficient and Threshold

We shall now evaluate the magnitude of the coupling coefficient

$$\mathcal{C} = \tilde{K}_B \left[\frac{\omega_A \omega_T \tilde{\omega}_B}{W_A W_T \tilde{W}_B} \right]^{1/2}.$$

Using (46) to evaluate W_M for each of the modes in terms of the RF electron velocity, we have

$$W_A = 2m_e n_o V_{eA}^2 \frac{v_{te}^2}{c_s^2}$$

$$W_T = 2m_e n_o V_{et}^2 \tag{48}$$

$$\tilde{W}_B = \frac{2m_e n_o \mathcal{N} V_{eB}^2}{(1-v_b/v_B)^3}.$$

We can simplify the expression for $\tilde{K}_B$ given in Eq. 30 by using our general knowledge of the frequency and the wave number of the interacting modes (see Fig. XIII-7):

$$v_B \approx v_b \qquad T_B \approx T_T \approx 1$$

$$v_T \approx -v_b \qquad T_A \approx -v_{te}^2/c_s^2$$

$$v_A = c_s \ll v_{te} \ll v_b \tag{49}$$

Using these approximations, we obtain

$$\tilde{K}_B \approx \frac{1}{c_s}\left[1 + \frac{\mathcal{N}}{2}\frac{v_{te}^2}{v_b^2}\frac{1}{(v_b/v_B - 1)^2}\right] = \frac{1}{c_s}\left[1 + \frac{1}{2}\frac{v_{te}^2}{v_b^2}\left(\frac{k^2}{k_z^2}\frac{\omega_B^2}{\omega_{pe}^2} - 1\right)\right], \tag{50}$$

where the contribution of the beam in the second term is in general small. The coupling coefficient $\mathscr{C}$ is therefore given by

$$\mathscr{C} = \frac{1}{2m_e n_o V_{eA} V_{eT} V_{eB}}\left\{\frac{1}{v_{te}}\left[1 + \frac{\mathcal{N}}{2}\frac{v_{te}^2}{v_b^2}\frac{1}{(v_b/v_B - 1)^2}\right]\left[\frac{\omega_A \omega_T \omega_B}{2m_e n_o \mathcal{N}}\left(1 - \frac{v_b}{v_B}\right)^3\right]^{1/2}\right\}. \tag{51}$$

To obtain some idea of the strength of this interaction, we use this coupling coefficient to calculate a threshold for the interaction, under the assumption of a strong pump. The relevant coupled-mode equations are then

$$\frac{dA_A}{ct} = j\mathscr{C}'^* A_{B'} A_T^*$$

$$\frac{dA_T}{dt} = j\mathscr{C}'^* A_{B'} A_A^*,$$

where $\mathscr{C}'$ is the term in brackets above. Assuming that A_A and A_T have an $e^{\gamma t}$ variation, we have

$$\gamma^2 \approx |\mathscr{C}'|^2 \left|\frac{W_B}{\omega_B}\right| = |K_B|^2 \frac{\omega_A \omega_T}{W_A W_T} m_e^2 n_o^2 V_{eA}^2 V_{eT}^2 V_{eB}^2. \tag{52}$$

At instability threshold $\gamma^2 \geq \gamma_A \gamma_T$,[11] where γ_A and γ_T are the linear damping rates of the A and T modes, respectively. Therefore the threshold for the instability is given by

$$\frac{V_{B,RF}^2}{v_{te}^2} > 16 \frac{\gamma_A \gamma_T}{\omega_A \omega_T} \frac{1}{\left[1 + \frac{\mathscr{N}}{2} \frac{v_{te}^2}{v_b^2} \frac{1}{(v_b/v_B - 1)^2}\right]^2}, \tag{53}$$

where $V_{B,RF} = 2V_{eB}$ is the RF induced electron velocity. This threshold, without the term in brackets, is identical to the result obtained for the parametric decay of a T mode into a lower frequency T mode and an A mode.[11] The correction factor in brackets results from the fact that a BP wave is being used here as a pump wave instead of a T wave. This correction is in general small unless $v_b \approx v_B$. While $(v_b - v_B)$ is a function of $\mathscr{N}$, it also depends independently on the particular value of ω_B/ω_{pe} that is used.

We can also obtain from Eq. 36 Manley-Rowe type relations that describe the power flow between the coupled modes. Taking $\left(A_2^* \frac{d}{dt} A_2 + A_2 \frac{d}{dt} A_2^*\right)$ and using the first two equations, we obtain

$$\frac{d}{dt} |A_A|^2 = \frac{d}{dt} |A_T|^2 = -\frac{d}{dt} 2 \operatorname{Re}\left(A_B A_{B'}^*\right), \tag{54}$$

so that the energy exchanged by the modes, ΔW, is related by

$$\left|\frac{\Delta W_B}{\Delta W_T}\right| = \left|\frac{\omega_B}{\omega_T}\right|; \qquad \left|\frac{\Delta W_T}{\Delta W_A}\right| = \left|\frac{\omega_T}{\omega_A}\right|. \tag{55}$$

Thus energy flows from the BP mode into the A and T modes in the ratio of their frequencies, as expected.

c. Nonlinear Stability

Equations 36 and 37 describe the temporal nonlinear evolution of the coupled system. The equations closely resemble those obtained for the usual three-wave case,[12] but are complicated by the complex nature of the coupling coefficient and the form taken by the BP wave when it acts as a pump. In the usual three-wave case, if the high-frequency pump were a negative-energy wave, the system would be explosively unstable.[10] As we

have stressed, however, the high-frequency pump wave for this interaction is not necessarily a negative-energy wave, so that there is no a priori reason to expect the system to be nonlinearly unstable.

A numerical study of the nonlinear evolution of the system indicates that the stability of the system depends upon the sign of the quantity Re $(\mathscr{C}^2) \sim$ Re $(\tilde{W}_B)$. This is shown in Fig. XIII-8, where we give three examples of the evolution of the wave amplitude. For Re $(\tilde{W}_B) < 0$ (Fig. XIII-8a), we see that at first the growing BP mode exhibits exponential growth, but on a longer time scale the nonlinear behavior quickly dominates to cause the system to exhibit explosive behavior. For Re $(\tilde{W}_B) > 0$ (Fig. XIII-8b), the usual linear growth of B' saturates via pump depletion and periodically exchanges energy with the other modes. The evolution of modes A, B, B' is shown in more detail for the stable system in Fig. XIII-8c. The phase angle of the coupling coefficient depends on specific system parameters, such as n_b, v_b, etc., so that whether or not a particular experiment

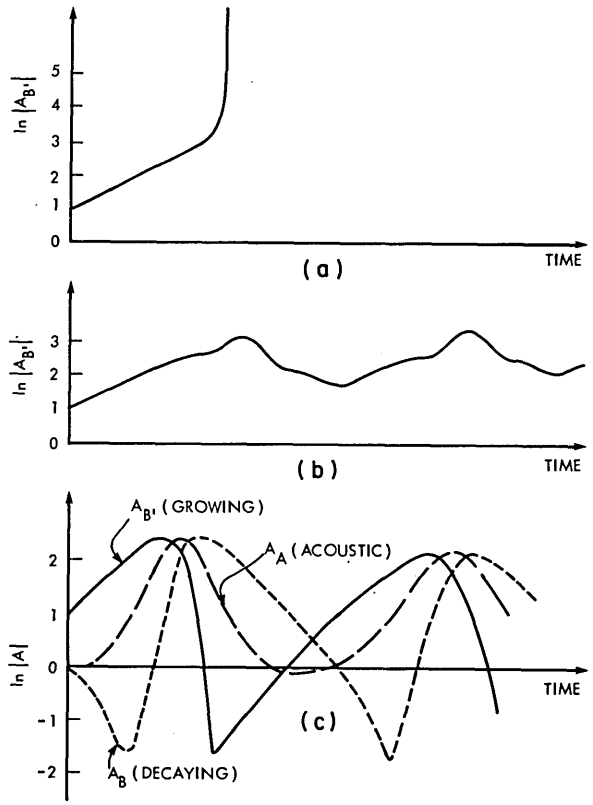

Fig. XIII-8. Nonlinear temporal evolution of the BP instability.
(a) Explosive behavior for Re $(\tilde{W}_B) < 0$.
(b) Stable behavior for Re $(\tilde{W}_{BP}) > 0$.
(c) Stable case showing the evolution of the three interacting waves.

would reveal saturation of the unstable BP wave because of pump depletion or some other nonlinear mechanism would depend on the specific operating parameters. Since a threshold exists for the decay instability, if the threshold were sufficiently large, it seems possible that the BP wave might saturate via some other mechanism, for example, by trapping, before pump depletion could become important. For our experiment, we find that $\mathrm{Re}\,(\tilde{W}_B) > 0$ over the whole operating regime, so that the system can be stabilized by pump depletion. The field strength required for the onset of trapping is estimated to be ~50 V/cm, while the decay instability threshold is estimated to be ~3 V/cm. Therefore it seems possible that for our particular experimental conditions the unstable BP wave might saturate via pump depletion before trapping can become important.

It is more difficult to demonstrate analytically the dependence of the stability of the system upon the sign of $\mathrm{Re}\,(\tilde{W}_B)$. If we neglect the γ terms in Eqs. 37, we can derive the following conservation theorems.

$$|A_B|^2 + \frac{|\mathscr{C}|^2}{2\,\mathrm{Re}\,(\tilde{W}_B)}\,|A_A|^2 = \text{constant}$$

$$\frac{d^2}{dt^2}\,|A_A|^2 - 4\left|\mathscr{C}^* A_{B'} + \mathscr{C} A_B\right|^2 |A_A|^2 + 2\,\mathrm{Re}\,(\tilde{W}_B)\left(|A_A|^2\right)^2 = 0. \tag{56}$$

The first equation demonstrates that the system must be stable for $\mathrm{Re}\,(\tilde{W}_B) > 0$, since the sum of the wave amplitudes is limited. The second equation demonstrates that the system is unstable for $\mathrm{Re}\,(W_B) > 0$. While these statements do not allow us to say much about the stability of the complete system as described by Eqs. 37, they do lend credence to the numerical results.

References

1. J. Apel, Phys. Fluids 12, 291 (1969).
2. J. Apel, Phys. Fluids 12, 640 (1969); Y. Fainberg, Czech. J. Phys. 18, 652 (1968); B. Quon et al., Phys. Rev. Letters 32, 406 (1974).
3. K. Gentle and J. Lohr, Phys. Fluids 16, 1464 (1973).
4. K. Papadopoulos, Bull. Am. Phys. Soc. 18, 1306 (1973).
5. L. Thode and R. Sudan, Phys. Rev. Letters 30, 732 (1973).
6. R. R. Parker and A. L. Throop, Phys. Rev. Letters 31, 1549 (1973).
7. A. L. Throop and R. R. Parker, Quarterly Progress Report No. 108, Research Laboratory of Electronics, M. I. T., January 15, 1973, pp. 154-166.
8. A. Bers and P. Penfield, Jr., IRE Trans., Vol. ED-9, No. 1, pp. 12-26, January 1962.
9. R. J. Briggs, Electron-Stream Interaction with Plasmas (The M. I. T. Press, Cambridge, Mass., 1964).

10. B. Coppi, M. Rosenbluth, and R. Sudan, Ann. Phys. (N. Y.) 55, 207 (1969).

11. A. Bers, Notes on Lectures: Linear Waves and Instabilities, given at Ecole d'Eté de Physique Théorique, Les Houches, France, July 1972 (Gordon and Breach Publishers, London, in press).

12. S. Tanaka and M. Raether, University of Illinois Report R-536, 1971; J. Chang, M. Raether, and S. Tanaka, Phys. Rev. Letters 27, 1263 (1971).

XIII. PLASMA DYNAMICS

G. General Theory

RESEARCH OBJECTIVES AND SUMMARY OF RESEARCH

1. Toroidal Transport Theory

We are interested in collisional and collective transport processes in toroidal plasmas of the Tokamak type.

a. Inertial Effects on Self-consistent Toroidal Confinement in the MHD Regime

U. S. Atomic Energy Commission (Contract AT(11-1)-3070)

James E. McCune, Paul W. Chrisman, Jr.

We are studying plasma fluid dynamics in the Pfirsch-Schlüter regime. An extensive review of the literature of self-consistent resistive MHD confinement in toroidal geometry, as well as associated loss rates and transport, has been completed. We have not found a completely satisfactory self-consistent MHD description of a resistive toroidal equilibrium (especially with inertial effects included). The "equilibria" predicted thus far are subject to rotational instability. We have formulated an invariant form for the viscosity that is useful for our purposes, and the investigation of self-consistent resistive equilibria with viscosity and inertia is under way.

b. Collisional and Anomalous Transport in the Long Mean-Free-Path Regime

U. S. Atomic Energy Commission (Contract AT(11-1)-3070)

Dieter J. Sigmar, Steven P. Hirshman, Hark C. Chan, David A. Ehst

Collisional transport theory of multi-ion species plasmas in the long mean-free path regime has been developed and applied to reactor plasmas. Besides neoclassical transport effects, anomalous diffusion driven by the impurity mode is being investigated in slab and toroidal geometries. The following papers have been submitted for publication, or are in preparation:

D. J. Sigmar, J. F. Clarke, R. V. Neidigh, and K. L. Vander Sluis, "Hot-Ion Distribution Function in the Oak Ridge Tokamak," Phys. Rev. Letters 33, 1376-1379 (1974).

D. J. Sigmar, S. P. Hirshman, J. E. McCune et al., "Alpha Particle Transport in Tokamak Plasma," a paper presented at the Fifth IAEA Conference on Plasma Physics and Controlled Nuclear Fusion Research, Tokyo, November 11-15, 1974, Paper CN-33/A15-3.

S. P. Hirshman, D. J. Sigmar, and J. F. Clarke, "Collisional Impurity Diffusion in the Banana Regime," to be submitted for publication; now available as ORNL TM-4839, March 1975.

D. J. Sigmar and H. C. Chan, "Anomalous Transport Due to Impurity Mode" (in preparation).

c. Effects of Turbulence on Trapped Particles in Toroidal Geometry

U. S. Atomic Energy Commission (Contract AT(11-1)-3070)
National Science Foundation (Grant GK-37979X1)

Thomas H. Dupree

Our study of the effects of turbulence on trapped particles in toroidal geometry continues. When the orbits are understood, we shall be able to predict the effects of trapped-particle instabilities on toroidal confinement. We are also investigating the driving and decay mechanisms of plasma vortices and the effect of vortices on plasma confinement. The doctoral research of David Ehst on anomalous diffusion arising from the dissipative trapped-particle mode is a part of this investigation.

2. Radio-Frequency Heating of Tokamak Plasmas

U. S. Atomic Energy Commission (Contract AT(11-1)-3070)

Abraham Bers, Charles F. F. Karney, Kim Theilhaber

The availability of large amounts of power at microwave frequencies (2-10 GHz) and the simplicity of coupling structures at these frequencies makes it attractive to consider their use for heating a Tokamak plasma. For typical Tokamak plasmas this frequency regime falls between the electron cyclotron and ion cyclotron frequencies, usually near and above the lower hybrid frequency. We have shown that an array of properly phased waveguides at the wall of a Tokamak can excite in the central (nearly homogeneous) part of the plasma a large-amplitude electrostatic electron plasma wave that can act as a pump for the parametric excitation of electrostatic ion cyclotron waves suitable for heating the ions.[1, 2]

We are now studying the excitation of large-amplitude waves of the whistler type in the same frequency regime by means of a suitable waveguide array. These waves can also be downconverted to electrostatic ion cyclotron waves (see Sec. XIII-G. 3). We plan to address ourselves to the toroidal magnetic field effects on the propagation and damping of these waves, to explore other possibilities of downconversion to kinetic modes, and to study the detailed nonlinear aspects of heating by RF fields. In all of our work we shall make extensive use of symbolic computation, using the MACYSMA System.

3. High-Frequency Microinstabilities in Tokamak Plasmas

U. S. Atomic Energy Commission (Contract AT(11-1)-3070)

Abraham Bers, Miloslav S. Tekula

We have previously studied microinstabilities in a homogeneous plasma driven by an electric field or current. We have focused on the fast-growing modes that occur at high frequencies (above the ion cyclotron frequency) and short wavelength (of the order of, or smaller than, the ion cyclotron radius). In these modes the effects of plasma density and magnetic field inhomogeneity may be ignored. The conditions under which these modes are growing sufficiently fast seem to occur in the initial stages of plasma buildup in Tokamaks where $n \sim 10^{12\text{-}13}/cm^3$, and $T_e \gg T_i$. The study of the turbulence caused by these modes is important in understanding plasma generation and heating in Tokamaks.

We plan to study the detailed effects of trapped-particle orbits on these instabilities, in order to determine their relevance in the quasi steady-state Tokamak plasma regime. In this regime trapped-particle effects also make the velocity distribution function anisotropic and this can lead to new high-frequency microinstabilities.

References

1. A. Bers and C. F. F. Karney, Proc. Annual Meeting on Theoretical Aspects of Controlled Thermonuclear Research, University of California, Berkeley, April 3-5, 1974, A. E. C. Publication CONF-740403 TID-4500, UC-20, p. 7 (Abstract).

2. A. Bers, C. F. F. Karney, and K. Theilhaber, Bull. Am. Phys. Soc. 19, 961 (1974).

1. A GENERAL TREATMENT OF RESONANCE BROADENING IN PLASMAS

National Science Foundation (Grant GK-37979X1)

Nathaniel J. Fisch, Abraham Bers

Introduction

Resonance broadening corrections to the weak-turbulence equations have been derived for some particular interactions with mathematical rigor.[1-7] These corrections may be obtained less rigorously but very quickly and to a good approximation by a generalizable procedure that is based on phenomenological considerations. Such a procedure offers several advantages. It may lead to greater insight into the underlying physics of perturbed orbit and wave theory. Rough corrections can be made to higher order weak-turbulence equations for which a rigorous perturbed orbit and wave theory has not yet been derived, and once derived the theory would probably be most useful in a reduced form such as ours. To illustrate our procedure, we shall derive corrections to the weak-turbulence equations describing one-dimensional wave-particle, wave-wave, and nonlinear Landau-damping interactions. We shall concentrate especially on the familiar case, the linear wave-particle interaction, stressing the analogy to the higher order interactions. We shall indicate the generalization to more complicated and higher order interactions and discuss the method. Incorporation of these corrections in the weak-turbulence equations in a manner that conserves energy and momentum will be shown.

Wave-Particle Interaction

In order for the coherent wave-particle interaction (trapping) to take place, the speed of the particle in the wave frame must roughly satisfy

$$\left|\frac{\omega}{k}-v\right| < v_{tr}=\sqrt{\frac{qE}{mk}} \tag{1}$$

or, in a less usual form,

$$\left|\omega-kv\right| < \omega_{mm}=\sqrt{\frac{qEk}{m}}, \tag{2}$$

where ω_{mm} is the allowable mismatch frequency between the wave frequency ω and the "particle frequency" kv such that the coherent interaction can still take place. It is no coincidence that, if trapping takes place, ω_{mm} is also the bounce frequency of the particle in the wave trough. The reason for this is that a particle starting off in exact resonance with the wave ($|\omega-kv| = 0$) develops a maximum frequency mismatch on the order

of ω_{mm}. The exact mismatch at any time is only an indication of the phase of the interaction, as long as it is less than ω_{mm}. Alternatively, we may say that in one bounce (or trapping) time, $\tau_{tr} = 1/kv_{tr}$, the wave-particle interaction cannot distinguish frequency mismatches of less than $1/\tau_{tr}$. In any case, we have the important relation

$$\omega_{mm} = \frac{1}{\tau_{tr}} = \sqrt{\frac{qEk}{m}}. \tag{3}$$

When a particle interacts with a single wave, the mismatch frequency ω_{mm} is calculated from Eq. 2, where E is the amplitude of the wave (Fig. XIII-9a). When many very closely spaced waves are present (Fig. XIII-9b) the E that is used must be based on the energy in all of the waves. In other words, one bounce time is calculated for the wave packet, rather than separate bounce times for each of the waves. Correspondingly, one large ω_{mm} will be found rather than many smaller ω_{mm} for each wave. In order to be considered essentially as one wave for the purpose of trapping, these waves must

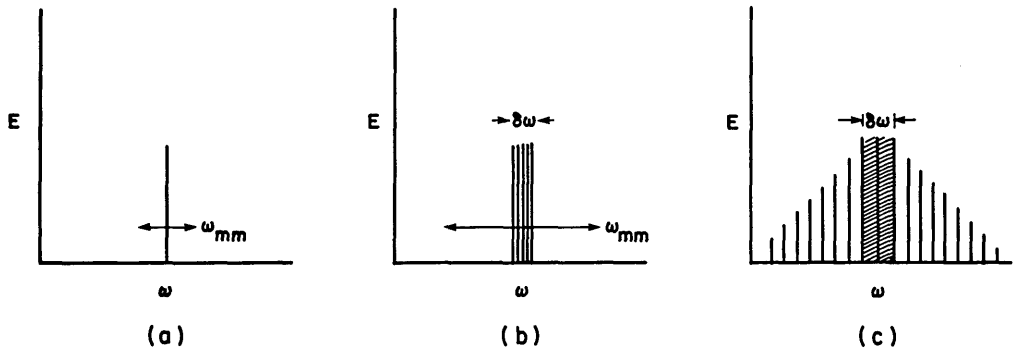

Fig. XIII-9. Mismatch frequency for (a) one wave, (b) many very closely spaced waves, (c) a wide spectrum of waves.

be so closely spaced that they do not get out of phase in a bounce time; that is, $\delta\omega$, the width of the "coherently acting" waves, must be no more than $1/\tau_{tr} = \omega_{mm}$ (Fig. XIII-9c). Thus we put

$$\delta\omega = \omega_{mm}. \tag{4}$$

In the many-wave case ω_{mm} may be identified as a resonance broadening width because it characterizes the allowable mismatch between wave and particle frequency so that the wave still interacts "resonantly" with the particle, in the sense that it acts in concert with other waves in trying to trap the particle.

From Eqs. 3 and 4 it is possible to estimate ω_{mm}, which we now call the resonance broadening width, in the case of a continuum of waves. Let $\mathscr{E}_k$ be the spectral energy density. Then Eq. 3 becomes

$$\omega_{mm} = \sqrt{\frac{qk}{m}(16\pi \mathscr{E}_k \delta k)^{1/2}}, \tag{5}$$

where δk is the width of coherently acting waves in k space and is related in turn to $\delta\omega$ by

$$\delta\omega = \delta(\omega - kv) = \delta k\left|\frac{\delta\omega}{\delta k} - v\right| + k\delta v. \tag{6}$$

Writing $\delta\omega/\delta k = v_g$, we note that

$$\delta v = \delta\left(\frac{\omega}{k}\right) = \frac{\delta k}{k}\left|v_g - v\right|. \tag{7}$$

That is, for self-consistency, the width of the "coherent" particle spectrum, δv, must be equal to the width of the (coherent) wave spectrum, $\delta(\omega/k)$, because if a wave can "reach out" a width $\delta\omega$ to interact with a particle, a particle must be able to reach out the same width to interact with a wave.

Solving Eqs. 4-7, we write

$$\omega_{mm} = \left(\frac{q^2k^2}{m^2}\,\frac{8\pi \mathscr{E}_k}{|v_g - v|}\right)^{1/3} = \left(\frac{k^2 D^R}{\pi}\right)^{1/3}, \tag{8}$$

where D^R is the quasi-linear diffusion coefficient for the resonant particles. Equation 8 is the reduced Dupree-Weinstock result for wave-particle resonance broadening (to within a numerical factor of nearly 1).

In deriving resonance broadening corrections for other interactions we make use of equations analogous to Eqs. 4-7. We find a width of "coherently acting" waves, $\delta\omega$, that we set equal to ω_{mm} (Eq. 4) which is expressed as a function of the "coherently acting" widths of the individual (wave or particle) modes (Eq. 5). Then it remains to relate these individual mode widths to each other (Eq. 7) and to $\delta\omega$ (Eq. 6).

Wave-Wave Interaction

In order for the wave-wave coherent interaction to take place, we must have (analogous to Eq. 2)

$$|\omega_1 - \omega_2 - \omega_3| < \omega_{mm} \tag{9}$$

and also (analogous to Eq. 3)

$$\omega_{mm} = \frac{1}{\tau_{tr}}, \tag{10}$$

where we define a transfer time τ_{tr} as the period in which the energy sloshes between the three waves. This is an extension of the idea of the bounce or trapping time for the wave-particle interaction which indicates the period in which energy is transferred between the wave and the particle.

In general, we have (analogous to Eq. 5)

$$\omega_{mm}^{-1} = \tau_{tr}\left(\mathscr{E}_{k1}\delta k_1, \mathscr{E}_{k2}\delta k_2, \mathscr{E}_{k3}\delta k_3\right), \tag{11}$$

where the exact functional dependence may be put in terms of elliptic integrals.[7] For the case $\omega_1 > \omega_2, \omega_3$ and $\mathscr{E}_{k1} \gg \mathscr{E}_{k3}$ but $\mathscr{E}_{k2} \gtrsim \mathscr{E}_{k1}$, we write for Eq. 3

$$\omega_{mm} = 8\sqrt{\pi}\ |V|\left(\mathscr{E}_{k1}\delta k_1 + \mathscr{E}_{k2}\delta k_2\right)^{1/2}, \tag{12}$$

where V is the usual nonlinear wave-wave coupling coefficient.

From Eq. 9 for $\delta k_j > \delta k_i, \delta k_k$, we have

$$\delta\omega = \delta k_i |v_{gi} - v_{gj}| + \delta k_k |v_{gk} - v_{gj}| = \omega_{mm}, \tag{13}$$

which is analogous to Eqs. 4 and 6. We can interpret ω_{mm} as the maximum frequency difference between interacting waves that satisfy $k_1 - k_2 - k_3 = 0$. We find (analogous to Eq. 7)

$$\frac{\delta k_1}{|v_{g2} - v_{g3}|} = \frac{\delta k_2}{|v_{g1} - v_{g3}|} = \frac{\delta k_3}{|v_{g1} - v_{g2}|} \tag{14}$$

which is the self-consistency relation requiring that the δk are related in such a fashion that if any two modes (k_i, k_j) together can reach out a width $\delta\omega$ to regenerate the third mode (k_k), then modes k_i, k_k should also be able to reach out to regenerate mode k_j, and so on. Alternatively, Eq. 14 may be obtained by requiring that each mode see the other two wave packets of coherently acting waves pass through it in the same amount of time.

Using Eqs. 11-14, we can solve for the resonance broadening width in wave-wave turbulence.

$$\omega_{mm} = 32\pi |V|^2 \frac{\mathscr{E}_{k1}|v_{g2} - v_{g3}| + \mathscr{E}_{k2}|v_{g1} - v_{g3}|}{|v_{gi} - v_{gj}|\,|v_{gj} - v_{gk}|}, \tag{15}$$

where $v_{gi} > v_{gj} > v_{gk} > 0$. If $v_{gj} \neq v_{gi}, v_{gk}$, then ω_{mm} is of the same form as the relaxation rate[11] (and hence is not a true resonance broadening correction). Otherwise,[8] ω_{mm} may be put in the form of Eq. 8, i.e., $\sim \mathscr{E}^{1/3}$. This will be treated in detail in a future report.

Nonlinear Landau-Damping Interaction

For the nonlinear Landau-damping interaction, we imagine a transfer time based on the trapping time of a particle in the (coherent) beat wave.[9] Hence (analogous to Eq. 3) we write

$$\omega_{mm} = \tau_{tr}^{-1} = \sqrt{\frac{qk\dot{E}_B}{m}}, \qquad E_B = AE_1E_2, \tag{16}$$

where A is the nonlinear coupling coefficient, E_1 and E_2 are the real wave amplitudes, and the coherent interaction will take place if

$$|\omega_1 - \omega_2 - kv| < \omega_{mm}. \tag{17}$$

For the many-wave case we write Eq. 16 (cf. Eq. 5) as

$$\omega_{mm} = \sqrt{\frac{qk}{m} A\left(16\pi \mathscr{E}_{k1}\delta k_1\right)^{1/2}\left(16\pi \mathscr{E}_{k2}\delta k_2\right)^{1/2}}. \tag{18}$$

From (10) we find

$$\delta\omega = \delta k_1 |v_{g1}-v| + \delta k_2 |v_{g2}-v| + k\delta v = \omega_{mm}, \tag{19}$$

which is analogous to Eqs. 4 and 6.

As for the linear wave-particle interaction (cf. Eq. 7) the beat wave width determines the (coherently acting) particle spectrum width

$$k\delta v = \delta\left(\frac{\omega_1 - \omega_2}{k_1 - k_2}\right) = \delta k_1 |v_{g1}-v| + \delta k_2 |v_{g2}-v|, \tag{20}$$

and we have (analogous to Eq. 13)

$$\frac{\delta k_1}{|v_{g2}-v|} = \frac{\delta k_2}{|v_{g1}-v|}. \tag{21}$$

Thus a nonlinearly resonant particle sees each packet of coherently acting waves for the same amount of time.

Solving Eqs. 18-21, we find a true resonance broadening correction (since $\omega_{mm} \sim \mathscr{E}$ whereas the diffusion rate $\sim \mathscr{E}^2$) to the nonlinear Landau-damping equations

$$\omega_{mm} = 16\pi \frac{qk}{m} A \left(\frac{\mathscr{E}_{k1}}{|v_{g1}-v|}\right)^{1/2}\left(\frac{\mathscr{E}_{k2}}{|v_{g2}-v|}\right)^{1/2}. \tag{21a}$$

Discussion and Generalization

The resonance broadening corrections describe the mathematical transition between the coherent and turbulent interaction formalisms. In a coherent interaction we examine the oscillatory sharing or sloshing of energy between a small number of oscillators. In a turbulent interaction we examine the irreversible approach to an equilibrium sharing of energy by a very large number of oscillators which is amenable to a Fokker-Planck type of description.[10] The "step" in the Fokker-Planck equation may be pictured as an instantaneously valid "coherent interaction" that has lost correlation (memory) with all previous coherent interactions. The origin of all so-called resonance broadening corrections lies in the coherent interaction which has a characteristic frequency mismatch associated with it that is built into the overall random process.

In the limit of zero-field energy, there are no resonance broadening corrections to the weak-turbulence equations. Since these equations are derived by an expansion in field energy, this result is expected. The opposite limit of interest is when the individual resonance-broadened mode widths δk_i exceed the wave spectrum widths Δk_i, as in Fig. XIII-9b. Then all waves associated with mode i act as one wave and a coherent interaction develops. The test of the ratio $(\delta k/\Delta k)_i$, which is crucial in determining whether the interaction is coherent or turbulent, is equivalent to the more usual consideration in terms of τ_{ac}/τ_{tr}, the ratio of the autocorrelation time of the fields to a trapping time, for the wave-particle case.[1] Similar characteristic times may be defined for higher order interactions; in general, there will be many "autocorrelation" times but only one trapping (transfer) time. In the event that $(\delta k/\Delta k)_i \ll 1$ for some but not all i, neither the turbulent nor the coherent formalism is valid, in general, without modification.

The general procedure to obtain resonance broadening corrections is the following. First, we determine the characteristic frequency mismatch associated with the appropriate coherent interaction as a function of the "coherently acting" energy in each of the interacting modes. This is expressed as

$$\omega_{mm} = \tau_{tr}^{-1}(E_1, E_2, \ldots, E_n) = \tau_{tr}^{-1}\left(\sqrt{\mathscr{E}_{k1}\delta k_1}, \sqrt{\mathscr{E}_{k2}\delta k_2}, \ldots, \sqrt{\mathscr{E}_{kn}\delta k_n}\right). \quad (22)$$

Note that the amount of energy in each mode that acts coherently is a function of ω_{mm}; it is the energy that does not get out of phase in a time $1/\omega_{mm}$. Therefore we write

$$\omega_{mm} = \delta k_1 v_{g1} + \delta k_2 v_{g2} + \ldots + \delta k_n v_{gn}. \quad (23)$$

Finally, we note that in the regeneration of any particular mode the other modes must participate coherently for the same amount of time, yielding n+1 equations for ω_{mm} and δk_i. The resonance broadening correction will be important only if significant mode perturbations take place. This will occur if two (or more) unperturbed group velocities are nearly equal or a particle mode is involved. It can be shown that in one dimension there

are only two classes of true resonance-broadening corrections; $\omega_{mm} \sim \mathscr{E}^{1/3}$ (as in Eq. 8) and $\omega_{mm} \sim \mathscr{E}$ (as in Eq. 21a).[8]

Incorporation of Corrections

We have argued that modes within the resonance-broadened mode width δk_i act as one mode. If $\delta k_i \ll \Delta k_i$, which is the total mode width, then the weak-turbulence description is still valid, but can be improved by replacing the exact (wave or particle) mode amplitudes by an average or smoothing over δk_i. For example, in the linear wave-particle interaction, we must replace

$$\mathscr{E}_k \rightarrow \overline{\mathscr{E}}_k \equiv \frac{1}{2\delta k} \int_{k-\delta k}^{k+\delta k} \mathscr{E}_k \, dk \tag{24}$$

and

$$\frac{\partial f_o}{\partial v} \rightarrow \frac{\overline{\partial f_o}}{\partial v} \equiv \frac{1}{2\delta v} \int_{v-\delta v}^{v+\delta v} \frac{\partial f_o}{\partial v} \, dv = \frac{f_o(v+\delta v) - f_o(v-\delta v)}{2\delta v}, \tag{25}$$

where δv and δk are calculated from Eqs. 5-8. The quasi-linear equations,[11] corrected by these driving terms, then become

$$\frac{\partial f_o(v,t)}{\partial t} = \frac{\partial}{\partial v} D(v) \frac{\overline{\partial f_o(v,t)}}{\partial v} \tag{26}$$

$$\frac{\partial \mathscr{E}_k(t)}{\partial t} = 2\gamma_k \overline{\mathscr{E}_k(t)}, \tag{27}$$

where

$$\gamma_k = -\frac{\epsilon_i}{\frac{\partial \epsilon_r}{\partial \omega}} \tag{28}$$

$$\epsilon_i = -\pi \frac{\omega_p^2}{k|k|} \frac{\overline{\partial f_o}}{\partial v}\bigg|_{v=\omega/k} \tag{29}$$

$$\epsilon_r = 1 + \frac{\omega_p^2}{k} P \int \frac{\frac{\overline{\partial f_o}}{\partial v} \, dv}{\omega - kv} \tag{30}$$

and

$$D(v) = 8\pi \frac{q^2}{m^2} \int \overline{\mathscr{E}}_k \frac{i}{\omega - kv} \, dk. \tag{31}$$

In fact, it can be shown that these equations do reduce to the quasi-linear equations in the limit $\mathscr{E}_k \to 0$ and, furthermore, they conserve energy and momentum.

Similarly, for the wave-wave and nonlinear Landau-damping interactions, we correct the conventional weak-turbulence equations by averaging over the driving terms, replacing

$$\mathscr{E}_{ki} \to \overline{\mathscr{E}}_{ki} \equiv \frac{1}{2\delta k_i} \int_{k_i-\delta k_i}^{k_i+\delta k_i} \mathscr{E}_{ki}\, dk_i, \tag{32}$$

where δk_i is found from the appropriate equations. The corrected wave-wave equations then become

$$\frac{1}{S_{k1}} \frac{\partial N_{k1}}{\partial t} = \frac{1}{S_{k2}} \frac{\partial N_{k2}}{\partial t} = \frac{1}{S_{k3}} \frac{\partial N_{k3}}{\partial t}$$

$$= 4\pi \iint dk_2 dk_3 \, |V|^2 \, \delta(k_1 - k_2 - k_3)\, \delta(\omega_1 - \omega_2 - \omega_3)$$

$$\cdot \left[S_{k1}\overline{N}_{k2}\overline{N}_{k3} - S_{k2}\overline{N}_{k1}\overline{N}_{k3} - S_{k3}\overline{N}_{k1}\overline{N}_{k2} \right] \tag{33}$$

and the corrected nonlinear Landau-damping equations may be written

$$\frac{\partial N_k}{\partial t} = -\overline{N}_k \int d\ell \, R_{k,\ell} \overline{N}_\ell \tag{34}$$

$$\frac{\partial f_o}{\partial t} = \frac{\partial}{\partial v} (D^R + D^{NR}) \frac{\overline{\partial f_o}}{\partial v} \tag{35}$$

$$R_{k,\ell} = \Gamma_{k,\ell} \frac{\overline{\partial f_o}}{\partial v} \tag{36}$$

$$D^R = \iint dk d\ell \, \overline{N}_k \overline{N}_\ell (k-\ell) \, |k-\ell| \, \Gamma_{k,\ell} \, \delta(\omega_k - \omega_\ell - (k-\ell)v), \tag{37}$$

where we have adopted much of Davidson's notation.[11] In Eq. 35 D^R is the nonlinearly resonant diffusion coefficient, whereas D^{NR} governs the nonresonant particle diffusion that is largely unaffected by the perturbed orbits, as in quasi-linear theory. It can be shown that Eqs. 33-37 obey the appropriate limits and conserve both energy and momentum.

Note that this approach to introducing corrections differs slightly from that of Dupree, who modified the quasi-linear equations by replacing the delta-function resonances with finite width resonances. That is,

$$\delta(\omega - kv) \rightarrow \frac{1}{2\omega_{mm}} \begin{cases} 1 & |\omega - kv| < \omega_{mm} \\ 0 & \text{otherwise} \end{cases} \tag{38}$$

A major step in his derivation was to approximate the first term in his series of operator-type corrections as a function. The operator can be shown to obey the appropriate limits and conserve energy and momentum.[12] The functional approximation, on the other hand, obeys the correct limits, conserves momentum, and qualitatively preserves the resonance broadening effect of the operator, but does not strictly conserve energy. Our "physical derivation" leads to a very similar result that preserves the resonance broadening character of Dupree's operator and obeys the same limits and conservation laws. Although our result lacks the mathematically esthetic nature (a simple functional correction) and rigorous derivation of Dupree's (reduced) result, it may be preferred because energy is conserved.

Conclusion

The implications of the resonance-broadening corrections to higher order interactions are similar to those often discussed for linear wave-particle resonance broadening. These effects may be characterized in two ways. First, a particular mode is driven by an average over a resonance broadening width of driving modes. If that width becomes large compared with the width of the driving mode, the driven mode may saturate at an earlier stage. Second, modes that previously could not be excited may become excited if they fall within a resonance broadening width of the exactly resonantly driven modes. These new modes may interact with other modes in the plasma, possibly in a manner in which the exactly resonantly excited modes could not. This may lead to many important effects, such as enhanced particle diffusion, quicker wave cascading, or a slowing down of an instability, because of removal of energy from the originally active region in ω-k space.

References

1. T. H. Dupree, Phys. Fluids 9, 1773 (1966).
2. J. Weinstock, Phys. Fluids 12, 1045 (1969).
3. A. N. Kaufman, Phys. Rev. Letters 27, 376 (1971).
4. L. I. Rudakov and V. N. Tsytovich, Plasma Phys. 113, 213 (1971).
5. S. A. Orzag and R. H. Kraichnan, Phys. Fluids 10, 1720 (1967).
6. T. J. Birmingham and M. Bornitici, Phys. Fluids 15, 1778 (1972).
7. V. N. Tsytovich, Nonlinear Effects in Plasma (Plenum Press, New York, 1970), p.48.
8. N. J. Fisch, "A General Treatment of Resonance Broadening in Plasmas," S.M. Thesis, Department of Electrical Engineering, M.I.T., January 1975.
9. E. Ott and C. T. Dum, Phys. Fluids 14, 959 (1971).

10. I. Prigogine, Non-Equilibrium Statistical Mechanics (John Wiley and Sons, Inc., New York, 1962), Chap. 2.

11. R. C. Davidson, Methods in Nonlinear Plasma Theory (Academic Press, Inc., New York, 1972).

12. T. H. Dupree (Private communication, 1974).

2. THREE-DIMENSIONAL THREE-WAVE AND FOUR-WAVE COUPLING COEFFICIENTS FOR MAGNETIZED WARM-FLUID PLASMA WITH DRIFTS

National Science Foundation (Grant GK-37979X1)

Duncan C. Watson, Abraham Bers

Introduction

Coherent wave-wave interactions in a medium caused by the nonlinear conductivity of the medium may be conveniently described in terms of coupling coefficients. We present general expressions for these coupling coefficients which embrace all three-wave and four-wave interactions in a warm-fluid plasma. The plasma may be permeated by a steady uniform magnetic field $\vec{B}_o$, and may contain arbitrarily many particle populations, each with its own temperature and drift velocity. Each interacting wave may propagate in an arbitrary direction and be polarized in an arbitrary direction.

Motivation for Use of Coupling Coefficients

Consider a homogeneous medium having an electrical conductivity that is the sum of a linear conductivity, a second-order nonlinear conductivity, a third-order nonlinear conductivity, and so on. The second-order nonlinear conductivity causes interaction between triplets of waves with wavevectors and frequencies satisfying the approximate sum rule

$$(\vec{k}_a, w_a) \tilde{=} (\vec{k}_b, w_b) + (\vec{k}_c, w_c). \tag{1}$$

Similarly, the third-order nonlinear conductivity causes interaction between quadruplets of waves with wavevectors satisfying the approximate sum rule

$$(\vec{k}_a, w_a) \tilde{=} (\vec{k}_b, w_b) + (\vec{k}_c, w_c) + (\vec{k}_d, w_d), \tag{2}$$

and so on. Suppose that the wave-wave interaction merely modulates each wave by a slowly varying envelope. Then the total electric field assumes the form

$$\vec{E}(\vec{x}, t) = \sum_a \vec{E}_a(\vec{x}, t) \exp(i\vec{k}_a \cdot \vec{x} - iw_a t). \tag{3}$$

Suppose that the effect of the interaction is small enough that the interacting waves are still separable in the wavevector-frequency domain. Then the envelope of each interacting wave satisfies a separate equation of the form

$$\vec{\vec{L}}(\vec{k}_a, w_a)\,\vec{E}_a(\vec{x},t) - i\frac{\partial\vec{\vec{L}}}{\partial\vec{k}}\frac{\partial\vec{E}_a}{\partial\vec{x}} + i\frac{\partial\vec{\vec{L}}}{\partial w}\frac{\partial\vec{E}_a}{\partial t}$$

$$-\frac{1}{2!}\frac{\partial^2\vec{\vec{L}}}{\partial\vec{k}\partial\vec{k}}\frac{\partial^2\vec{E}_a}{\partial\vec{x}\partial\vec{x}} + \frac{\partial^2\vec{\vec{L}}}{\partial\vec{k}\partial w}\frac{\partial^2\vec{E}_a}{\partial\vec{x}\partial t} - \frac{1}{2!}\frac{\partial^2\vec{\vec{L}}}{\partial w^2}\frac{\partial^2\vec{E}_a}{\partial t^2} + \cdots =$$

$$\sum_{(b,\,c)} \exp[i(-\vec{k}_a + \vec{k}_b + \vec{k}_c)\cdot\vec{x} - i(-w_a + w_b + w_c)t](-i\mu_o)\left(w_b + w_c + i\frac{\partial}{\partial t}\right)$$

$$\left\{\vec{\vec{G}}^{NL(2)}(\vec{k}_b, w_b, \vec{k}_c, w_c)\,\vec{E}_b(\vec{x},t)\,E_c(\vec{x},t) - i\frac{\partial\vec{\vec{G}}^{NL(2)}}{\partial\vec{k}_b}\frac{\partial\vec{E}_b}{\partial\vec{x}}\vec{E}_c\right.$$

$$\left. + i\frac{\partial\vec{\vec{G}}^{NL(2)}}{\partial w_b}\frac{\partial\vec{E}_b}{\partial t}\vec{E}_c - i\frac{\partial\vec{\vec{G}}^{NL(2)}}{\partial\vec{k}_c}\vec{E}_b\frac{\partial\vec{E}_c}{\partial\vec{x}} + i\frac{\partial\vec{\vec{G}}^{NL(2)}}{\partial w_c}\vec{E}_b\frac{\partial\vec{E}_c}{\partial t} + \cdots\right\}$$

$$+ \sum_{(b,\,c,\,d)} \exp[i(-\vec{k}_a + \vec{k}_b + \vec{k}_c + \vec{k}_d)\cdot\vec{x} - i(-w_a + w_b + w_c + w_d)t](-i\mu_o)\left(w_b + w_c + w_d + i\frac{\partial}{\partial t}\right)$$

$$\left\{\vec{\vec{G}}^{NL(3)}(\vec{k}_b, w_b, \vec{k}_c, w_c, \vec{k}_d, w_d)\,\vec{E}_b(\vec{x},t)\,\vec{E}_c(\vec{x},t)\,\vec{E}_d(\vec{x},t) + \cdots\right\}$$

$$+ \cdots\cdots \tag{4a}$$

Here $\vec{\vec{L}}$ is the linear dispersion tensor

$$\vec{\vec{L}}(\vec{k}, w) \equiv \vec{k}\,\vec{k} - k^2 + \mu_o\epsilon_o w^2 + i\mu_o w\vec{\vec{G}}^{LIN}(\vec{k}, w). \tag{4b}$$

The tensors $\vec{\vec{G}}^{LIN}$, $\vec{\vec{G}}^{NL(2)}$, $\vec{\vec{G}}^{NL(3)}$, ... are linear, second-order nonlinear, third-order nonlinear, ... conductivities of the medium in the wavevector frequency domain. The first summation on the right-hand side of (4) is over pairs of waves (b, c) that satisfy (1). The phase factor immediately following the summation sign is thus a slowly varying function in the space-time domain. The second summation on the right-hand side of (4) is over triplets of waves (b, c, d) satisfying (2), and so on. The set of differential equations of the form (4), one for each wave envelope $\vec{E}_a$ belonging to (3), constitutes the set of coupled-mode equations. The set of wave envelopes occurring in (3) are slowly varying insofar as their space-time derivatives can be neglected in (4) beyond some small finite order.

The wave envelopes present in (3), whose space-time variations are described by

the set of coupled nonlinear differential equations of the form (4), may vary in polarization, as well as in complex amplitude. Express each electric field wave envelope in terms of its polarization components referred to a fixed triad of basis vectors:

$$\vec{E}_a(\vec{x}, t) = \sum_A E_{Aa}(\vec{x}, t)\, \vec{e}_{Aa}. \tag{5}$$

Choose the fixed triad in a physically appropriate way; that is, choose it to comprise eigenvectors of the linear dispersion tensor $\vec{\vec{L}}(\vec{k}_a, w_a)$. Then the space-time variation of each polarization component is described by an equation of the form

$$(D_a)_{AA} E_{Aa} + \sum_{A'} \left\{ -i \frac{\partial}{\partial \vec{k}} \left(\frac{w^2}{c^2} (D_a)_{AA'} \right) \frac{\partial E_{A'a}}{\partial \vec{x}} + i \frac{\partial}{\partial w} \left(\frac{w^2}{c^2} (D_a)_{AA'} \right) \frac{\partial E_{A'a}}{\partial t} \right\} + \cdots =$$

$$\sum_{(b,c)} \exp[i(-\vec{k}_a + \vec{k}_b + \vec{k}_c) \cdot \vec{x} - i(-w_a + w_b + w_c)t]$$

$$\left\{ - \sum_B \sum_C \left({}_aF^{NL(2)}_{b,c} \right)_{BC} E_{Bb}(\vec{x}, t)\, E_{Cc}(\vec{x}, t) + \cdots \right\}$$

$$+ \sum_{(b,c,d)} \exp[i(-\vec{k}_a + \vec{k}_b + \vec{k}_c + \vec{k}_d) \cdot \vec{x} - i(-w_a + w_b + w_c + w_d)t]$$

$$\left\{ - \sum_B \sum_C \sum_D \left({}_aF^{NL(3)}_{b,c,d} \right)_{BCD} E_{Bb}(\vec{x}, t)\, E_{Cc}(\vec{x}, t)\, E_{Dd}(\vec{x}, t) + \cdots \right\}$$

$$+ \cdots . \tag{6}$$

Here some of the higher space-time derivatives have been omitted for clarity. The elements of the dimensionless dispersion tensor D are defined by

$$(D_a)_{AA'} = \vec{f}_{Aa} \cdot \frac{c^2}{w^2} \vec{\vec{L}}(\vec{k}_a, w_a)\, \vec{e}_{A'a}, \tag{7}$$

where the fixed triad of basis vectors $\vec{f}$ are chosen to be eigenvectors of the transposed linear dispersion tensor $\vec{\vec{L}}(\vec{k}_a, w_a)$. The dispersion tensor thus has a diagonal representation, although its wavevector and frequency derivatives may not have. The quantities F are the coupling coefficients. They describe interactions between waves which are specified by wavevector, frequency, and polarization. They are defined as follows:

$$\left({}_aF^{NL(2)}_{b,c} \right)_{ABC} \equiv i \vec{f}_{Aa} \cdot \vec{\vec{G}}^{NL(2)}(k_b, w_b, k_c, w_c)\, \vec{e}_{Bb} \vec{e}_{Cc} / \epsilon_o w_a \tag{8}$$

$$\left({}_{a}F^{NL(3)}_{b,c,d}\right)_{ABCD} \equiv \frac{i\vec{f}_{Aa} \cdot \vec{\vec{\vec{G}}}^{NL(3)}(k_b, w_b, k_c, w_c, k_d, w_d)\, \vec{e}_{Bb} \vec{e}_{Cc} \vec{e}_{Dd}}{\epsilon_o w_a} \tag{9}$$

and so on. These coupling coefficients will be shown to satisfy certain symmetry relations. Thus the amount of labor involved in setting up equations of type (6) is reduced.

In conclusion, the coupling coefficients are useful because they enable us to follow the behavior of specific polarized components of interacting waves and satisfy certain symmetry relations which will be displayed later.

Coupling Coefficients from the Warm-Fluid Plasma Model

If we neglect many-body correlations in a one-species plasma, such a plasma may be described by a smoothed-out distribution function $f(\vec{x}, \vec{v}, t)$ of six-dimensional phase space and time. By neglecting the discreteness of the plasma particles, and hence neglecting the evolution of the distribution function caused by collisions, we obtain the Vlasov equation

$$\frac{\partial f}{\partial t} + \vec{v} \cdot \frac{\partial f}{\partial \vec{x}} + \frac{q}{m}(\vec{E} + \vec{v} \times \vec{B}) \cdot \frac{\partial f}{\partial \vec{v}} = 0. \tag{10}$$

Multiplying the Vlasov equation by successive powers of the velocity $\vec{v}$ and integrating over velocity space, we form a hierarchy of equations relating successive moments of the velocity. This hierarchy may be truncated in such a way as to contain only a fluid conservation equation

$$\frac{\partial n}{\partial t} + \frac{\partial}{\partial \vec{x}} \cdot n\langle \vec{v} \rangle = 0, \tag{11}$$

and a momentum conservation equation with a pressure term

$$\frac{\partial \langle \vec{v} \rangle}{\partial t} + \langle \vec{v} \rangle \cdot \frac{\partial \langle \vec{v} \rangle}{\partial \vec{x}} + \frac{\gamma v_{To}^2}{n_o}\left(\frac{n}{n_o}\right)^{\gamma-2} \frac{\partial n}{\partial \vec{x}} = \frac{q}{m}(\vec{E} + \langle \vec{v} \rangle \times \vec{B}). \tag{12}$$

Using the results of Vlasov theory as a guide, we choose the value of γ. Equations 11 and 12 constitute the warm-fluid plasma model. Frequently each particle species in a plasma is modeled as such a warm fluid. If a single particle species contains beams or unequal temperature components that warrant treatment as separate populations, each such population may be modeled by (11) and (12) with the appropriate choice of number density, thermal velocity, and drift velocity.

To find the response of the warm-fluid model to an electric field, (11) and (12) are supplemented by a specification of the dc magnetic field $\vec{B}_o$: an equation expressing the

remainder of the magnetic field as a subsidiary quantity

$$\frac{\partial \vec{B}}{\partial t} = -\frac{\partial}{\partial \vec{x}} \times \vec{E}, \tag{13}$$

a specification of the dc component of the fluid velocity for each particle population π

$$\langle \vec{v}_\pi \rangle_{dc} = \vec{v}_{o\pi}, \tag{14}$$

and an equation expressing the current in the plasma as a sum of the currents that are due to each particle population

$$\vec{J}(\vec{x}, t) = \sum_\pi q_\pi n_\pi(\vec{x}, t) \langle \vec{v}_\pi \rangle (\vec{x}, t). \tag{15}$$

The coupling coefficients are defined in terms of conductivities by (8) and (9). These conductivities describe the constitutive relation for electric current and electric field in the medium. This allows us to find the conductivities of a warm-fluid plasma by calculating the response of the system defined by (11)-(15) to an arbitrary electric field. The actual form of the electric field is determined at a later stage, by substituting the calculated conductivities in the mode-coupling equations (4), or equivalently by substituting the calculated coupling coefficients in the mode-coupling equations taken in the form (6).

The second-order conductivity of the system (11)-(15) gives rise to three-wave coupling coefficients according to (8). These coupling coefficients will be written in terms of quantities pertaining to the linear response of the system. This linear response is found by imposing upon the medium an electric field containing a single complex wave

$$\vec{E}(\vec{x}, t) = \vec{E}_a \exp(i\vec{k}_a \cdot \vec{x} - iw_a t) \tag{16}$$

whose particle populations have drift velocities

$$\langle \vec{v}_\pi \rangle = \vec{v}_{o\pi} \tag{17}$$

in the absence of the wave. The wave evokes a linear response at the same wavevector and frequency $(\vec{k}_a, w_a)$ from each particle population. This response comprises a fluid velocity of complex amplitude

$$\vec{V}_a^\pi = \vec{\vec{M}}_a^\pi \frac{iq_\pi \vec{E}_a^\pi}{m_\pi w_a^\pi} \tag{18}$$

and a fluid density of complex amplitude

$$N_o^\pi = n_{o\pi} \frac{\vec{k}_a \cdot \vec{V}_a^\pi}{m_\pi w_a^\pi}. \tag{19}$$

Here $\vec{E}_a^\pi$ and w_a^π are respectively the electric vector and the frequency of the imposed field as seen by an observer moving with the drift velocity of the particle population in question:

$$\vec{E}_a^\pi \equiv \vec{E}_a + \vec{v}_{o\pi} \times \vec{B}_a = \vec{E}_a + \vec{v}_{o\pi} \times \frac{\vec{k}_a \times \vec{E}_a}{w_a} \tag{20}$$

$$w_a^\pi \equiv w_a - \vec{k}_a \cdot \vec{v}_{o\pi}. \tag{21}$$

$\vec{\vec{M}}_a^\pi$ is the mobility tensor, normalized so that in the absence of the fluid pressure and the steady magnetic field it becomes the identity

$$\vec{\vec{M}}_a^\pi = \left(\vec{\vec{1}} - \frac{\gamma v_{T\pi}^2 \vec{k}_a \vec{k}_a}{\left(w_a^\pi\right)^2} \cdot + \frac{iq_\pi \vec{B}_o}{m_\pi w_a^\pi} \times \right)^{-1}. \tag{22}$$

Now find the second-order nonlinear conductivity of the plasma. Impose an electric field, comprising the superposition of 2 complex waves indexed b and c, upon the medium defined by (11)-(15):

$$\vec{E}(\vec{x}, t) = \vec{E}_b \exp(i\vec{k}_b \cdot \vec{x} - iw_b t) + \vec{E}_c \exp(i\vec{k}_c \cdot \vec{x} - w_c t). \tag{23}$$

This field evokes a second-order nonlinear response at the sum wavevector and sum frequency

$$(\vec{k}_{b+c}, w_{b+c}) \equiv (\vec{k}_b, w_b) + (\vec{k}_c, w_c). \tag{24}$$

This second-order nonlinear response comprises a fluid velocity of complex amplitude

$$\begin{aligned} \vec{V}_{b,c}^\pi = \vec{\vec{M}}_{b+c}^\pi \Bigg[& \frac{\vec{k}_{b+c}}{w_{b+c}^\pi} \vec{V}_b^\pi \cdot \vec{V}_c^\pi \\ & + \frac{\gamma v_{To}^2 \vec{k}_{b+c} \vec{k}_{b+c}}{\left(w_{b+c}^\pi\right)^2} \cdot \left(\vec{V}_b^\pi \frac{N_c^\pi}{n_{o\pi}} + \vec{V}_c^\pi \frac{N_b^\pi}{n_{o\pi}} \right) + \gamma(\gamma-2) v_{To}^2 \frac{\vec{k}_{b+c}}{w_{b+c}^\pi} \frac{N_b^\pi N_c^\pi}{n_{o\pi}^2} \\ & + \vec{V}_b^\pi \times \left(\frac{\vec{k}_c}{w_c^\pi} \times \left(\frac{iq_\pi \vec{B}_o}{m_\pi} \times \vec{V}_c^\pi \right) \right) + \vec{V}_c^\pi \times \left(\frac{\vec{k}_b}{w_b^\pi} \times \left(\frac{iq_\pi \vec{B}_o}{m_\pi} \times \vec{V}_b^\pi \right) \right) \Bigg] \end{aligned} \tag{25}$$

and a fluid density of complex amplitude

$$N^{\pi}_{b,c} = \frac{\vec{k}_{b+c}}{w^{\pi}_{b+c}} \cdot \left(n_{o\pi} \vec{V}^{\pi}_{b,c} + N^{\pi}_{b} \vec{V}^{\pi}_{c} + N^{\pi}_{c} \vec{V}^{\pi}_{b} \right). \tag{26}$$

Here $\vec{V}^{\pi}_{b}, N^{\pi}_{b}$ constitute the linear response to the field $\vec{E}_{b}$ at the wavevector and frequency $(\vec{k}_{b}, w_{b})$ and satisfy (18)-(21) with a replaced by b; $\vec{V}^{\pi}_{c}, N^{\pi}_{c}$ are defined analogously. The second-order nonlinear current response is given in terms of (25) and (26) by

$$\vec{J}_{b,c} = \sum_{\pi} q_{\pi} \left(n_{o\pi} \vec{V}^{\pi}_{b,c} + N^{\pi}_{b} \vec{V}^{\pi}_{c} + N^{\pi}_{c} \vec{V}^{\pi}_{b} + N^{\pi}_{b,c} \vec{V}_{o\pi} \right). \tag{27}$$

Now we may calculate the three-wave coupling coefficient defined by (8). That definition depends on $(\vec{k}_{a}, w_{a})$ only through the vector $\vec{f}_{Aa}$. For purposes of calculating (8), the basis polarization vectors $\vec{f}_{Aa}, \vec{e}_{Bb}, \vec{e}_{Cc}$ are regarded as given and the functional relationship of the coupling coefficient to these vectors then only involves $(\vec{k}_{b}, w_{b})$ and $(\vec{k}_{c}, w_{c})$. This functional relationship may be brought into a convenient form by defining

$$(\vec{k}_{\bar{a}}, w_{\bar{a}}) \equiv -(\vec{k}_{b}, w_{b}) - (\vec{k}_{c}, w_{c}), \tag{28}$$

$$\vec{e}_{A\bar{a}} \equiv \vec{f}_{Aa}. \tag{29}$$

Then the three-wave coupling coefficient (8) has a functional dependence on the basis polarization vectors which may be expressed as

Three-Dimensional Three-Wave Coupling Coefficient for Magnetized Warm-Fluid Plasma with Drifts

$$\begin{aligned} \left({}_{a}F^{NL(2)}_{b,c} \right)_{ABC} = -\sum_{\pi} \frac{m_{\pi}}{\epsilon_{o}} \Bigg\{ & n^{\pi}_{A\bar{a}} \vec{v}^{\pi}_{Bb} \cdot \vec{v}^{\pi}_{Cc} \\ & + n^{\pi}_{Bb} \vec{v}^{\pi}_{Cc} \cdot \vec{v}^{\pi}_{A\bar{a}} + n^{\pi}_{Cc} \vec{v}^{\pi}_{A\bar{a}} \cdot \vec{v}^{\pi}_{Bb} \\ & + \gamma(\gamma-2) v^{2}_{T\pi} \frac{n^{\pi}_{A\bar{a}} n^{\pi}_{Bb} n^{\pi}_{Cc}}{n^{2}_{o\pi}} \\ & + n_{o\pi} \frac{\vec{v}^{\pi}_{A\bar{a}} \cdot \left(v^{\pi}_{Bb} \times \vec{v}^{\pi}_{Cc} \right)}{w^{\pi}_{a} w^{\pi}_{b} w^{\pi}_{c}} \left(\vec{k}_{b} w^{\pi}_{c} - \vec{k}_{c} w^{\pi}_{b} \right) \cdot \frac{i q_{\pi} \vec{B}_{o}}{m_{\pi}} \Bigg\} \end{aligned} \tag{30}$$

Here the normalized fluid velocities $\vec{v}$ and normalized fluid densities n are the linear responses of the particle populations to the normalized fields $\vec{e}$. They are given by (18) and (19) with $\vec{E}$ replaced by $\vec{e}$ and the appropriate wavevectors and frequencies inserted. Explicitly,

$$\vec{v}^{\pi}_{A\bar{a}} \equiv \vec{\vec{M}}^{\pi}_{\bar{a}} \frac{iq_{\pi}\vec{e}^{\pi}_{A\bar{a}}}{m_{\pi}w^{\pi}_{\bar{a}}} \tag{31}$$

$$n^{\pi}_{A\bar{a}} \equiv n_{o\pi} \frac{\vec{k}_{\bar{a}} \cdot \vec{v}_{A\bar{a}}}{w^{\pi}_{\bar{a}}} \tag{32}$$

$$\vec{v}^{\pi}_{Bb} \equiv \vec{\vec{M}}^{\pi}_{b} \frac{iq_{\pi}\vec{e}^{\pi}_{Bb}}{m_{\pi}w^{\pi}_{b}} \tag{33}$$

$$n^{\pi}_{Bb} \equiv n_{o\pi} \frac{\vec{k}_{b} \cdot \vec{v}^{\pi}_{Bb}}{w^{\pi}_{b}} \tag{34}$$

$$\vec{v}^{\pi}_{Cc} \equiv \vec{\vec{M}}^{\pi}_{c} \frac{iq_{\pi}\vec{e}^{\pi}_{Cc}}{m_{\pi}w^{\pi}_{c}} \tag{35}$$

$$n^{\pi}_{Cc} \equiv n_{o\pi} \frac{\vec{k}_{c} \cdot \vec{v}^{\pi}_{Cc}}{w^{\pi}_{c}} . \tag{36}$$

Consider the symmetry properties of the expression (30). The coupling coefficient is certainly symmetric under simultaneous interchanges of the pair of indices B, C and the pair of indices b, c. This symmetry is obvious by inspection and from the method of derivation. The expression (30) is also invariant under simultaneous identical permutations of the three indices A, B, C and the three indices $\bar{a}$, b, c. To show this for the last term requires the use of vector algebra and the use of the wavevector-frequency sum relation (28).

The third-order conductivity of the system (11)-(15) gives rise to four-wave coupling coefficients according to (9). These coupling coefficients will be written in terms of quantities pertaining to the linear response and the second-order nonlinear response of the system. The third-order nonlinear conductivity of the plasma is found as follows. Impose an electric field, comprising the superposition of 3 complex waves indexed b, c, and d, upon the medium defined by (11)-(15):

$$\vec{E}(\vec{x}, t) = \vec{E}_b \exp(i\vec{k}_b \cdot \vec{x} - iw_b t)$$

$$+ \vec{E}_c \exp(i\vec{k}_c \cdot \vec{x} - iw_c t)$$

$$+ \vec{E}_d \exp(i\vec{k}_d \cdot \vec{x} - iw_d t). \tag{37}$$

This field evokes a third-order nonlinear response at the sum wavevector and sum frequency

$$(\vec{k}_{b+c+d}, w_{b+c+d}) \equiv (\vec{k}_b, w_b) + (\vec{k}_c, w_c) + (\vec{k}_d, w_d). \tag{38}$$

This response comprises a fluid velocity $\vec{V}^{\pi}_{b,c,d}$ and a fluid density $N^{\pi}_{b,c,d}$ for each particle population in the plasma. In terms of these third-order nonlinear responses, together with the second-order nonlinear responses given by (25)-(26), and the linear responses given by (18)-(21), the third-order nonlinear current may be written

$$\vec{J}_{b,c,d} = \sum_{\pi} q_{\pi}\Big(n_{o\pi}\vec{V}^{\pi}_{b,c,d}$$

$$+ N^{\pi}_{b}\vec{V}^{\pi}_{c,d} + N^{\pi}_{c}\vec{V}^{\pi}_{d,b} + N^{\pi}_{d}\vec{V}^{\pi}_{b,c}$$

$$+ N^{\pi}_{b,c}\vec{V}^{\pi}_{d} + N^{\pi}_{c,d}\vec{V}^{\pi}_{b} + N^{\pi}_{d,b}\vec{V}^{\pi}_{c}$$

$$+ N^{\pi}_{b,c,d}\vec{v}_{o\pi}\Big). \tag{39}$$

Now we may calculate the four-wave coupling coefficient defined by (9). Set

$$(\vec{k}_{\bar{a}}, w_{\bar{a}}) \equiv -(\vec{k}_b, w_b) - (\vec{k}_c, w_c) - (\vec{k}_d, w_d) \tag{40}$$

$$\vec{e}_{A\bar{a}} \equiv \vec{f}_{Aa}. \tag{41}$$

Then the four-wave coupling coefficient has a functional dependence on the basic polarization vectors which may be expressed as

Three-Dimensional Four-Wave Coupling Coefficient for Magnetized Warm-Fluid Plasma with Drifts

$$
\begin{aligned}
\left({}_{a}F^{NL(3)}_{b,c,d}\right)_{ABCD} = &- \sum_{\pi} \frac{m_{\pi}}{\epsilon_{o}} \\
&\Bigg\{ \left(n^{\pi}_{A\bar{a}}\vec{v}^{\pi}_{Bb} + n^{\pi}_{Bb}\vec{v}^{\pi}_{A\bar{a}}\right) \cdot \vec{v}^{\pi}_{Cc,\,Dd} + \left(n^{\pi}_{Cc}\vec{v}^{\pi}_{Dd} + n^{\pi}_{Dd}\vec{v}^{\pi}_{Cc}\right) \cdot \vec{v}^{\pi}_{A\bar{a},\,Bb} \\
&+ \left(n^{\pi}_{A\bar{a}}\vec{v}^{\pi}_{Cc} + n^{\pi}_{Cc}\vec{v}^{\pi}_{A\bar{a}}\right) \cdot \vec{v}^{\pi}_{Dd,\,Bb} + \left(n^{\pi}_{Dd}\vec{v}^{\pi}_{Bb} + n^{\pi}_{Bb}\vec{v}^{\pi}_{Dd}\right) \cdot \vec{v}^{\pi}_{A\bar{a},\,Cc} \\
&+ \left(n^{\pi}_{A\bar{a}}\vec{v}^{\pi}_{Dd} + n^{\pi}_{Dd}\vec{v}^{\pi}_{A\bar{a}}\right) \cdot \vec{v}^{\pi}_{Bb,\,Cc} + \left(n^{\pi}_{Bb}\vec{v}^{\pi}_{Cc} + n^{\pi}_{Cc}\vec{v}^{\pi}_{Bb}\right) \cdot \vec{v}^{\pi}_{A\bar{a},\,Dd} \\
&+ n_{o\pi}\left(\vec{v}^{\pi}_{A\bar{a},\,Bb} \cdot \vec{v}^{\pi}_{Cc,\,Dd} + \vec{v}^{\pi}_{A\bar{a},\,Cc} \cdot \vec{v}^{\pi}_{Dd,\,Bb} + \vec{v}^{\pi}_{A\bar{a},\,Dd} \cdot \vec{v}^{\pi}_{Bb,\,Cc}\right) \\
&- \frac{\gamma v^{2}_{T\pi}}{n_{o\pi}}\left(n^{\pi}_{A\bar{a},\,Bb}n^{\pi}_{Cc,\,Dd} + n^{\pi}_{A\bar{a},\,Cc}n^{\pi}_{Dd,\,Bb} + n^{\pi}_{A\bar{a},\,Dd}n^{\pi}_{Bb,\,Cc}\right) \\
&+ \frac{\gamma(\gamma-2)(\gamma-3)\,v^{2}_{T\pi}}{n^{3}_{o\pi}}\, n^{\pi}_{A\bar{a}}n^{\pi}_{Bb}n^{\pi}_{Cc}n^{\pi}_{Dd} \\
&- \frac{iq_{\pi}\vec{B}_{o}}{m_{\pi}n_{o\pi}} \cdot \Bigg[\frac{\left(n_{o\pi}\vec{v}^{\pi}_{A\bar{a},\,Bb} + n^{\pi}_{A\bar{a}}\vec{v}^{\pi}_{Bb} + n^{\pi}_{Bb}\vec{v}^{\pi}_{A\bar{a}}\right) \times \left(n_{o\pi}\vec{v}^{\pi}_{Cc,\,Dd} + n^{\pi}_{Cc}\vec{v}^{\pi}_{Dd} + n^{\pi}_{Dd}\vec{v}^{\pi}_{Cc}\right)}{w^{\pi}_{c+d}} \\
&+ \frac{\left(n_{o\pi}\vec{v}^{\pi}_{A\bar{a},\,Cc} + n^{\pi}_{A\bar{a}}\vec{v}^{\pi}_{Cc} + n_{Cc}\vec{v}^{\pi}_{A\bar{a}}\right) \times \left(n_{o\pi}\vec{v}^{\pi}_{Dd,\,Bb} + n_{Dd}\vec{v}^{\pi}_{Bb} + n_{Bb}\vec{v}^{\pi}_{Dd}\right)}{w^{\pi}_{d+b}} \\
&+ \frac{\left(n_{o\pi}\vec{v}^{\pi}_{A\bar{a},\,Dd} + n^{\pi}_{A\bar{a}}\vec{v}^{\pi}_{Dd} + n_{Dd}\vec{v}^{\pi}_{A\bar{a}}\right) \times \left(n_{o\pi}\vec{v}^{\pi}_{Bb,\,Cc} + n^{\pi}_{Bb}\vec{v}^{\pi}_{Cc} + n^{\pi}_{Cc}\vec{v}^{\pi}_{Bb}\right)}{w^{\pi}_{b+c}} \Bigg] \\
&+ \frac{iq_{\pi}\vec{B}_{o}n_{o\pi}}{m_{\pi}w^{\pi}_{\bar{a}}} \cdot \Bigg[\left(\left(\frac{\vec{k}_{c}}{w^{\pi}_{c}} - \frac{\vec{k}_{b}}{w^{\pi}_{b}}\right)\frac{\vec{k}_{d}}{w^{\pi}_{d}} + \left(\frac{\vec{k}_{d}}{w^{\pi}_{d}} - \frac{\vec{k}_{c}}{w^{\pi}_{c}}\right)\frac{\vec{k}_{c+d}}{w^{\pi}_{c+d}} + \left(\frac{\vec{k}_{b}}{w^{\pi}_{b}} - \frac{\vec{k}_{d}}{w^{\pi}_{d}}\right)\frac{\vec{k}_{b+d}}{w^{\pi}_{b+d}}\right) \cdot \vec{v}^{\pi}_{Dd}\left(\vec{v}^{\pi}_{A\bar{a}} \times \vec{v}^{\pi}_{Bb} \cdot \vec{v}^{\pi}_{Cc}\right) \\
&+ \left(\left(\frac{\vec{k}_{d}}{w^{\pi}_{d}} - \frac{\vec{k}_{c}}{w^{\pi}_{c}}\right)\frac{\vec{k}_{b}}{w^{\pi}_{b}} + \left(\frac{\vec{k}_{b}}{w^{\pi}_{b}} - \frac{\vec{k}_{d}}{w^{\pi}_{d}}\right)\frac{\vec{k}_{d+b}}{w^{\pi}_{d+b}} + \left(\frac{\vec{k}_{c}}{w^{\pi}_{c}} - \frac{\vec{k}_{b}}{w^{\pi}_{b}}\right)\frac{\vec{k}_{c+b}}{w^{\pi}_{c+d}}\right) \cdot \vec{v}^{\pi}_{Bb}\left(\vec{v}^{\pi}_{A\bar{a}} \times \vec{v}^{\pi}_{Cc} \cdot \vec{v}^{\pi}_{Dd}\right) \\
&+ \left(\left(\frac{\vec{k}_{b}}{w^{\pi}_{b}} - \frac{\vec{k}_{d}}{w^{\pi}_{d}}\right)\frac{\vec{k}_{c}}{w^{\pi}_{c}} + \left(\frac{\vec{k}_{c}}{w^{\pi}_{c}} - \frac{\vec{k}_{b}}{w^{\pi}_{b}}\right)\frac{\vec{k}_{b+c}}{w^{\pi}_{b+c}} + \left(\frac{\vec{k}_{d}}{w^{\pi}_{d}} - \frac{\vec{k}_{c}}{w^{\pi}_{c}}\right)\frac{\vec{k}_{d+c}}{w^{\pi}_{d+c}}\right) \cdot \vec{v}^{\pi}_{Cc}\left(\vec{v}^{\pi}_{A\bar{a}} \times \vec{v}^{\pi}_{Dd} \cdot \vec{v}^{\pi}_{Bb}\right) \Bigg] \Bigg\}
\end{aligned}
\tag{42}
$$

Here the normalized fluid velocities $\vec{v}$ and normalized fluid densities n are the linear and second-order nonlinear responses of the particle population to the normalized fields $\vec{e}$. They are given by (18), (19), (25), and (26) with $\vec{E}$ replaced by $\vec{e}$ and the appropriate wavevectors and frequencies inserted.

Consider the symmetry properties of the expression (42). The coupling coefficient is certainly symmetric under simultaneous identical permutations of the three indices B, C, D and the three indices b, c, d. This symmetry is obvious by inspection and from the method of derivation. The expression (42) is also invariant under simultaneous identical permutations of the four indices A, B, C, D and the four indices $\bar{a}$, b, c, d. To show this for the term involving $\vec{B}_o$ requires the use of vector algebra and the use of the wavevector-frequency sum relation (40). To show the symmetry for the last group of three terms proved too difficult by hand, and we resorted to MACSYMA — Project MAC's SYmbolic MAnipulation system.[1] This is a highly interactive computer system, implemented and maintained at M.I.T.'s Project MAC under the direction of Professor Joel Moses. Details of the symmetry proof, and of the calculations leading to (30) and (42), will be presented in a forthcoming thesis.

Application of Warm-Fluid Coupling Coefficients and Extension to Vlasov Plasma

We have already employed the expressions (30) and (42) for wave-wave coupling coefficients. They were used in dealing with the problem of laser-driven instabilities in unmagnetized plasma, so that $\vec{B}_o$ terms did not appear. First, electrostatic instabilities were considered.[2] Then a formalism was set up which systematically yielded all of the laser-driven instabilities.[3] The coupling coefficients were approximated physically, and used to derive the three-dimensional dispersion relations[4] for certain of the instabilities. Continued progress in this work is reported in Section XIII-B.1.

In the description of laser-driven instabilities in our previous reports[2-4] and in Section XIII-B.1 the four-wave coupling coefficients are essential. They describe how three-wave decay processes are modified at high values of the laser pump intensity. They also lead to instabilities that are intrinsically four-wave interactions and cannot be constructed from decay processes. Among these are the oscillating two-stream,[5] filamentation,[6] and modulation[7] instabilities, which can alter the gross time-average density distribution in the plasma.

The forms (30) and (42), with the $\vec{B}_o$ terms retained, will be used for investigating laser-driven instabilities in a pellet plasma with self-magnetic fields.[8] They will also be used in investigating the coupling to warm-fluid modes of injected microwave energy in Tokamaks.[9] These applications will make use of the three-dimensional nature of the expressions (30) and (42).

The expressions for the coupling coefficients have the units of energy density. They

were derived by expanding the equations of motion in terms of all but one of the interacting waves, and then were brought a posteriori to a form that is symmetric in all of the interacting waves. This symmetrization was accomplished through using somewhat involved algebra. We hope to rederive the coupling coefficients in a manner that is a priori symmetric in all interacting waves and less involved algebraically. We hope to do this by finding a quantity, analogous to energy density, that satisfies a conservation theorem, and then expanding this quantity in terms of the interacting waves. The second-order part of this quantity will regenerate the linear dispersion tensor. The third-order part of the conserved quantity will furnish three-wave coupling coefficients, the fourth-order part four-wave coupling coefficients, and so on.

If this scheme proves successful, it will be tried on the magnetized Vlasov plasma. Again, expressions for the coupling coefficients have been derived[10] by expanding the equations of motion. These coupling coefficients were limited to three-wave interactions, and further limited to certain directions of propagation. The proof of their symmetry is indirect. We hope to generate coupling coefficients as coefficients in the expansion of some conserved quantity, thereby obtaining them in a straightforward manner and in an a priori symmetric form. Such a simplified systematic derivation of three-dimensional coupling coefficients in magnetized Vlasov plasma is needed before a certain practical possibility can be investigated. This is the possibility of injecting microwave energy into Tokamaks and heating the plasma by coupling to ion-cyclotron modes, rather than to the warm-fluid modes envisaged in a previous report.[9]

The computation of coupling coefficients in unmagnetized Vlasov plasma, and of coupling coefficients for electrostatic waves propagating parallel to the magnetic field in magnetized Vlasov plasma, presents no difficulty. The plasma is regarded as a continuous superposition of cold beams, and the sums in (15), (30), and (42) are replaced by integrals, evaluated according to the Landau prescription.

References

1. "MACSYMA REFERENCE MANUAL," The Mathlab Group, Project MAC-M.I.T., Version Seven, September 1974.
2. D. C. Watson and A. Bers, Quarterly Progress Report No. 111, Research Laboratory of Electronics, M.I.T., October 15, 1973, pp. 84-98.
3. D. C. Watson and A. Bers, Quarterly Progress Report No. 113, Research Laboratory of Electronics, M.I.T., April 15, 1974, pp. 117-126.
4. D. C. Watson and A. Bers, Quarterly Progress Report No. 113, op. cit., pp. 59-74.
5. K. Nishikawa, J. Phys. Soc. Japan 24, 916-922 (1968).
6. J. W. Shearer and J. L. Eddleman, Phys. Fluids 16, 1953 (1973).
7. J. Drake, P. K. Kaw, Y. C. Lee, G. Schmidt, C. S. Liu, and M. N. Rosenbluth, Phys. Fluids 17, 778 (1974).
8. J. A. Stamper, K. Papadopoulos, R. N. Sudan, S. O. Dean, E. A. McLean, and J. M. Dawson, Phys. Rev. Letters 26, 1012 (1971).
9. A. Bers and C. F. F. Karney, Quarterly Progress Report No. 114, Research Laboratory of Electronics, M.I.T., July 15, 1974, pp. 123-131.
10. B. Coppi, M. N. Rosenbluth, and R. N. Sudan, Ann. Phys. (N.Y.) 55, 207-270 (1969).

3. WHISTLER WAVE EXCITATION AND ITS PARAMETRIC DOWN-CONVERSION TO ELECTROSTATIC ION CYCLOTRON WAVES

U. S. Atomic Energy Commission (Contract AT(11-1)-3070)

Abraham Bers, Charles F. F. Karney, Kim Theilhaber

Introduction

This report continues our study of the possibility of supplementary heating of Tokamak-type plasmas by RF energy applied externally. We have previously described the excitation of electrostatic electron plasma waves in the plasma above the lower hybrid frequency by an array of waveguides at the plasma wall, and studied the parametric down-conversion of these electrostatic electron plasma waves to electrostatic ion cyclotron waves in the homogeneous part of the plasma. The efficient excitation of the electrostatic electron plasma wave is restricted to a narrow range of wave numbers parallel to B_o, limited from below by accessibility restrictions and from above by electron Landau damping in the density gradient. The latter becomes particularly severe for high-temperature plasmas ($T_e \gtrsim 5$ keV). These waves are known to penetrate into the plasma in narrow resonance cone field structures that introduce a finite pump-extent threshold on the parametric down-conversion process. Both of these restrictions, the range of parallel wave numbers and the parametric threshold, require an array of waveguides at the plasma walls.

In this report we consider the excitation of the whistler wave in the same frequency regime, and study its parametric down-conversion to electrostatic ion cyclotron waves. As we shall show, this wave is much less damped in the density gradient by hot electrons, its propagation is not limited to a resonance cone structure, and its parametric coupling coefficient to electrostatic ion cyclotron waves is essentially the same as for the electrostatic electron plasma wave. Its main disadvantage is that it has a larger cutoff region near the wall than the electrostatic electron plasma wave has. We shall show that this, coupled with the accessibility condition, also leads to the requirement of an array of waveguides at the wall but these waveguides have very different characteristics from those for the electrostatic wave.

Linear Dispersion Relation for Homogeneous Plasma

Whistler waves are "cold" in the sense that neither the electron nor the ion pressure terms are important in the two-fluid momentum equations. The dielectric tensor $\overline{\overline{K}}$ may be written

$$\overline{\overline{K}} = \begin{bmatrix} K_\perp & iK_x & 0 \\ -iK_x & K_\perp & 0 \\ 0 & 0 & K_\parallel \end{bmatrix} \tag{1}$$

The electromagnetic dispersion relation[1-3] is

$$An^4 + Bn^2 + C = 0, \tag{2}$$

where

$n = kc/\omega$, with c the velocity of light

$$A = K_\perp \xi^2 + K_\parallel \zeta^2$$

$$B = -\left[\left(K_\perp^2 - K_x^2\right)\xi^2 + (1+\zeta^2)K_\perp K_\parallel\right]$$

$$C = \left(K_\perp^2 - K_x^2\right)K_\parallel$$

and $\xi = \sin\theta$ and $\zeta = \cos\theta$ are the direction cosines of $\overline{k}$.

We consider waves such that

$$\frac{\Omega_i}{\zeta} \ll \omega \ll \frac{\omega_{LH}^2}{\Omega_i}\zeta, \tag{3}$$

where ω_{LH} is the lower hybrid frequency

$$\omega_{LH}^2 = \frac{\omega_{pi}^2}{1 + \dfrac{\omega_{pe}^2}{\Omega_e^2}} \approx \min\left(\omega_{pi}^2, |\Omega_e|\Omega_i\right).$$

This expression for ω_{LH} is valid for $\omega_{pi}^2 \gg \Omega_i^2$, which is also the condition that (3) can be satisfied for some ω and ζ. When (3) holds

$$K_\parallel \approx -\omega_{pe}^2/\omega^2 \tag{4}$$

$$K_\perp \approx 1 + \frac{\omega_{pe}^2}{\Omega_e^2} - \frac{\omega_{pi}^2}{\omega^2} \tag{5}$$

$$K_x \approx -\frac{\omega_{pe}^2}{|\Omega_e|\omega} \tag{6}$$

$$AC \gg B^2$$

and so the solution to (2) is

$$n^2 = +\sqrt{-C/A} \approx |K_x|/|\zeta| \tag{7}$$

or

$$\omega \cong \frac{k^2c^2}{\omega_{pe}^2}|\Omega_e||\zeta|. \tag{8}$$

The region of validity of this dispersion relation is given by (3) and is illustrated in Fig. XIII-10.

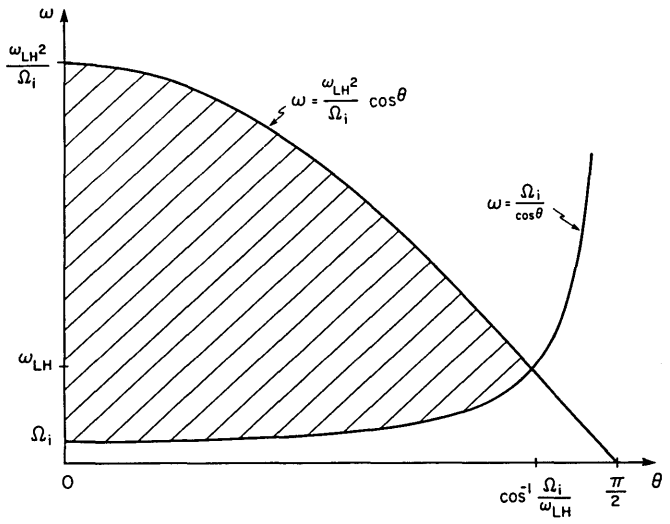

Fig. XIII-10. Region of validity of approximate whistler wave dispersion relation (Eq. 8). For simplicity, the region is shown extended until the inequalities in Eq. 3 become equalities.

Polarizations and Group Velocity for Homogeneous Plasma

The electric polarization of the whistler mode is found by taking the eigenvector of the dispersion tensor and by making use of (3) and (7). From $\overline{E}$ we can then easily find $\overline{B}$, $\overline{v}_e$, and $\overline{v}_i$. We find

$$\bar{E} = E_x \left[1,\ i|\zeta|,\ \frac{\omega}{|\Omega_e|}\ \frac{\xi|\zeta|}{\zeta}\right] \tag{9}$$

$$\bar{B} = E_x k/\omega[-i\zeta|\zeta|, \zeta, i\xi|\zeta|] \tag{10}$$

$$\bar{v}_e = E_x/B_o[i|\zeta|, -1, -i\xi|\zeta|/\zeta] \tag{11}$$

$$\bar{v}_i = iq_i\bar{E}/m_i\omega. \tag{12}$$

Note that $|E_z/E_x| = \xi\omega/|\Omega_e| \ll \zeta/\xi$ by (3), so $\bar{E}$ lies much closer to the perpendicular (x, y) plane than $\bar{k}$. Contrast this with electrostatic modes where $\bar{E}$ and $\bar{k}$ are parallel.

The group velocity can be obtained by differentiating (8) with respect to $\bar{k}$:

$$\bar{v}_g = \frac{\partial\omega}{\partial\bar{k}} = \frac{\omega}{k}\left[\xi,\ 0,\ \frac{1+\zeta^2}{\zeta}\right]. \tag{13}$$

Power Flow, Dissipation, and Damping Rate for Homogeneous Plasma

In general the power flow in a dielectric medium[2] is

$$\bar{S} = \frac{1}{2}\,\mathrm{Re}\,E \times H^* - \frac{\omega}{4}\epsilon_o \frac{\partial K_{ij}}{\partial\bar{k}} E_i^* E_j.$$

For a cold plasma $\partial K_{ij}/\partial\bar{k} = 0$, so by evaluating S_x, specializing to whistler waves, and using (3) and (7), we obtain

$$S_x = \frac{1}{2}\epsilon_o |E_x|^2 v_{gx} n_{\|}^2, \tag{14}$$

where from (13) $v_{gx} = \xi\omega/k$.

The power dissipation is given by

$$p = \frac{\epsilon_o\omega}{2} E^* \cdot \bar{\bar{K}}^a \cdot \bar{E}, \tag{15}$$

where $\bar{\bar{K}}^a$ is the anti-Hermitian component of the dielectric tensor. For a collisionless plasma this anti-Hermitian component is a result of the wave-particle interactions that lead to Landau and cyclotron damping. Since $\omega \gg \Omega_i$ from (3), we consider the ions unmagnetized. The Landau-damping terms for the ions then vary as $\exp\left[-\omega^2/k_z^2 a_i^2\right]$, where $a_s^2 \equiv 2T_s/m_s$. We evaluate these terms in the cold limit $|\omega/k_z a_s| \gg 1$ and $|\Omega_e/k_x a_e| \gg 1$.

With the electrons, Landau-damping terms in $\overline{\overline{K}}^a$ vary as $\exp\left[-\omega^2/k_z^2 a_e^2\right]$ and the electron cyclotron damping terms vary as $\exp\left[-(\omega-|\Omega_e|)^2/k_z^2 a_e^2\right]$. Since $\omega \ll |\Omega_e|$ from (3), the cyclotron damping terms are exponentially small compared with the Landau-damping terms. This is also true for approximately isothermal plasmas ($T_i \lesssim T_e$) $a_e^2 \gtrsim \frac{m_e}{m_i} a_i^2$, and so the electron Landau-damping terms are exponentially larger than the ion terms.

$\overline{\overline{K}}^a$ then becomes

$$\begin{bmatrix} 0 & 0 & 0 \\ 0 & K_\perp^a & iK_x^a \\ 0 & -iK_x^a & K_\parallel^a \end{bmatrix} \tag{16}$$

where

$$K_\perp^a = A2\lambda/z^2$$

$$K_x^a = A\sqrt{2\lambda}$$

$$K_\parallel^a = A2$$

$$A = \sqrt{\pi}\,\frac{\omega_{pe}^2}{\omega^2}\, z^3\, e^{-z^2}$$

$$z = \omega/k_z a_e, \qquad \lambda = \frac{1}{2}\left[\frac{k_x a_e}{|\Omega_e|}\right]^2.$$

We evaluate p, using (9) and (15),

$$p = \epsilon_o |E_x|^2\, \frac{\omega\omega_{pe}^2 \xi^2}{|\Omega_e|^2}\, \sqrt{\pi}\, e^{-z^2}\, z^3. \tag{17}$$

The largest term contributing to this expression is $\frac{\epsilon_o \omega}{2} |E_z|^2 K_\parallel^a$. Recall that E_z is much smaller than it would be if the mode were electrostatic, and so the dissipation is correspondingly smaller.

The spatial damping rate k_{xi} is then

$$k_{xi} = \frac{p}{2S_x} = \sqrt{\pi}\, e^{-z^2}\, z^3 \frac{\omega^2}{|\Omega_e|} \frac{\xi^2}{|\zeta|} \frac{1}{v_{gx}}. \tag{18}$$

The temporal damping rate for these waves has also been given by Akhiezer et al.[4] Our results are larger by a factor of two.

Accessibility Conditions for Whistler Waves

We now consider wave propagation into an inhomogeneous density profile. The Tokamak geometry is modeled as two-dimensional (see Fig. XIII-11). The plasma is homogeneous along a confining field $\underline{B}_o$ in the z direction. The density gradient in the x direction is transverse to $\underline{B}_o$. The density profile, where particle density $n_o(x)$ is plotted, has 2 parts: a linear portion extending over ($0 \leq x \leq L_n$) and, beyond $x = L_n$, a flat profile of constant density, the "interior" of the plasma. An array of open-ended waveguides, placed at the boundary of the enclosure, is shown in the diagram. A high-frequency wave (a whistler for our choice of parameters) propagates from the waveguide

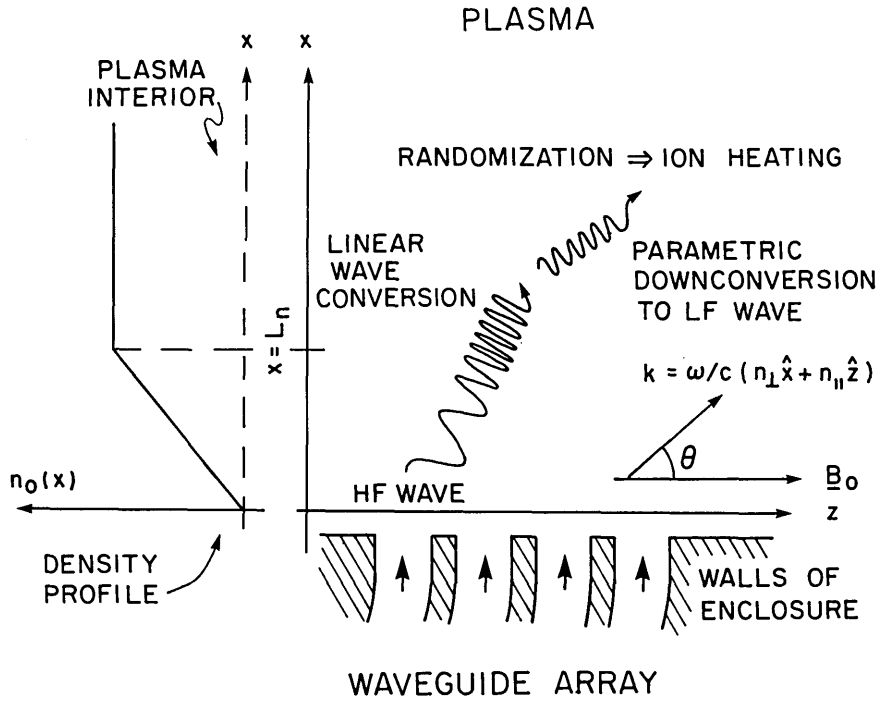

Fig. XIII-11. Geometry for the RF heating scheme.

apertures into the plasma. Inside the plasma the wave transfers energy to the medium by a parametric down-conversion to ion cyclotron waves, as we shall show. The "accessibility" conditions ensure that the wave reaches the plasma interior without excessive attenuation. Thus ion heating will not be confined to the edges of the density profile, but will occur over an appreciable part of the plasma.

The fields imposed along the boundary at x = 0 will be involved functions of z. For simplicity, we consider a single sinusoidal component of these functions, $\exp(ik_{\parallel}z)$. Superposition of the fields resulting from the propagation of each component would then provide a more complete picture. At any given particle density we consider a "local" dispersion relation corresponding to a homogeneous medium. The local wave dependence is of the form $\exp[i(k_{\parallel}z + k_{\perp}x)]$. Introducing an index of refraction $\bar{n}$, we have $\bar{k} = \frac{\omega}{c}\bar{n} = \frac{\omega}{c}(n_{\parallel}\hat{z} + n_{\perp}\hat{x})$. For fixed $n_{\parallel}$, $n_{\perp}$ is obtained from the cold-plasma dispersion relation (Eq. 2):

$$K_{\perp}n_{\perp}^4 + \left\{(K_{\parallel}+K_{\perp})\left(n_{\parallel}^2 - K_{\perp}\right) - K_x^2\right\} n_{\perp}^2 + K_{\parallel}\left\{\left(n_{\parallel}^2 - K_{\perp}\right)^2 + K_x^2\right\} = 0. \tag{19}$$

The K are elements of the dielectric tensor.[1] In the regime $\Omega_i \ll \omega \ll |\Omega_e|$ they are given by Eqs. 4-6.

Parker[5] and Troyon[6] have described the behavior of the solutions of (19) when $n_{\perp}^2$ is plotted as a function of density and $n_{\parallel}$ is considered a variable parameter. In particular, they have derived accessibility conditions on $n_{\parallel}$ which guarantee that $n_{\perp}^2$ remains real for $0 \leq x \leq L_n$ and is only negative close to the x = 0 boundary. Let $\omega_g = (\Omega_e\Omega_i)^{1/2}$ denote the mean of the cyclotron frequencies. Let the normalized variables Ω and Ω_{pi} be defined by

$$\Omega = \frac{\omega}{\omega_g} \qquad \Omega_{pi} = \frac{\omega_{pi}(L_n)}{\omega_g}.$$

Then the plasma interior is "accessible" for $n_{\parallel} > n_{\parallel\ell}$, where $n_{\parallel\ell}$ is given by

Case 1. For $\Omega^2 < 1$ and $\Omega^2 < \frac{\omega_{pi}^2(L_n)}{\omega^2}(1-\Omega^2)$

$$n_{\parallel\ell}^2 = \frac{1}{1-\Omega^2} \tag{20}$$

Case 2. For $\frac{\omega_{pi}^2(L_n)}{\omega^2}(1-\Omega^2) < \Omega^2 < 1$ or $\Omega^2 > 1$

$$n_{\parallel \ell}^2 = 1 + \left(2 - \frac{1}{\Omega^2}\right) \Omega_{pi}^2 + 2\Omega_{pi}\left[\left(1+\Omega_{pi}^2\right) - \Omega_{pi}^2/\Omega^2\right]^{1/2}. \tag{21}$$

Figure XIII-12 shows $n_\perp^2$ as a function of density, corresponding to these two cases. Both slow and fast modes are shown. In each case, $n_\parallel \cong n_{\parallel \ell}$. The upper branches of the dispersion curves correspond to the slow electrostatic wave.

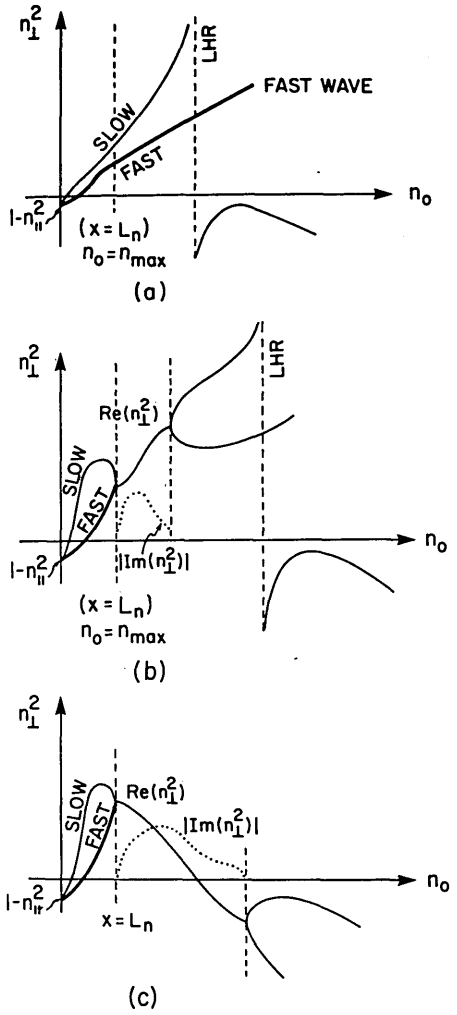

Fig. XIII-12.

$n_\perp^2$ vs density n_o for three cases. $n_u = n_o(L_n)$. In each case $n_\parallel = n_{\parallel \ell}$. For $n_\parallel > n_{\parallel \ell}$ the left-hand lobes and the cutoffs of the lower branches would be shifted outward. Lower branches correspond to the fast wave. For cases 1 and 2a where $\omega < \omega_g$, lower hybrid resonance occurs for the electrostatic mode at the line marked "LHR." In regions where $n_\perp^2$ is complex, $|\mathrm{Im}\,(n_\perp^2)|$ is indicated by a dotted line.

We shall be concerned with the lower branch, which corresponds to a fast electromagnetic wave. This mode is evanescent over $0 \leq x \leq x_c$, where the cutoff point x_c is obtained from $\omega_{pe}^2(x_c) = \omega\Omega_e\left(n_\parallel^2 - 1\right)$. For the linear density profile of length L_n

$$x_c = \frac{\omega_{pe}^2(x_c)}{\omega_{pe}^2(L_n)} L_n = \frac{\omega|\Omega_e|}{\omega_{pe}^2(L_n)} \left(n_\parallel^2 - 1\right) L_n. \tag{22}$$

The width of the cutoff region is critical. If it is too large, the wave launched at the boundary of the enclosure cannot tunnel across the cutoff region into regions of higher density, where evanescence ceases completely. Now at x = 0, we have

$$|k_\perp(0)| = \frac{\omega}{c}\sqrt{n_\parallel^2 - 1}. \tag{23}$$

The loss in amplitude because of tunneling through the cutoff region is roughly by a factor of $\exp(-|k_\perp(0)|x_c)$. In fact, since $|k_\perp|$ decreases as we move toward cutoff, this is an overestimate. For reasonable transmission through the cutoff region the exponent must be small, say, no larger than one. With $\frac{2\pi}{\lambda_g} = \frac{\omega_g}{c}$, we write in normalized form

$$|k_\perp(0)\,x_c| = 2\pi\sqrt{\frac{m_e}{m_i}\frac{\Omega^2}{\Omega_{pi}^2}}\left(n_\parallel^2-1\right)^{3/2}\left(\frac{L_n}{\lambda_g}\right) \leq 1.$$

The inequality sets an upper bound on $n_\parallel$. Thus

$$n_{\parallel u}^2 = 1 + \left(\frac{1}{2\pi}\sqrt{\frac{m_i}{m_e}}\right)^{2/3}\left(\frac{\lambda_g}{L_n}\right)^{2/3}\left(\frac{\Omega_{pi}}{\Omega}\right)^{4/3} = 1 + 3.6\left(\frac{\omega_{pi}^2(L_n)}{\omega\,\omega_g}\frac{\lambda_o}{L_n}\right)^{2/3} \tag{24}$$

where $m_i/m_e = 1836$ and λ_o is the free-space wavelength. This should be compared with the electrostatic mode cutoff conditions $x_c = L_n\frac{m_e}{m_i}\left(\frac{\omega}{\omega_{pi}(L_n)}\right)^2$. Correspondingly, $n_{\parallel u}^2 = 1 + \left(\frac{m_i}{2\pi m_e}\right)^2\left(\frac{\omega}{\omega_{pi}(L_n)}\right)^2\left(\frac{\lambda_o}{L_n}\right)^2$, which yields a much larger value for $n_{\parallel u}$ than (24) does.

The accessibility condition can now be stated:

$$n_{\parallel \ell}(\Omega, \Omega_{pi}) \leq n_\parallel \leq n_{\parallel u}\left(\Omega, \Omega_{pi}, \frac{L_n}{\lambda_g}\right).$$

For fixed Ω_{pi}, curves of $n_{\parallel \ell}$ and $n_{\parallel u}$ have been plotted as functions of ω in Fig. XIII-13. Six special cases are considered, corresponding to B_o = 2.5, 5, 10T and $n_o(L) = 10^{13}$ and 10^{14} cm^{-3}. In each case, $n_{\parallel u}$ is plotted for a series of values of L: L = 5, 10, 25, 50, and 100 cm.

Consider, first, the case of a fixed density with a variable magnetic field. Increasing B_o will shift <u>downward</u> the region of accessible $n_\parallel$, and decrease the absolute width of the

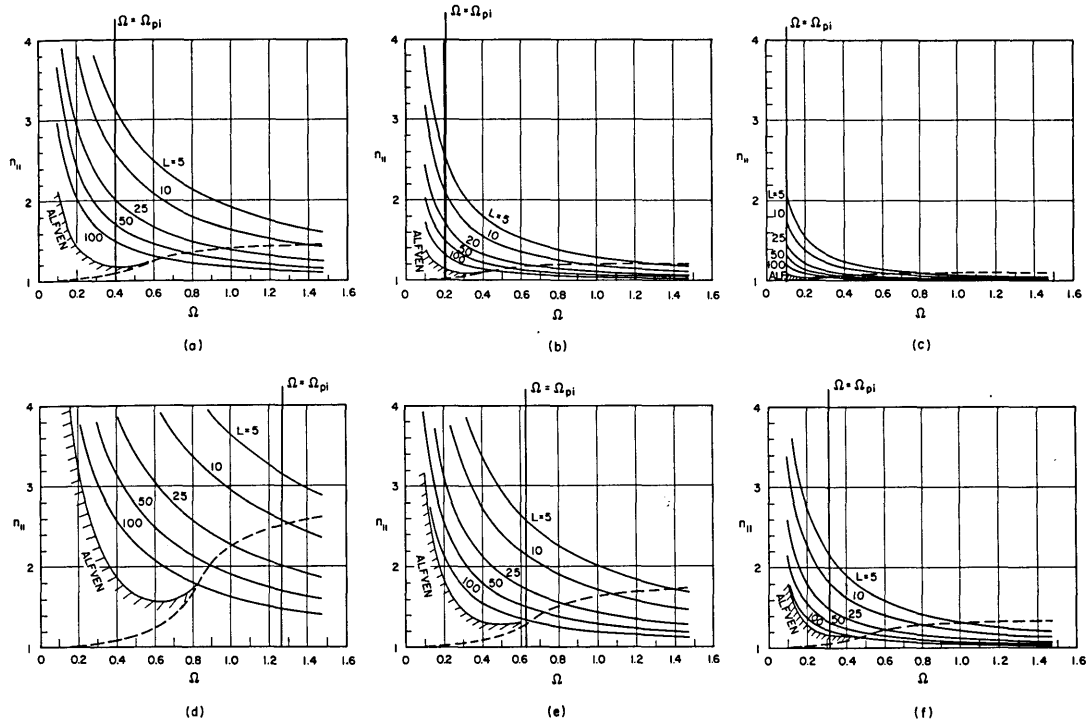

Fig. XIII-13. $n_{\|\ell}$ (dashed lines) and $n_{\|u}$ (solid lines) vs the normalized frequency $\Omega = \omega/(\Omega_e \Omega_i)^{1/2}$. In each case $n_{\|u}$ is plotted for several values of L (in cm). Given Ω and L, the accessible range of $n_{\|}$ is between the $n_{\|\ell}$ and the corresponding $n_{\|u}$ curves. Below the line marked "ALFVEN," high-frequency Alfvén waves propagate. With a pump frequency $\omega > \omega_{pi}$, only the region to the right of $\Omega = \Omega_{pi}$ (heavy vertical line) need be considered.

(a) $n_o = 10^{13}$ cm^{-3}, $B_o = 2.5$T, $\omega_g = 10.6$G-rad/sec
(b) $n_o = 10^{13}$ cm^{-3}, $B_o = 5$T, $\omega_g = 21.2$G-rad/sec
(c) $n_o = 10^{13}$ cm^{-3}, $B_o = 10$T, $\omega_g = 42.5$G-rad/sec
(d) $n_o = 10^{14}$ cm^{-3}, $B_o = 2.5$T, $\omega_g = 10.6$G-rad/sec
(e) $n_o = 10^{14}$ cm^{-3}, $B_o = 5$T, $\omega_g = 21.2$G-rad/sec
(f) $n_o = 10^{14}$ cm^{-3}, $B_o = 10$T, $\omega_g = 42.5$G-rad/sec

region somewhat. For instance, let $\omega = 9 \times 10^9$ sec^{-1}, corresponding to $\omega/\omega_g = 0.8$ at $B_o = 2.5$T (Fig. XIII-13a). In this case, density profiles with $L_n > 50$ cm are not accessible, since for such lengths $n_{\|u} < n_{\|\ell}$. On the other hand, for $L_n = 10$ cm the interior of the plasma is accessible to components with roughly $1.4 \leq n_{\|} \leq 1.8$. If B_o is doubled (Fig. XIII-13b), $\omega/\omega_g = 0.4$ and the lengths $L_n = 50$ cm and 100 cm are now accessible, albeit for small ranges of $n_{\|}$. The accessible range for $L_n = 10$ cm has been shifted downward. It is now $1.1 \leq n_{\|} \leq 1.5$. At still higher magnetic fields ($B_o = 10$T, $\omega/\omega_g = 0.2$), the width of this range decreases slightly. It is now $1.05 \leq n_{\|} \leq 1.4$ (Fig. XIII-13c).

Similarly, for fixed B_o and ω, increasing particle density results in a wider range of accessible $n_{\|}$ which is shifted upward too. Increasing n_o also makes larger L_n accessible.

One can determine from the graphs which waves will propagate at the maximum density. For $1 < n_{\|}^2 \ll (\omega_{pi}/\omega)^2$ large-angle, "high-frequency" Alfvén waves will propagate. The dispersion relation, according to Stringer,[7] is

$$\omega = kC_A \tag{25}$$

where C_A is the Alfvén velocity, $C_A^2 = B_o^2/(\mu_o n_o m_i)$. The range of validity of (25) is shown at the left of the line marked "ALFVEN" in Fig. XIII-13. For $\omega > \omega_{pi}$, Alfvén

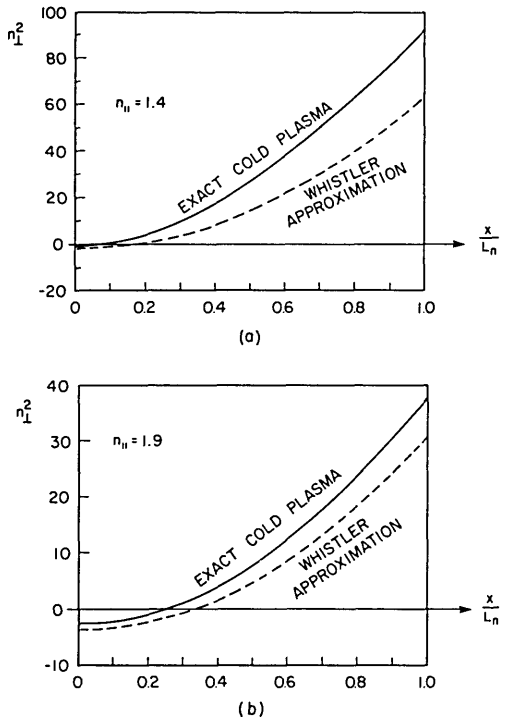

Fig. XIII-14.

$n_\perp^2$ vs relative position in the density profile. In each case $B_o = 10$ T and $n_o(L_n) = 10^{14}$ cm^{-3}. (a) $n_{\|} = 1.4$, for which lengths $L_n \leq 25$ cm are accessible. (b) $n_{\|} = 1.9$, only profiles with $L_n \leq 5$ cm are accessible. In each case a plot of the whistler wave approximation (26) is shown.

waves propagate only in a narrow region, hugging the $n_{\|\ell}$ curve. But for $n_{\|}^2 \gg (\omega_{pi}/\omega)^2$ and $n_{\|}^2 \gg 1$ whistler waves propagate with the dispersion relation (Eq. 8) $\omega = \frac{k^2C^2}{\omega_{pe}^2}\Omega_e \cdot \cos(\theta)$. Figure XIII-14 shows a comparison of the approximate and exact dispersion relations for two values of $n_{\|}$.

Polarization and Propagation of Whistler Waves in the Density Gradient

As the electromagnetic wave propagates from the boundary of the plasma enclosure it undergoes linear wave conversion; that is, its wavelength and polarization change. In the whistler regime the expression for $n_\perp^2$ as a function of position in the density profile, under the assumption $n_{\|}^2 \gg 1$, from Eqs. 3 and 7, is

$$n_\perp^2(x) \cong \left(\frac{\omega_{pe}^2(x)}{n_{\|}\omega|\Omega_e|}\right)^2 - n_{\|}^2, \tag{26}$$

which yields an approximate expression for the cutoff in $n_\perp$, $\omega_{pe}^2(x_c) \cong n_{\|}^2\omega|\Omega_e|$.

The field polarizations are obtained from the general cold-plasma expressions

$$\frac{E_y}{E_x} = \frac{+iK_x}{n_\perp^2 + n_{\|}^2 - K_\perp} \tag{27}$$

$$\frac{E_z}{E_x} = \frac{n_{\|}n_\perp}{n_\perp^2 - K_{\|}}. \tag{28}$$

In particular, at the edge of the density profile ($x = 0$, $n_o = 0$) the fast cold-plasma wave is linearly polarized in the y direction. From (9) we have

$$\frac{E_y}{E_x} \cong i\left(\frac{\omega|\Omega_e|}{\omega_{pe}^2(x)}\right)n_{\|}^2 \tag{29}$$

$$\frac{E_z}{E_x} \cong \frac{\omega^2}{\omega_{pe}^2(x)}\left[\left(\frac{\omega_{pe}^2(x)}{\omega\Omega_e}\right)^2 - n_{\|}^4\right]^{1/2} < \frac{\omega}{\Omega_e}. \tag{30}$$

The magnetic fields can be obtained from Faraday's law:

$$B_x \cong \frac{i}{c} \frac{\omega|\Omega_e|}{\omega_{pe}^2(x)} n_{\|}^3 E_x \tag{31}$$

$$B_y \cong \frac{n_{\|}}{c} E_x \tag{32}$$

$$B_z \cong \frac{in_{\|}}{c} \left[1 - n_{\|}^2 \frac{\omega\Omega_e}{\omega_{pe}^2(x)}\right]^{1/2} E_x. \tag{33}$$

Thus at cutoff ($x = x_c$) the wave is circularly polarized and propagates parallel to B_o. At larger densities the inequalities $|E_x| \gg |E_y| \gg |E_z|$ hold.

The x component of the power density for the fields of the whistler wave (Eq. 14) is given by

$$S_x = \frac{1}{2} \cdot c\epsilon_o |E_y(x)|^2 n_{\perp}(x). \tag{34}$$

Since S_x must be conserved with increasing density, it follows that $|E_y(x)| \sim \frac{1}{\sqrt{n_{\perp}(x)}}$, which is the usual WKB approximation for the propagation of a simple wave in an inhomogeneous medium. Near cutoff Eq. 34 is no longer valid. Far from cutoff $\omega_{pe}^2(x)/\omega\Omega_e \gg n_{\|}^2$, and the field intensity (Eqs. 26 and 29) varies as

$$|E|^2 \cong |E_x|^2 \sim n_{\perp}(x) \sim x. \tag{35}$$

Ray trajectories are useful in predicting how energy propagates in the plasma when the source is of finite extent. The group velocity for the whistler wave is given by

$$\bar{v}_g = \frac{\omega}{k}\left[\sin\theta, 0 \frac{1 + \cos^2\theta}{\cos\theta}\right].$$

The ray trajectory is parallel to $\bar{v}_g$ at each point of its path. Let α denote the angle between $\bar{v}_g$ and $\bar{B}_o$. The equation for the ray is then

$$\frac{dz}{dx} = \frac{\cos\theta + \frac{1}{\cos\theta}}{\sin\theta} \equiv \cot(\alpha), \tag{36}$$

where θ is a function of density, and hence of x. Let L_n denote the width of the density gradient. Integration of (36) yields

$$z(x, n_{\|}) = L_n n_{\|}^2 \frac{\omega\Omega_i}{\omega_{pi}^2(L_n)} \cdot I(\sec\theta), \tag{37}$$

where $I(\sec\theta)$ is defined by

$$I(\sec\theta) = \frac{1}{2}\left[3\log(\sec\theta+\tan\theta)+\tan\theta\sec\theta\right] \tag{38}$$

and, from Eq. 7, we have

$$\cos\theta = \frac{n_{\|}^2\omega\Omega_i}{\omega_{pi}^2(x)}. \tag{39}$$

The initial condition chosen for (36) is $z(x_c) = 0$. The wave is assumed to penetrate perpendicular to $\overline{B}_o$, as long as it remains in the cutoff region. In Fig. XIII-15 Eq. 37 is

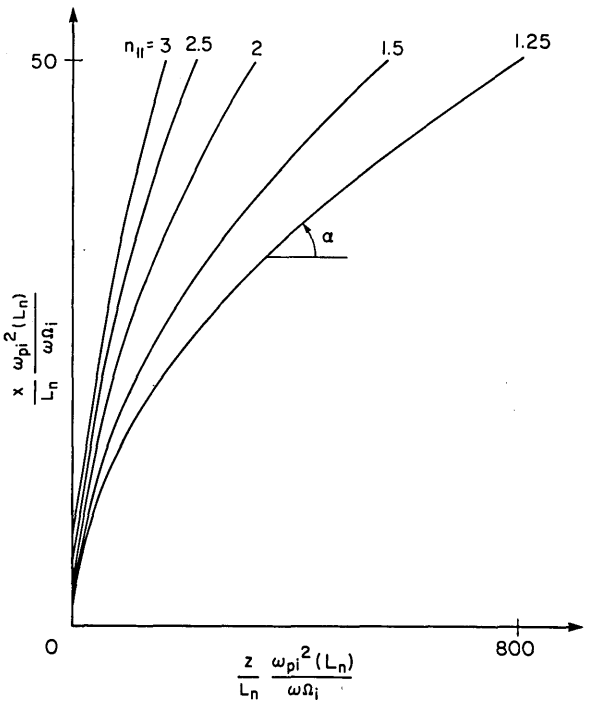

Fig. XIII-15. Ray paths for whistler waves according to Eq. 37. Note scale distortion by a factor of 20.

plotted against x for various $n_{\|}$. For $n_{\|}^2 \ll \left|\frac{\omega_p^2(L_n)}{\omega\Omega}\right|$ (or $\cos(\theta) \ll 1$), (37) reduces to

$$z(L_n) \cong \frac{1}{2}\cdot\frac{\omega_p^2(L_n)}{\omega\Omega n_{\|}^2}\,L_n. \tag{40}$$

Hence components with large $n_{||}$ do not propagate as far down the magnetic field.

Nonlinear Coupling to Electrostatic Ion Cyclotron Waves

We now consider coupling from a whistler wave (mode a), whose dispersion relation is given by (8), to an electron plasma wave (mode b), with an approximate dispersion relation

$$\omega_b^2 \approx \omega_{pi}^2 + \omega_{pe}^2 \cos^2 \theta, \tag{41}$$

and an electrostatic ion cyclotron wave $\left(\omega_n^2 = \Omega_i^2 + k_{\perp n}^2 c_s^2\right)$ satisfying the usual resonance conditions (see Fig. XIII-16)

$$\omega_n = \omega_a + \omega_b$$

$$\bar{k}_n = \bar{k}_a + \bar{k}_b.$$

(Note that we consider $\omega_a > |\omega_b| > \omega_{pi}$. Hence mode a cannot be an Alfvén mode; see the condition preceding Eq. 25.) This interaction is similar to the nonlinear interaction of two electron plasma waves and an electrostatic ion cyclotron wave, which has been

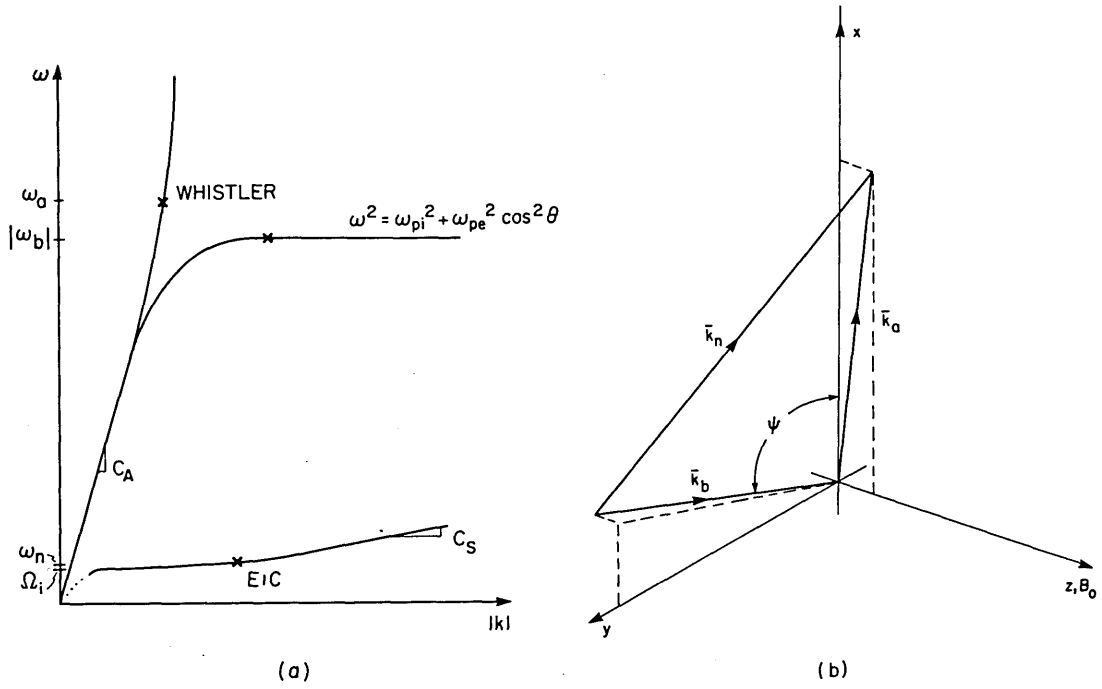

Fig. XIII-16. (a) ω, k and (b) $\bar{k}$ diagrams for the modes taking part in the parametric reaction.

studied previously.[8-10] In that case the dominant contribution to the coupling coefficient arose from the z component of the convective term in the nonlinear driving term to the electron momentum equation

$$P_{z\,conv} = -\frac{1}{2} mn_o[(\bar{v}_a \cdot i\bar{k}_b) v_{bz} + (\bar{v}_b \cdot i\bar{k}_a) v_{az}]. \tag{42}$$

The problem is different now in two respects. First, $\bar{E}_a$ is closer to being perpendicular to $\bar{B}_o$ than $\bar{k}_a$ (see Eq. 9) so v_{az} is much smaller than v_{bz} (b is still an electrostatic mode so $\bar{E}_b /\!/ \bar{k}_b$), and hence we may neglect the $(\bar{v}_b \cdot i\bar{k}_a) v_{az}$ term. Second, a is now an electromagnetic mode and so we must include the z component of the Lorentz contribution to $\bar{P}$:

$$P_{z\,Lor} = \frac{1}{2} qn_o(\bar{v}_b \times \bar{B}_a)_z. \tag{43}$$

Evaluating the first terms of (42) and (43) by using the polarizations given in Eqs. 9-11, we obtain

$$P_z = \frac{1}{2} qn_o \frac{E_{ax}}{B_o} E_{by} \frac{k_{nz}}{\omega_a}. \tag{44}$$

Hence the nonlinear charge fluctuation at $(\omega_n, \bar{k}_n)$ caused by modes a and b is

$$\rho^{(2)}_{a,b} = -\frac{1}{2} \epsilon_o \frac{\omega^2_{pe}}{v^2_{Te}} \frac{E_{ax}}{B_o} \frac{E_{by}}{\omega_a}, \tag{45}$$

and the growth rate γ_o is given by

$$\frac{\gamma_o}{(|\omega_b|\omega_n)^{1/2}} = \frac{|E_n \rho^{(2)}_{a,b}|}{4k_n (W_b W_n)^{1/2}}$$

$$= \frac{1}{4} \frac{k_{n\perp} c_s}{\omega_n} \frac{\omega_{pe}}{\omega_a} \frac{v_{a\perp}}{v_{Te}} \sin\psi, \tag{46}$$

where $v_a = |E_{ax}|/B_o$, and ψ is defined in Fig. XIII-16b. Equation 46 is formally identical to this equation for the growth rate for exciting EIC waves by the electrostatic pump.[9]

Array Design Considerations

The exciting structure that we assume is a waveguide array as shown in Fig. XIII-17. Note that the waveguides support TE_{01} with the $\bar{E}$ field in the y direction. This excites

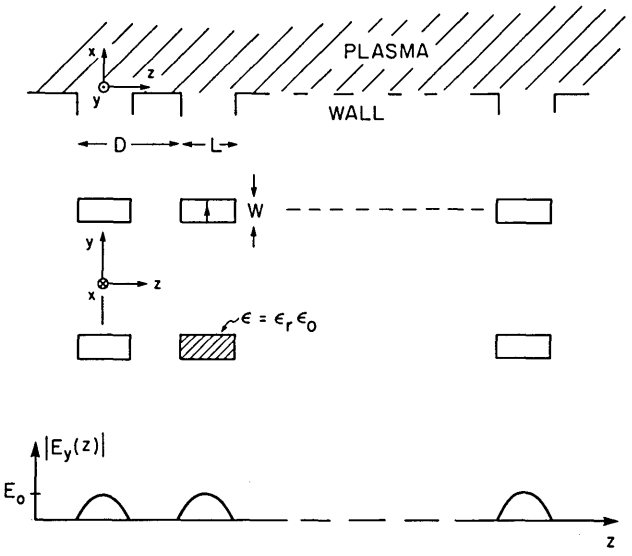

Fig. XIII-17. Waveguide array and the field pattern at the wall (x = 0).

the electromagnetic modes in preference to the electrostatic mode considered in a previous report.[11] The spectrum for the fields produced by this structure (Fig. XIII-18) is

$$E_y(k_z) = E_o \cos\left(\frac{L}{2} k_z\right) \frac{2\pi L}{\pi^2 - k^2 L^2} \frac{\sin\left[\frac{ND}{2}(k_z - \phi/D)\right]}{\sin\left[\frac{D}{2}(k_z - \phi/D\right]}. \tag{47}$$

For a given plasma and operating frequency we can find which range of $n_{||}$, ($n_{||\ell}$ - $n_{||u}$) is accessible, by using Eqs. 20, 21, 24 and Fig. XIII-13. Thus for a plasma with $n_o = 10^{14}$ cm^{-3}, $B_o = 5$T, and a density scale length $L_n = 50$ cm, when operating slightly above ω_{pi} we find that $n_{||}$ between approximately $n_{||\ell} = 1.3$ and $n_{||u} = 1.5$ are accessible. This is the plasma that we use as an example here.

For evacuated waveguides we require $L > \lambda_o/2$, where λ_o is the free-space wavelength ($2\pi c/\omega$). Since $D > L$, the separation of peaks in the k_z spectrum is $2\pi/D < 2\omega/c_L$, which, of course, is a separation of 2 in $n_{||}$. Since the inaccessible region always extends at least from $n_{||} = -1$ to $n_{||} = 1$, we would always end up with the largest peak in the central inaccessible portion, with a resulting drop in efficiency. This situation may be remedied by loading the waveguides with dielectric, $\epsilon = \epsilon_r \epsilon_o$ (in practice, a similar effect may be realized by using ridged waveguides). In that case $L > \frac{\lambda_{o/2}}{\sqrt{\epsilon_r}}$, which gives a separation of at most $2\sqrt{\epsilon_r}$ in $n_{||}$. In our example, we wish to put the peaks at $n_{||} = \pm\frac{1}{2}(n_{||u} + n_{||\ell}) = \pm 1.4$. This we can do with, say, $\epsilon_r = 4$, $\phi = \pi$, $L = 1.2$, $\frac{\lambda_{o/2}}{\sqrt{\epsilon_r}} = 0.3\,\lambda_o$

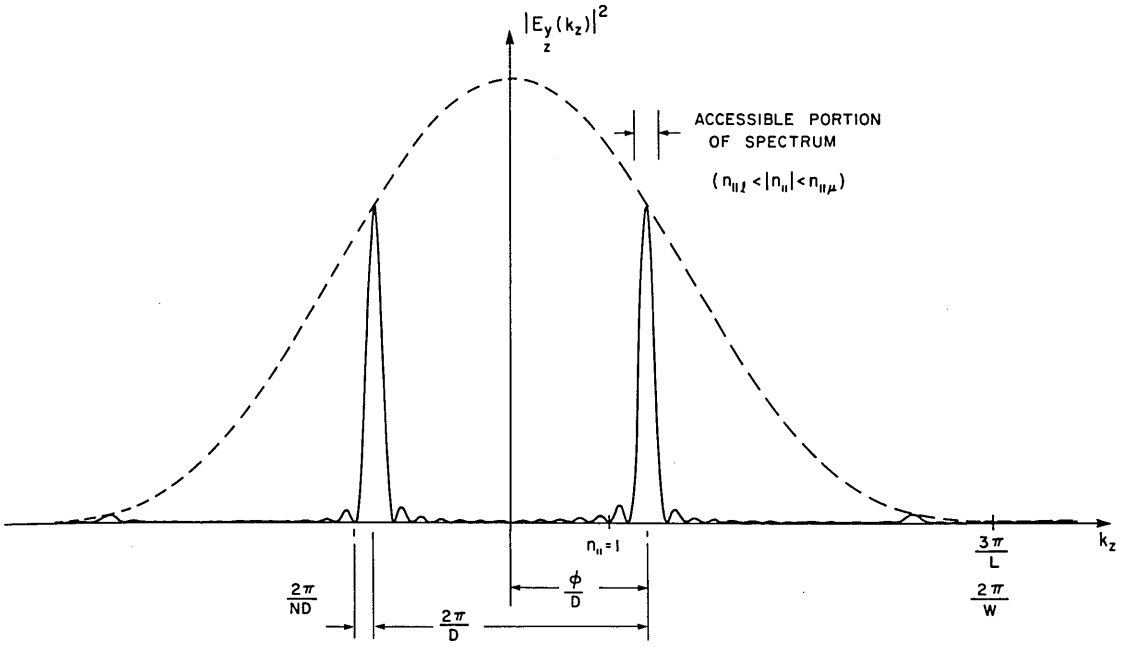

Fig. XIII-18. Spectrum of fields at the wall. $N = 14$, $L = 0.3\ \lambda_o$, $D = 0.36\ \lambda_o$, $\phi = \pi$.

and $D = 1.2$, $L = 0.36\ \lambda_o$.

The final consideration in designing an array is that the width of the peaks in the k_z spectrum be such that their half-power points lie in the accessible region. This puts a lower bound on N. The separation of the first two zeros in a single peak is $4\pi/ND$, and the half-power width is $\sim 2\pi/ND$. Thus if $\Delta n_\parallel = n_{\parallel u} - n_{\parallel \ell}$ is the accessible range of $n_\parallel$, $\Delta n_\parallel > \frac{c}{\omega}\frac{L}{ND}\frac{2\pi}{ND}$. In our example, $\Delta n_\parallel = 1.5 - 1.3 = 0.2$ and $D = 0.36\ \lambda_o$, we find $N \geq 14$. (Note that Fig. XIII-18 is plotted with these parameters.) If we take $\omega \approx \omega_{pi} = 1.3 \times 10^{10}\ s^{-1}$, the z extent of the array is $ND \approx 70$ cm. It should be noticed that the condition on the half-power points lying inside the accessible region may be too stringent, if we consider the variations that may be expected in plasma parameters. It may be more reasonable to choose a lower value for N to ensure that some power will be coupled for a range of plasma parameters.

Field Structure inside the Plasma

We have designed an array to produce a relatively narrow band of $n_\parallel$ that is accessible to the plasma. As these $n_\parallel$ penetrate the plasma, they follow slightly different rays, and this leads to a dispersion of the pump field. In fact, if we trace rays at $n_{\parallel u}$ and $n_{\parallel \ell}$, starting at the same point at $x = 0$, then, from (37), at $x = L_n$ we have

$$\delta z = z(n_{\|\ell}) - z(n_{\|u}) = \frac{\omega\Omega_i}{\omega_{pi}^2} L_n \left[n_{\|\ell}^2 I\left(\frac{\omega_{pi}^2}{\omega\Omega_i n_{\|\ell}^2}\right) - n_{\|u}^2 I\left(\frac{\omega_{pi}^2}{\omega\Omega_i n_{\|u}^2}\right)\right], \tag{48}$$

where I is defined in (38). These rays for $L_n = 50$ cm and $n_{\|\ell} = 1.3$, $n_{\|u} = 1.5$ are shown in Fig. XIII-19. In this case $\delta z \approx 100$ cm. Since rays can start anywhere, if there are waveguides the total extent of the pump inside the plasma is roughly $\Delta z = \delta z + ND \approx 170$ cm. The x extent is found by multiplying Δz by $\tan \alpha$, where α, the angle of the ray path, is given in (36). Since $\sin\theta \approx 1$, $\tan\alpha \approx \cos\theta \approx n_{\|} \frac{\omega|\Omega_e|}{\omega_{pe}^2} \approx 0.07$, and thus $\Delta x \approx 12$ cm.

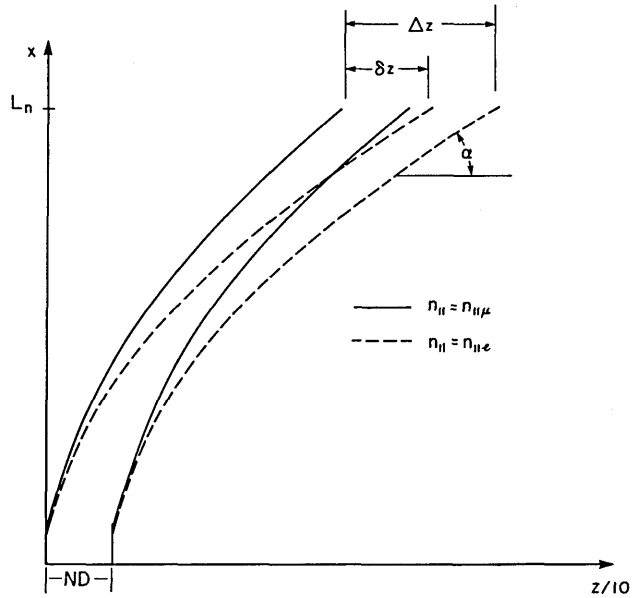

Fig. XIII-19. Rays with $n_{\|} = n_{\|\ell} = 1.3$ and $n_{\|} = n_{\|u} = 1.5$, starting at $z = 0$ and $z = ND = 70$. $L_n = 50$ cm.

We also need to know the field strength inside the plasma compared with its value at the waveguides. We can estimate this field strength by requiring that the total x-directed power flow is independent of x. Beyond cutoff, from (14), we have

$$\int S_x \, dz \sim \Delta z(x) \left| E_x(x) \right|^2 \cos\theta(x). \tag{49}$$

In order to relate the fields inside the plasma ($x = L_n$) to those at cutoff ($x = x_c$), we remove the singularity at cutoff predicted by WKB theory, by extending the region of validity of (49) to cutoff. Then

$$\left|\frac{E_x(L_n)}{E_x(x_c)}\right|^2 \approx \frac{\Delta_z(x_c)}{\Delta z(L_n)} \frac{\cos\theta(x_c)}{\cos\theta(L_n)} \approx \frac{ND}{\delta z + ND} \frac{1}{\cos\theta}. \tag{50}$$

Here we have neglected the effect of Landau damping because k_{xi} for these modes is $\sim 10^{-5}$ m^{-1} for $T_e \sim 5$ keV and so can be neglected. When operating near the maximum lower hybrid frequency the field at cutoff is related to the waveguide field.

$$\frac{E_x(x_c)}{E_o} \approx \exp\left(-\sqrt{n_{\|}^2 - 1}\, \frac{\omega}{c} x_c\right) \sim \exp\left(-\sqrt{n_{\|}^2 - 1}\, \frac{\Omega_i}{c} L_n\right). \tag{51}$$

For our example we get

$$E_x(L_n) \sim 2E_o. \tag{52}$$

Threshold for Parametric Interaction

As in a previous report,[10] we take the threshold condition to be the requirement that an unstable pulse e-fold many times during the time when the center of the pulse remains in the pump region. The velocity of the pulse center[10] is $\frac{1}{2}(\bar{v}_b + \bar{v}_n) \approx \frac{1}{2}\bar{v}_b$, since $v_b \gg v_n$. The time τ when the pulse remains in the pump region is

$$\tau \approx \frac{2\Delta z}{v_{bz}} \left|1 - \frac{v_{az} v_{bx}}{v_{ax} v_{bx}}\right|^{-1} \approx \frac{2\Delta z}{v_{bz}}. \tag{53}$$

Now from the dispersion relation for b (41)

$$v_{bz} = \frac{\omega_{pe}^2 \cos\theta_b}{\omega_b k_b} \approx \frac{\sqrt{\omega_b^2 - \omega_{pi}^2}}{\Omega_i} v_{Te}, \tag{54}$$

since $k_b \sim k_n \sim \Omega_i/c_s$. Therefore the threshold condition is

$$\gamma_o \tau = \frac{2\gamma_o \Delta z}{v_{Te}} \frac{\Omega_i}{\sqrt{\omega_b^2 - \omega_{pi}^2}} \gg 1. \tag{55}$$

Using our example with $E_o = 10$ kV/cm, $T_e = 5$ keV, $\omega_b = 1.1\,\omega_{pi}$ and γ_o given by (46), we find $\gamma_o \tau \approx 3$.

Conclusion

We have examined the coupling from whistler waves in a large Tokamak, with the design objective of achieving efficient coupling from the waveguides to the plasma. There

are, however, other criteria for designing an array. The first is to see what powers are required to produce measurable ion heating in a present Tokamak (for example, T_i from 200 eV to 300 eV for ATC) with only a few phased waveguides, say, 2 or 3. Second, the design of the array might be optimized so as to produce an efficient coupling of the waveguide power into the plasma. Again, this should be designed for present Tokamaks, so that the efficiency of RF heating can be measured. Finally, we need to know the array design required for a large Tokamak such as the ETR to heat the ions to ignition temperature as we did for heating by electrostatic waves.[11] Detailed comparison of these designs, when electrostatic and whistler modes are excited, will form the basis of a future report.

References

1. W. P. Allis, S. J. Buchsbaum, and A. Bers, Waves in Anisotropic Plasmas (The M. I. T. Press, Cambridge, Mass., 1963).
2. A. Bers, "Linear Waves and Instabilities," in Plasma Physics (Les Houches 1972), (Gordon and Breach Publishers, London, in press); also M. I. T. Plasma Research Report 7210, July 1972 (unpublished).
3. T. H. Stix, The Theory of Plasma Waves (McGraw-Hill Book Company, New York, 1962).
4. A. I. Akhiezer, I. A. Akhiezer, R. V. Polovin, A. G. Sitenko, and K. N. Stepanov, Collective Oscillations in a Plasma (The M. I. T. Press, Cambridge, Mass., 1967).
5. R. R. Parker, "Alcator Lower Hybrid-Heating Experiment," Quarterly Progress Report No. 102, Research Laboratory of Electronics, M. I. T., July 15, 1971, pp. 97-111.
6. F. Troyon and F. W. Perkins, "Lower Hybrid Heating in a Large Tokamak," Proc. Second Topical Conference on RF Plasma Heating, Texas Technical University, June 1974.
7. T. E. Stringer, "Low Frequency Waves in an Unbounded Plasma," J. Nucl. Energy, Part C, 5, 93 (1963).
8. C. F. F. Karney, "Parametric Coupling to Low-Frequency Plasma Waves," S. M. Thesis, Department of Electrical Engineering, M. I. T., 1974.
9. C. F. F. Karney and A. Bers, Quarterly Progress Report No. 111, Research Laboratory of Electronics, M. I. T., October 15, 1973, pp. 71-84.
10. C. F. F. Karney and A. Bers, Quarterly Progress Report No. 113, Research Laboratory of Electronics, M. I. T., April 15, 1974, pp. 105-112.
11. A. Bers and C. F. F. Karney, Quarterly Progress Report No. 114, Research Laboratory of Electronics, M. I. T., July 15, 1974, pp. 123-131.